ISTANBUL TECHNICAL UNIVERSITY ★ EURASIA INSTITUTE OF EARTH SCIENCES

UPPER CRETACEOUS STRATIGRAPHY AND VOLCANISM IN İĞNEADA REGION, PONTIDES, NW TURKEY

M.Sc. THESIS

Ezgi SAĞLAM

Solid Earth Sciences Department

Geodynamics Programme

JULY 2020

ISTANBUL TECHNICAL UNIVERSITY ★ EURASIA INSTITUTE OF EARTH SCIENCES

UPPER CRETACEOUS STRATIGRAPHY AND VOLCANISM IN İĞNEADA REGION, PONTIDES, NW TURKEY

M.Sc. THESIS

Ezgi SAĞLAM
(602171006)

Solid Earth Sciences Department

Geodynamics Programme

Thesis Advisor: Prof. Dr. Aral I. OKAY

JULY 2020

İSTANBUL TEKNİK ÜNİVERSİTESİ ★ AVRASYA YER BİLİMLERİ ENSTİTÜSÜ

İĞNEADA'DA (BATI PONTİDLER, KB TÜRKİYE) ÜST KRETASE STRATİGRAFİSİ VE VOLKANİZMASI

YÜKSEK LİSANS TEZİ

Ezgi SAĞLAM
(602171006)

Katı Yer Bilimleri Anabilim Dalı

Jeodinamik Programı

Tez Danışmanı: Prof. Dr. Aral I. OKAY

TEMMUZ 2020

Ezgi Sağlam, a M.Sc. student of ITU Eurasia Earth Science Institute with student ID 602171006, successfully defended the thesis/dissertation entitled "UPPER CRETACEOUS STRATIGRAPHY AND VOLCANISM IN İĞNEADA REGION, PONTIDES, NW TURKEY", which she prepared after fulfilling the requirements specified in the associated legislations, before the jury whose signatures are below.

Thesis Advisor :	**Prof. Dr. Aral I. OKAY** İstanbul Technical University	....
Jury Members :	**Prof. Dr. Gültekin TOPUZ** İstanbul Technical University	....
	Prof. Dr. Timur USTAÖMER İstanbul University	....

Date of Submission : 10 June 2020
Date of Defense : 24 July 2020

FOREWORD

Firstly, I would like to express my sincere gratitude and appreciation to my supervisor Prof. Dr. Aral I. Okay for his invaluable guidance, continuous support, patience, constructive critisim and sharing his knowledge during the preparation of my thesis. Also, I would like to give my grateful thanks to my colleague Res. Asst. Turgut Duzman for his precious support and help during the field and laboratory studies and writing of my thesis.

I would like to give my special thanks to Prof. Dr. Gültekin Topuz for providing age data and, also for his precious help during sample preparation for geochemical analysis and interpretation of analysis results. I also would like to thank Prof. Dr. Timur Ustaömer for his constructive critisim and suggestions. I would like to thank Assoc. Prof. Dr. Gürsel Sunal for his important help during interpretation of age data and diagram preparation. I would like to thank Prof. Dr. Demir Altıner for his precious help in identification and dating of foraminifera. Additionally, I would like to give my thanks to Prof. Dr. Emin Çiftçi for his important help in imaging of zircons before dating. Also, I would like to thank Prof. Dr. Ercan Özcan for his important help in dating foraminifera. I would like to send my special thanks to Prof. Dr. Boris A. Natalin for sharing his precious suggestions about my study area and my thesis. I also would like to give my special thanks to Dr. Alp Ünal for his important help in preparation of geochemical diagrams and interpreting them. Also, I would like to thank Mehmet Ali Oral for preparation of thin sections, Mahir Altınbağa for his help in preparation of zircons for dating analysis.

Also, I would like to give my special thanks to my parents Bağdat Sağlam and Salih Sağlam, and my uncle İbrahim Sağlam for their continuous love and support. I would like to thank my best friend Elifsu Nemli, who is a sister to me, for always being there for me.

Additionally, I would especially like to thank my beloved friends Res. Asst. Işık Su Yazıcı, Korhan Uysal, Res. Asst. Ali Akın, Res. Asst. Işıl Nur Güraslan and Res. Asst. Yağmur Güneş for their suggestions and constructive critisim during the preparation of my thesis.

Finally, I would like to thank the people of İğneada, Limanköy and Beğendik for their hospitality. I also have to thank the beautiful forests of İğneada, the sun, the sea, warm breeze, cute puppies and birds for embellishing the field study for us.

May 2020

Ezgi SAĞLAM
(Geological Engineer)

TABLE OF CONTENTS

Page

ABBREVIATIONS

App	: Appendix
ASI	: Aluminum saturation index
Ca	: Calcite
Ch:	: Chlorite
Fds	: Feldspar
GPS	: Global positioning system
HFSE	: High field strength elements
LA-ICP-MS	: Laser Ablation Inductively Coupled Plasma Mass Spectrometry
LILE	: Large-ion lithophile elements
LOI	: Loss on ignition
Lt	: Lithic fragment
Mg#	: Magnesium number
OIB	: Ocean island basalt
Opq	: Opaque mineral
Plg	: Plagioclase
Prh	: Prehnite
Prx	: Pyroxene
Q	: Quartz
REE	: Rare earth element
TAS	: Total Alkali Silica

LIST OF TABLES

Page

LIST OF FIGURES

Page

UPPER CRETACEOUS STRATIGRAPHY AND VOLCANISM IN İĞNEADA REGION, WESTERN PONTIDES, NW TURKEY

SUMMARY

The Pontide Upper Cretaceous magmatic arc can be traced for over 1000 km along the southern Black Sea coast from Georgia to Bulgaria. The arc extrusive sequence is well-exposed in İğneada region in Thrace close to the Bulgarian border. The Upper Cretaceous sequence in İğneada region overlies the schists and phyllites of Strandja Massif with an unconformity. The sequence consists at the base of Cenomanian shallow marine limestone, which pass up into carbonate-rich sandstone, marl and calcareous siltstone indicating deepening upwards. The sedimentary rocks pass up into a volcanic-volcaniclastic sequence of andesitic tuff, lapilli-tuff, lapillistone, agglomerate, andesitic and basaltic-andesitic lava flows. The volcanic-volcaniclastic sequence is divided into three domains for a detailed investigation and they are indicated on the prepared geological map as D1, D2 and D3. The volcaniclastic rocks are intercalated with lava flows, rare pelagic limestone and shale beds. The sequence starts with andesitic volcaniclastic rocks and lava flows, and changes to basaltic-andesitic and then, to andesitic and dacitic rocks. The calc-alkaline characteristic of volcanic rocks and negative Nb-Ta anomaly indicate a volcanic arc setting. Although it is disrupted by several normal faults, the volcanic sequence can be traced from older to younger along the coast of İğneada. The sea floor alteration, which is found in all volcaniclastic and volcanic rocks, the intercalated pelagic limestones, and turbiditic sedimentary structures show that the rocks were deposited in deep submarine conditions in an intra-arc to fore-arc environment.

The beginning of the sedimentation in İğneada region is suggested as Albian based on rudist ages or Cenomanian based on foraminifera ages from the basal carbonate-rich sandstones. In this study, the start of the volcaniclastic deposition and hence the beginning of the volcanism is determined as Turonian based on a biomicritic limestone bed in the volcanic rocks. The limestone sample contains the planktonic foraminifera *Marginotruncana pseudolinneana*, *Marginotruncana marginata*, *Whitenella* sp., *Whitenella praehelvetica*, *Muricohedbergella* sp. Additionally, the planktonic foraminifera *Marginotruncana pseudolinneana*, *Marginotruncana coronate* and *Muricohedbergella flanderini*, which are identified in another biomicrite level, give age range between uppermost Turonian and Santonian. U-Pb zircon ages obtained from andesitic and dacitic tuffs from two different locations reveal Santonian (84.85 ± 0.42 Ma) and Campanian (80.6 ±1.5 Ma) ages indicating a continued volcanism from Turonian to Campanian.

İĞNEADA'DA (BATI PONTİDLER, KB TÜRKİYE) ÜST KRETASE STRATİGRAFİSİ VE VOLKANİZMASI

ÖZET

Üst Kretase magmatik yayı, Pontidler boyunca gözlemlenen 1000 kilometreden uzun bir magmatik kuşaktır. Tetis'in kuzeye doğru dalması sonucu oluşan Üst Kretase yaşlı volkanik ve volkaniklastik kayalar, Trakya İğneada'da çok iyi yüzlek vermektedir. Istranca Masifi'ne ait şist ve fillatlar bölgenin temel kayasını oluşturmaktadır. Bölgede bu metamorfik temeli uyumsuzlukla örten Üst Kretase yaşlı bir istif gözlemlenmektedir. Sedimanter, volkanik ve volkaniklastik kayalardan oluşan bu istif İğneada Grubu olarak isimlendirilmiştir. İğneada Grubu'nun tabanında, en iyi İğneada liman bölgesinde yüzlek veren sığ denizel kireçtaşları ve onun üzerine gelen karbonatlı kumtaşları yer almaktadır. Daha önceki çalışmalarda, sığ denizel kireçtaşlarındaki rudist ve karbonatlı kumtaşlarındaki Orbitolina fosillerine bakılarak bu birimin yaşı Albiyen ve Senomaniyen olarak belirlenmiştir. Bu birimin üzerine gelen marn, karbonatlı silttaşı ve laminasyonlu radyolaryalı silt/kiltaşı birimleri, istifin yukarı doğru derinleştiğini göstermektedir. Bu birimlerden yapılan ince kesitlerde volkanik malzeme bulunmaması, volkanizmanın henüz başlamadığını göstermektedir.

İğneada Grubu'nun sedimanter kayalarının üzerine gelen volkanik-volkaniklastik istif Limanköy limanından başlayarak Bulgaristan sınırına kadar gözlemlenmeye devam etmektedir. Ayrıca, volkanik-volkaniklastik kayaların Bulgaristan sahillerindeki devamlılığı Beğendik Köyü'nden görülebilmektedir. Bu volkanik-volkaniklastik istifin doğru bir şekilde yaşlıdan gence izlenebilmesi için istif, aşağıda açıklanacak yapısal unsurlardan dolayı tabaka yönelimlerinin değişimine göre D1, D2 ve D3 olarak üç bölüme ayrılarak incelenmiştir. Kaya türlerinin ve bileşimlerinin değişmesi de istifin bölünerek incelenmesinde etkili olmuştur.

Volkanik-volkaniklastik istif, İğneada Grubu'nun sedimanter kayalarının üzerine uyumlu bir şekilde gelen ve volkanizmanın başlangıcını temsil eden andezitik tüf seviyesiyle başlamaktadır. Bu andezitik tüf seviyesinden yapılan U-Pb zirkon yaşlandırmasının sonucunda Kampaniyen (80.6 ±1.5 My) yaşı elde edilmiştir. Volkanik-volkaniklastik istif, andezitik lapilli-tüf, aglomera, şeyl, karbonatça zengin kum/silttaşı-volkaniklastik kaya ardalanmaları ile devam etmektedir. Bu ardalanmalardaki sedimanter tabakalarda çok iyi gözlemlenemeyen türbiditik sedimanter yapılar bulunmaktadır. Bu kayaları önce 50 metre boyunca, yer yer içine bloklar alarak devam eden andezit, daha sonra bazaltik andezit lav akıntıları takip etmektedir. Bazaltik andezitlerde önce iyi gelişmemiş daha sonra iyi gelişmiş bazaltik andezit sütun çatlakları görülmektedir. Bazaltik andezit lav akıntılarının üzerine gelen andezitik/bazaltik andezitik tüf ve aglomeralar, volkanojenik kum/silttaşlarıyla ardalanmalı olarak görülmektedirler. Bu ardalanmaların arasında yer alan biyomikrit seviyelerinde bulunan planktonik foraminiferler *Marginotruncana pseudolinneana, Marginotruncana marginata, Whitenella* sp., *Whitenella praehelvetica, Muricohedbergella* sp. Turoniyen yaşını ve *Marginotruncana pseudolinneana, Marginotruncana coronate, Muricohedbergella flanderini* en üst Turoniyen-Santoniyen

yaşını vermektedir. Bölgede volkaniklastik çökelmenin başlama yaşı ve dolayısıyla volkanizmanın başlama yaşı, bu planktonik foraminiferlere dayanarak Turoniyen olarak belirlenmiştir. İstifin yukarılarına doğru kum ve silttaşlarında türbiditik sedimantasyonu gösteren konvolüt laminasyon gibi sedimanter yapılar çok iyi gözlemlenebilmektedir. Yukarılara doğru volkanik ve volkaniklastik kayaların bileşimleri asidik olmaya ve dasit lav akıntıları ve dasitik tüfler görülmeye başlanmaktadır. Bu dasitik kayalardan yapılan U-Pb zirkon yaşlandırmasının sonuçları Santoniyen (84.85 ± 0.42 My) yaşını vermektedir. İstifin en yukarılarına doğru tekrar bazik bileşime geçiş göstermesiyle, andezitik ve bazaltik andezitik volkaniklastik kayalar tekrar görülmektedir. Limanköy'den başlayan volkanik-volkaniklastik istif, Beğendik Köyü sahilinde dasitik, andezitik ve bazaltik andezitik tüflerin kum/silttaşı ardalanmaları ile sona ermektedir.

İstif boyunca alınan örneklerle yapılan petrografik incelemelerde bütün örneklerin alterasyondan etkilendiği ve örneklerde kalsit, klorit ve prehnit oluşumunun yoğun olduğu görülmektedir. Tüflerin ince kesitlerinde mineral bileşimi genel olarak plajiyoklaz, klorit, litik taneler ve kuvarstan oluşmaktadır. Andezit ve bazaltik andezitlerin bileşimi is plajiyoklaz, piroksen ve prehnitten oluşmaktadır. İnce kesitlerde mafik mineral olarak, bir tek az sayıda piroksen görülebilmektedir.

Stratigrafik ve petrografik incelemeler sonucunda, istifin bütün volkaniklastik ve volkanik kayalarında görülen deniz tabanı alterasyonu, aralarda görülen pelajik kireçtaşı seviyeleri ve andezitik tüf-aglomera seviyelerinin aralarında bulunan türbiditik çökeller, tüm kayaların denizaltı koşullarında ve bir yay önü havzasında derin denizel bir çökelme ortamında oluştuklarını göstermektedir.

Volkanik-volkaniklastik istifin jeokimyasal evrimini anlamak için istif boyunca jeokimya örnekleri alınarak tüm kaya analizleri yapılmıştır. Jeokimya analizlerinin sonuçlarına göre, tüm örneklerde ateşte kayıp değerlerinin yüksek olması (2.1 – 4.9 % arasında), örneklerin altere olduğunu göstermektedir. Alterasyonun bileşime etkisini önlemek için tüm örnekler kuru baza göre normalleştirilmiş ve sonuçlar normalleştirme sonrasında değerlendirilmiştir. % 77 SiO_2 değerine sahip olan dasit örneği dışında, andezit ve bazaltik andezitlerin ortalama SiO_2 değeri % 57 olarak belirlenmiştir. Yüksek SiO_2 değerine sahip dasit örneği dışında diğer örnekler andezit/bazaltik andezit alanında kalmaktadır. Bütün örnekler için hesaplanan magnezyum numaraları (Mg#) 65'ten küçük olduğu için örneklerin yüksek oranda diferansiye oldukları görülmüştür. Hesaplanan alüminyum doygunluk indekslerine (ASI) göre andezit ve bazaltik andezit örnekleri 1'den küçük, dasit örneği ise 1'den büyük değere sahiptir. Bu da andezit ve bazaltik andezitler metalüminyumlu özellik gösterirken, dasit örneğinin peralüminyumlu olduğunu göstermektedir. Örneklerde alterasyon etkili olduğu için, alterasyona daha duyarlı olan immobil elementler baz alınarak oluşturulmuş olan ayrım diyagramları kullanılmıştır. Hazırlanan diyagramlara göre, tüm örnekler volkanik yay alanı içerisinde yer almaktadır ve örneklerin tamamında kalk-alkalen magmatizmanın etkili olduğu görülmektedir. Bazı örnekler yüksek K içerikli kalk-alkalen/şoşonit serisinde bulunmaktadır. Ayrıca bütün örneklerde, negatif Nb-Ta anomalisi, ve yüksek çekim alanlı elementlere (HFSE) kıyasla büyük iyon yarıçaplı litofil elementlerce (LILE) ve hafif nadir toprak elementlerince zenginleşme görülmektedir. Bu jeokimya verilerine göre bölgedeki kayaların dalma-batma ile ilişkili oldukları ve bir volkanik yay ortamında oluştukları ortaya konmuştur.

Çalışma alanı içerisindeki bütün birimler büyük ve küçük ölçekli normal faylarla kesilmiştir. Bu normal faylar yoğunlukla sahil boyunca volkanik-volkaniklastik istifi keserek yarattığı cep sahiller olarak ve İğneada Grubu'nun sedimanter kayalarında basamak fayları olarak gözlemlenebilmektedir. Bölgedeki normal faylar, baskın olarak KB-

GD yönlü bir açılma sonucu oluşmuştur. Normal fayların yanısıra, yarısından fazlası açılma çatlağı olan ikili ve üçlü çatlak sistemleri de görülmektedir. Bazı bölgelerde kalsit veya kuvars ile doldurulmuş olan bu çatlak sistemleri genellikle volkanik-volkaniklastik istifin içinde bulunmaktadır. Normal fayların ve açılma çatlaklarının varlığı bölgede hakim olmuş olan genişlemeli bir sistemi işaret etmektedir. Yapılan KD-GB yönlü enine kesitte de görülebileceği gibi bölgede volkanik-volkaniklastik birimlerde büyük ölçekli bir senklinal görülmektedir. İstifin stratigrafisi yaşlıdan gence doğru incelenirken, bütün bu yapısal unsurlar istifin bölümlere ayrılmasında etkili olmuştur.

Sonuç olarak, İğneada bölgesinde bulunan, sedimanter kayalarla başlayıp volkaniklastik ve volkanik kayalarla devam eden, andezitik, bazaltik andezitik ve dasitik kayalardan ve bunların volkanojenik sedimanter kayalarla ardalanmalarından oluşan bu istifte volkaniklastik çökelimin başlama yaşı planktonik foraminiferlerle Turoniyen olarak belirlenmiştir. Bu nedenle, Turoniyen'de bölgede volkanizmanın aktif olduğu düşünülmektedir. Ayrıca, yapılan U-Pb zirkon yaşlandırmalarının sonucu olarak elde edilen Santoniyen ve Kampaniyen yaşları da bölgedeki yay volkanizmasının Turoniyen'den Kampaniyen'e kadar devam ettiğini göstermektedir.

1. INTRODUCTION

1.1 Description of the Study Area

The following section describes the studied area emphasizing its geographical location, morphology, climate and flora.

1.1.1 Geographical location

The study area is located in Limanköy and Beğendik villages of the town of İğneada in Demirköy District of Kırklareli Province. Limanköy Village is 7 km away from the town of İğneada. Beğendik Village is a village on Turkey-Bulgaria frontier and 14 km away from the the town of İğneada. The studied and mapped area comprises approximately 10 km^2 around Limanköy and Beğendik villages (Figure 1.1). It bounded by the Turkey-Bulgaria border in the north, Black Sea in the east and south, and Sislioba Village in the west.

Figure 1.1 : The location of the study area in NW Turkey.

1.1.2 Morphology, climate and flora

There are steep cliffs and pocket beaches continuing along the coasts of İğneada. The height reaches up to 150 meters in the western part of the study area. In the eastern part of the study area that is seaside, there are some valleys, two of which are deep.

The İğneada floodplain forests comprise most of the vegetation cover of the study area. Therefore, the best outcrops and continuous stratigraphic sequences can be observed in the sea cliffs along the coasts of the İğneada. The İğneada floodplain forests are completely covered with water during winter and spring and it is mostly composed of forest trees of 8-15 m tall (nationalparksofturkey.com). The climate in İğneada is warm and temperate. There is significant rainfall throughout the year (tr.climate-data.org).

1.2 Aim and Method of the Study

This study aims to reveal stratigraphy, petrography, geochemistry, and tectonic evolution of volcaniclastic and volcanic sequence in and around İğneada. Field geology, petrography, geochemistry and structural geology studies on sedimentary, volcanic and volcaniclastic units are conducted.

The geological map of the study area and stratigraphic sequence of the volcanic and volcaniclastic rocks along the coastline are prepared. The field study is done during the June, July and October 2018. During the field study, geological hammer, GPS, hand-lens, Silva type compass are used. The main objectives of this study are specified as the followings: to make detailed geological map of the Upper Cretaceous volcanic rocks and surrounding rocks, to determine the structural elements and to establish contact relationships of units, to make systematic sampling for geochemical analyses and petrographic studies from specified locations, to reveal the petrographic properties of the rocks, to determine the geochemical characteristics of Upper Cretaceous volcanism in İğneada region of the Pontides.

Whole rock samples are analyzed for major oxides and trace elements at AcmeLabs, Bureau Veritas Mineral Laboratories in Ankara, Turkey. U-Pb dating is applied to zircons separated from volcaniclastic rocks in order to reveal the initiation and duration of the Upper Cretaceous volcanism in İğneada region. The zircons are separated in ITU Sample Preparation and Mineral Separation Laboratory and their cathodoluminescence images are captured in ITU Geochemical Instrumental Laboratory. The planktonic foraminifera are identified from thin sections and used also to constrain the age of the volcaniclastic rocks in the region.

1.3 Previous Studies

Pamir and Baykal (1947) defined the rock units in İğneada region and the relationship between them. The sedimentary and volcanic sequence starting from İğneada and continuing to Limanköy is first studied by them. They asserted that the age of the sequence including sedimentary, volcaniclastic and volcanic rocks is Cenomanian based on ages of foraminifera.

Çağlayan and Yurtsever (1998) mapped the geological units in the region and defined the "İğneada Group" and separated it into three formations.

Okay et al. (2001) indicated that the northern part of the Strandja Massif is composed of a magmatic arc and an intra-arc basin during Senonian, and as a result, calc-alkaline volcanic rocks and volcaniclastic rocks which have at least 3 km thickness and the Senonian granodioritic plutons which intruded the metamorphic rocks of the Strandja Massif are observed.

Okay et al. (2006) described the lithostratigraphic units in the region by revealing their lithological properties, boundaries, distribution, ages and fossil contents.

S. Georgiev et al. (2009) conducted geochemical studies on the eastern Sredna-Gora segment of the L-shaped Apuseni – Banat – Timok – Sredna-Gora Upper Cretaceous magmatic belt which extends from Romania to the Black Sea. According to their results, the East Sredna-Gora segment exhibits a geochemical diversity from the initially mafic magma to the intermediate magma unlike the other segments of the Carpathian-Balkan orogen.

N. Georgiev et al. (2009) indicated that the Upper Cretaceous (86 - 75 Ma) aged granites were found in the southwest of the Sredna-Gora region in Bulgaria and that the emplacement of these granites may be related to the shear zone created by a regional right lateral strike-slip fault.

Karacık and Tüysüz (2010) revealed the characteristics of the Demirköy pluton, which is a part of Upper Cretaceous magmatic belt comprising also the volcanic and volcaniclastic rocks. The Demirköy igneous complex is located in the west of İğneada. The age of the complex is given as 71 – 84 Ma by combining K-Ar, Ar-Ar and U-Pb datings from studies on different parts of the complex (Moore et al., 1980; Aydın, 1982; Handler et al., 2004; von Quadt et al., 2005; Kouzmanov et al., 2009; Peytcheva et al., 2009). The geochemistry of all of the magmatic rocks in Demirköy pluton indicates the subduction origin, but various petrological processes like deep crustal melting, slab-derived fluids and crustal contamination. According to their geochemical studies, the Demirköy Igneous Complex has calc-alkaline, medium-K and metaluminous characteristics. The sources of the pluton are a typical subduction-related enriched lithospheric mantle and a lower crustal source, based on geochemical data.

Gallhofer et al. (2015) explained the tectonic evolution of the Upper Cretaceous magmatic arc which was active for 25 Ma and can be followed along the Apuseni – Banat – Timok – Sredna-Gora magmatic belts, by comparing the geochemical characteristics of different segments. They asserted that these segments in the Carpathian-Balkan orogen show typical geochemical characteristics of a magmatic arc formed at the plate margin due to the subduction.

Marchev et al. (2015) defined the eastern Sredna-Gora Zone as Upper Cretaceous cumulates, ankaramites which contain normative nepheline and shoshonitic basalts. They indicated that the ankaramitic magma was formed by melting of a mantle source which does not contain garnet and is exposed to metasomatism instead of melting of cumulates of lower crust.

Keskin and Tüysüz (2018) claimed that the Western Pontides are formed from two different magma series corresponding to two different volcanic periods. During the first period in Middle Turonian – Early Santonian, the magma is derived from a depleted mantle associated with the subduction of the Tethys Ocean. The volcanism is paused in the late Santonian permitting the deposition of a thin pelagic limestone layer. During the second period of volcanism in Campanian, the magmas are derived from two different sources which are a depleted lithospheric mantle and an enriched asthenospheric mantle similar to ocean island basalts (OIB).

Boehm et al. (2019) suggested that Upper Cretaceous volcanic/volcaniclastic units are separated by pelagic limestone, which means that the main volcanic activity occurred as two different periods that are Turonian-Santonian and early-mid Campanian. The geochemical characteristics show dominantly volcanic arc setting. There are subalkaline and more tholeiitic series which are found in the second period of volcanism.

1.4 Geological Setting

The study area is located within the Upper Cretaceous magmatic complex in the Strandja Massif, which is metamorphosed and deformed during late Jurassic - early Cretaceous (Okay et al., 2001). After its exhumation in the Upper Cretaceous (Cattò et al., 2018), the massif is overlain by Upper Cretaceous sedimentary, volcaniclastic and volcanic rocks, which are best observed in İğneada on the Black Sea coast (Okay et al., 2019). They represent a part of the Upper Cretaceous Pontide magmatic arc (Okay et al., 2001). The Upper Cretaceous magmatic arc is formed as a result of the subduction of the Tethys Ocean to the north under the Eurasia (S. Georgiev et al., 2009; Gallhofer et al., 2015; Keskin and Tüysüz, 2018). The Upper Cretaceous magmatic arc, which is divided into segments as Apuseni – Banat – Timok – Sredna-Gora, has remained active for 25 million years. All segments show the typical geochemical properties of a subduction-related magmatic arc (Gallhofer et al., 2015). The magmatic belt has a width of approximately between 30 - 70 km and it can be observed for 1000 km along Romania, Serbia, Bulgaria, Turkey and Georgia (S. Georgiev et al., 2009). It can be traced in Turkey (Figure 1.2) starting from İğneada, continuing along Istanbul Zone and Pontides (Aysal et al., 2018). The eastern Sredna-Gora segment, which is adjacent to the Black Sea, is located in the easternmost part of the Apuseni – Banat – Timok – Sredna-Gora belt. The İğneada volcanic – volcaniclastic rocks are located within the eastern Sredna-Gora segment.

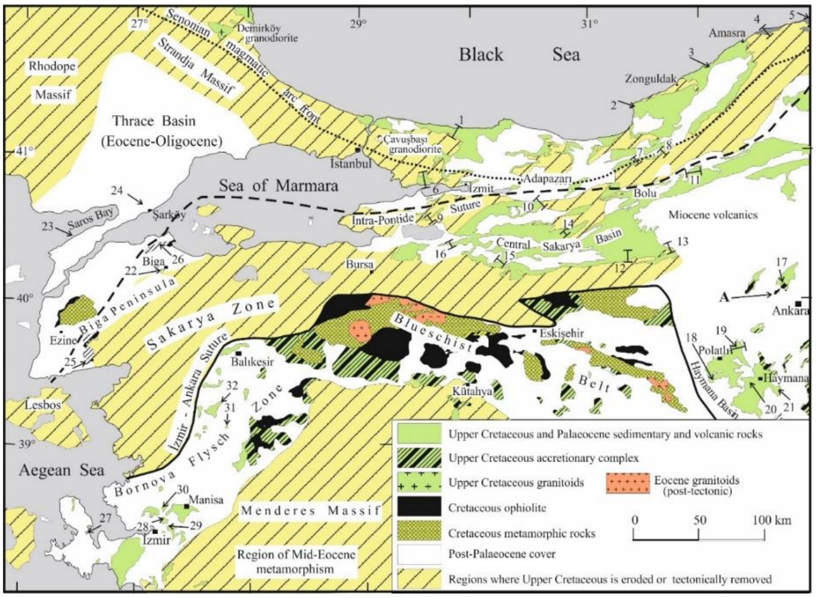

Figure 1.2 : The distribution of the Upper Cretaceous and Paleocene rocks in the western Turkey (modified from Okay et al., 2001).

2. STRATIGRAPHY AND PETROGRAPHY

2.1 Introduction to the Stratigraphy of the Study Region

The metamorphic rocks of the Strandja Massif, which is affected by Variscan orogeny and then by the Late Jurassic – Early Cretaceous metamorphism and deformation, constitutes the basement rocks in the study area. The basement is unconformably covered by sedimentary rocks of İğneada Group. As it will be explained in the following section, the beginning age of the sedimentation of the sedimentary rocks is suggested as Albian or Cenomanian according to different authors (Pamir and Baykal, 1947; Çağlayan and Yurtsever, 1998; Arca, 2012). There are volcanic and volcaniclastic rocks on the top of the sedimentary rocks, and they make up most of the stratigraphic section. In this study, the beginning age of the volcaniclastic deposition and hence the beginning of the volcanism is determined as Turonian based on the planktonic foraminifera, which will be presented in the following sections. In addition, U-Pb zircon ages from two different locations reveal Santonian and Campanian ages indicating a continued volcanism from Turonian to Campanian.

The rock units, which are exposed in the study area, are listed as the following: the Mahya Schists of the Strandja Massif; the İğneada Group including 3 sedimentary packages in which limestone, marl, carbonate-rich sandstone, siltstone, radiolarian calcareous siltstone are present; the volcanic and volcaniclastic rocks in the İğneada Group; the unconsolidated Neogene sediments as a cover unit in some places in the study area. The geological map of the study area, the observation points and the sample locations for dating and analyses are given in Figure 2.1 and App-A. The close up view showing İğneada harbour and surrounding is also given in Figure 2.2.

The generalized stratigraphy of the region is demonstrated in Figure 2.3. The stratigraphy is explained in detail separately for sedimentary and volcanic-volcaniclastic rocks, within the following parts.

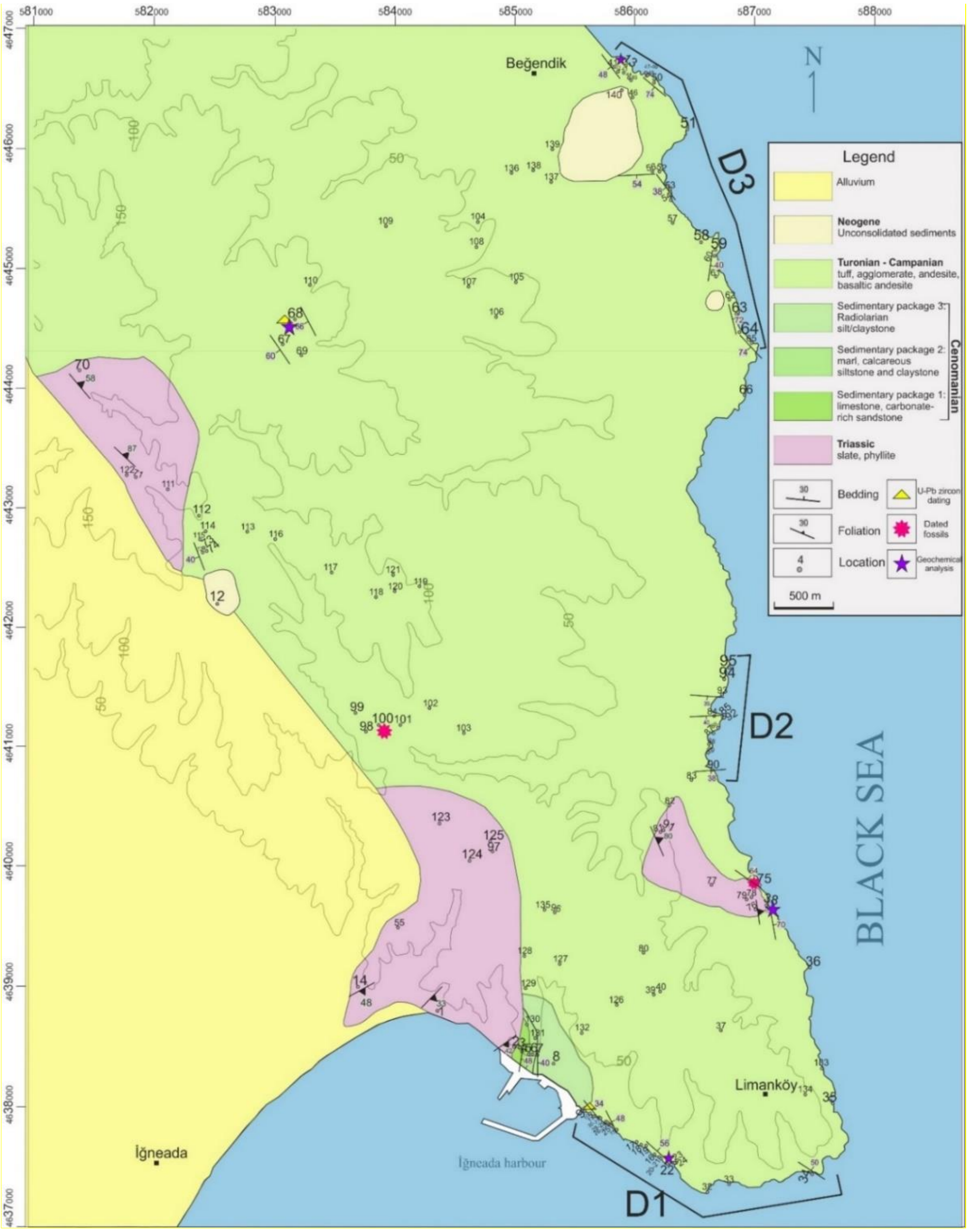

Figure 2.1 : The geological map of the study area showing the volcanic-volcaniclastic domains D1, D2 and D3.

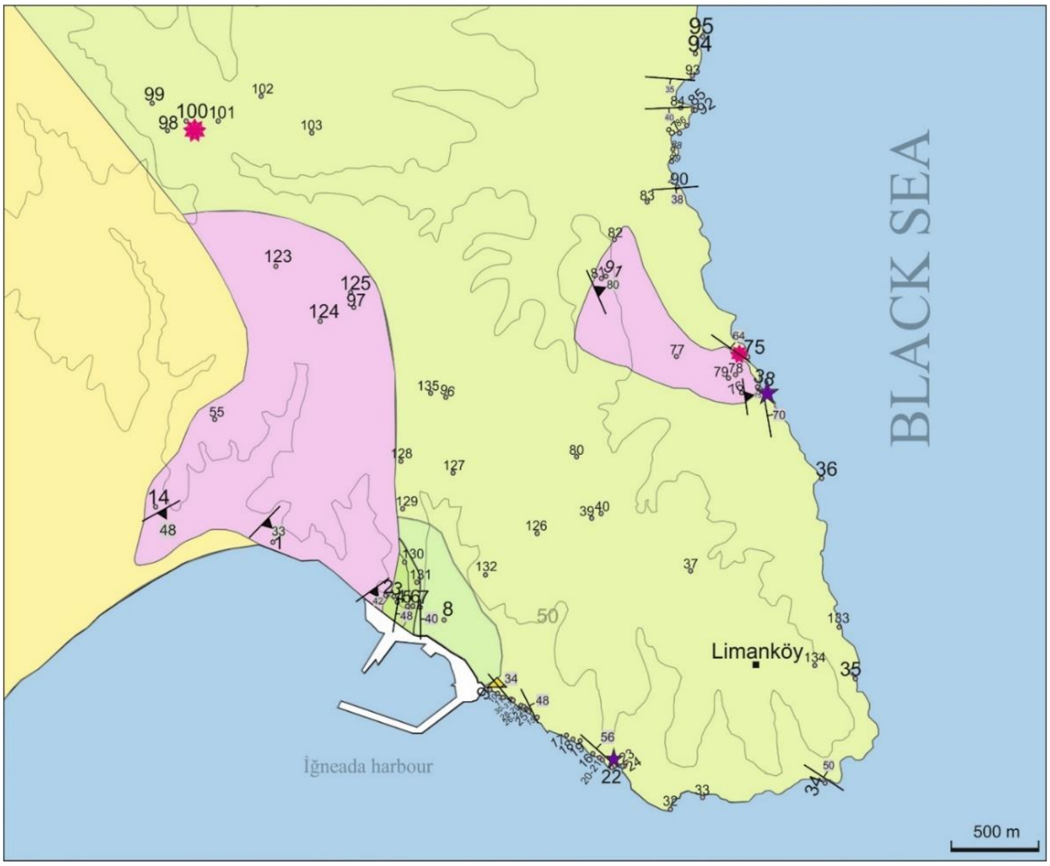

Figure 2.2 : The detailed geological map of the İğneada harbour and surrounding region.

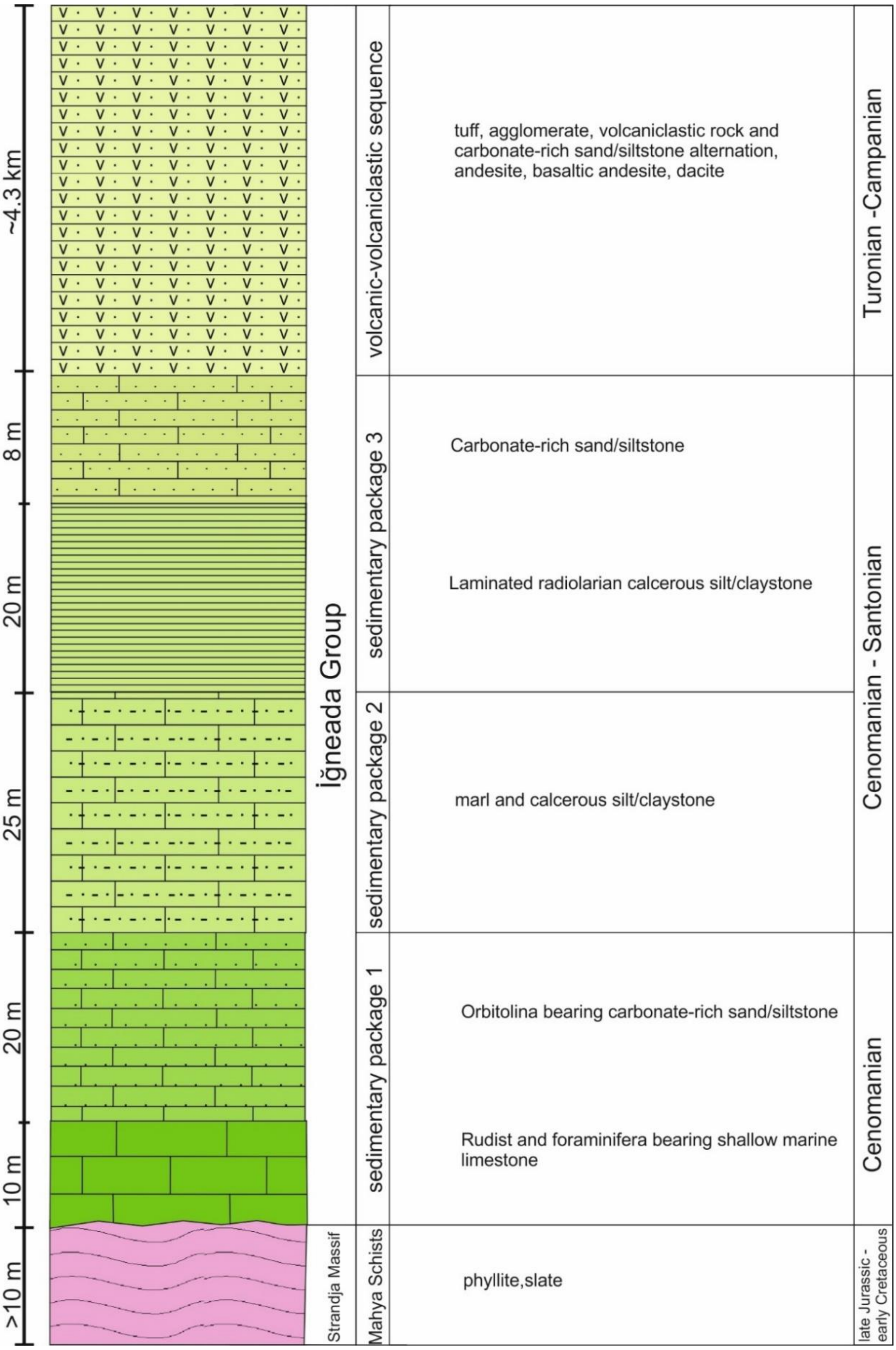

Figure 2.3 : The generalized stratigraphic section including all units in the study area.

2.2 Mahya Schists

The metamorphic rocks, which are phyllites and slates belonging to the Mahya Schists are observed as the basement rocks underlying the İğneada Group. The sedimentary rocks are deposited on this metamorphic basement with an unconformity which can be observed in the study area. Additionally, the volcanic rocks directly overlie the slates and phyllites in some places in the study area.

Pamir and Baykal (1947) defined Mahya Schists as phyllites, quartzites, micaschists and calcschists. Üşümezsoy and Öztunalı (1981) identified Mahya Complex as Triassic quartz schist, micaschist and phyllite. In 1998, for the first time Çağlayan and Yurtsever named this unit as the Mahya Complex which is considered as a combination of Triassic phyllites and partly carbonate schists. Natalin et al. (2016) revealed that the age of the deformation and greenschist facies metamorphism of the Mahya Schists is middle Jurassic – early Cretaceous. The phyllites and slates have wavy foliation indicating the subsequent folding of the main foliation. The schistosity varies between outcrops. The crenulation cleavage, asymmetric microfolding and kink folding are also observed (Figure 2.4). The protoliths of these fine grained metamorphic rocks are presumably silt/claystone.

Figure 2.4 : The field photo of the phyllites with the asymmetric folding.

2.3 İğneada Group

The İğneada Group covers most of the study area. It is exposed at the north, south and southeast comprising approximately 8 km^2 of the study area. The best outcrops are observed along the coast of Limanköy and Beğendik villages, and at the roadside opposite to the İğneada Harbour.

The Cretaceous sedimentary, volcaniclastic and volcanic rocks in İğneada are firstly defined by Pamir and Baykal (1947). They asserted that the sedimentary rocks are conformably overlying the micaschists of the Strandja Massif. Aydın (1982) first used the name “İğneada Formation” for the sedimentary and volcaniclastic rocks in İğneada and Limanköy. The stratigraphy of this formation is described from base upwards as tuffite, agglomerate, mudstone and fine sandstone. Çağlayan and Yurtsever (1998) described this sedimentary rocks as the “İğneada Group” which is well exposed in the town of İğneada, Limanköy, Beğendik and Rezve villages. According to their study, the İğneada Group is separated into three formations which are Avcılar Conglomerates, Rezve Formation and Limanköy Formation. Okay et al. (2006) defined the İğneada Group as a volcanosedimentary sequence which has approximately 400 m thickness and divided it into four formations which are Sislioba sandstone, Kadembaba, Rezve and Limanköy formations; they explained the stratigraphy in detail and asserted that the depositional age of the İğneada Group is Cenomanian – Campanian. The İğneada Group is composed of sedimentary, volcaniclastic and volcanic rocks which are well exposed in the study area. The sedimentary rocks of İğneada Group unconformably overlie the phyllites and slates of the Strandja Massif. The volcanic -volcaniclastic rocks of İğneada Group overlie the sedimentary rocks conformably. The volcaniclastic rocks are also found overlying directly the phyllites and slates in a few places.

2.3.1 Sedimentary sequence in İğneada Group

The sedimentary rocks are best observed at the roadside north of the İğneada Harbour and at the Limanköy Beach. The sedimentary sequence can be divided into three sedimentary packages (Figure 2.6) which are distinguished according to their rock type and fossil content. They can be observed from the oldest to the youngest starting from the roadside at the north of the İğneada Harbour to the entrance of Limanköy Beach. They are explained from the oldest to the youngest and indicated as sedimentary package 1, 2, and 3 in the stratigraphic section (Figure 2.5). The fossil contents of each sedimentary package are revealed in the previous studies and they are also indicated in the stratigraphic section.

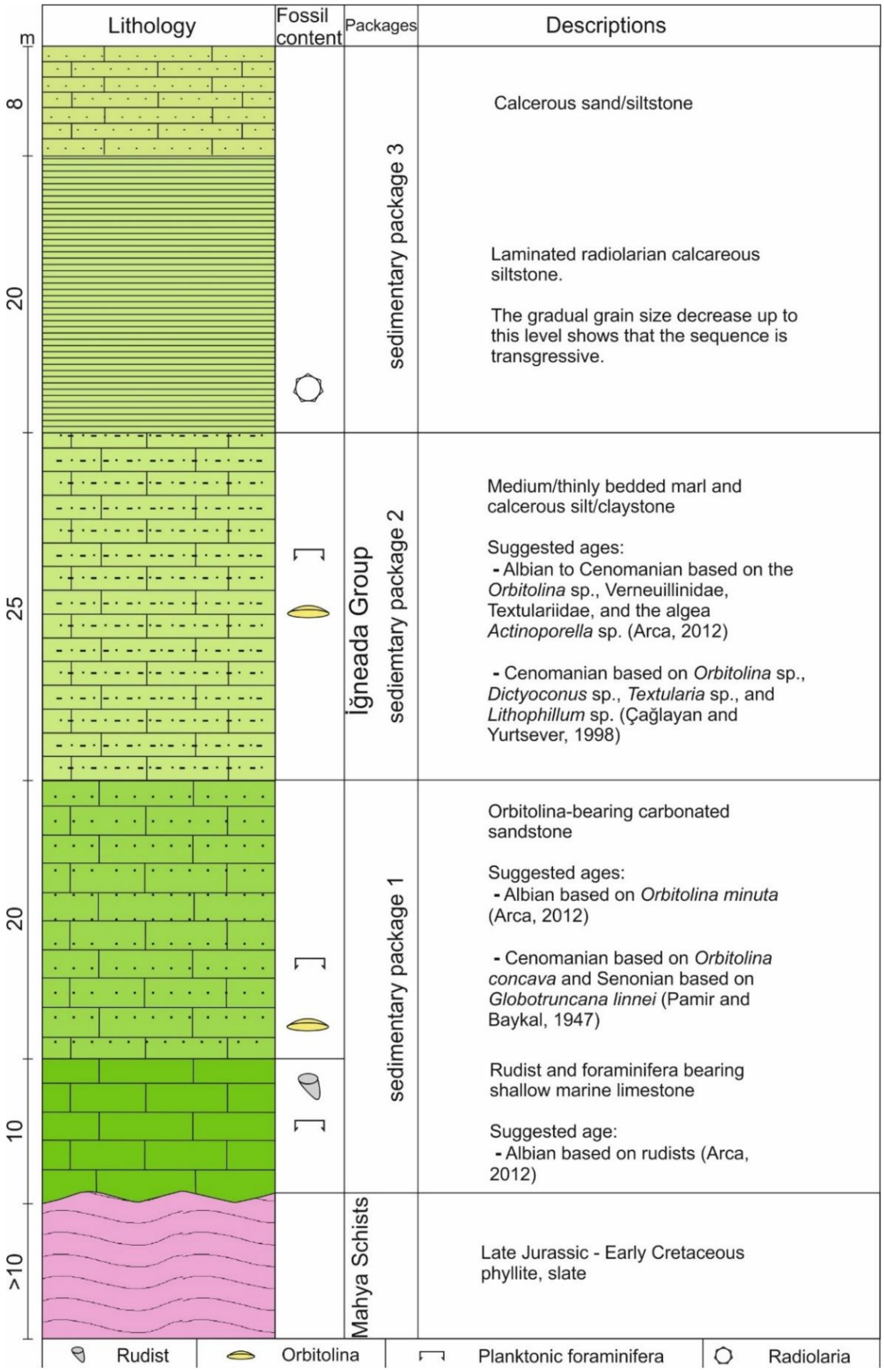

Figure 2.5 : The stratigraphic section of sedimentary sequence of İğneada Group.

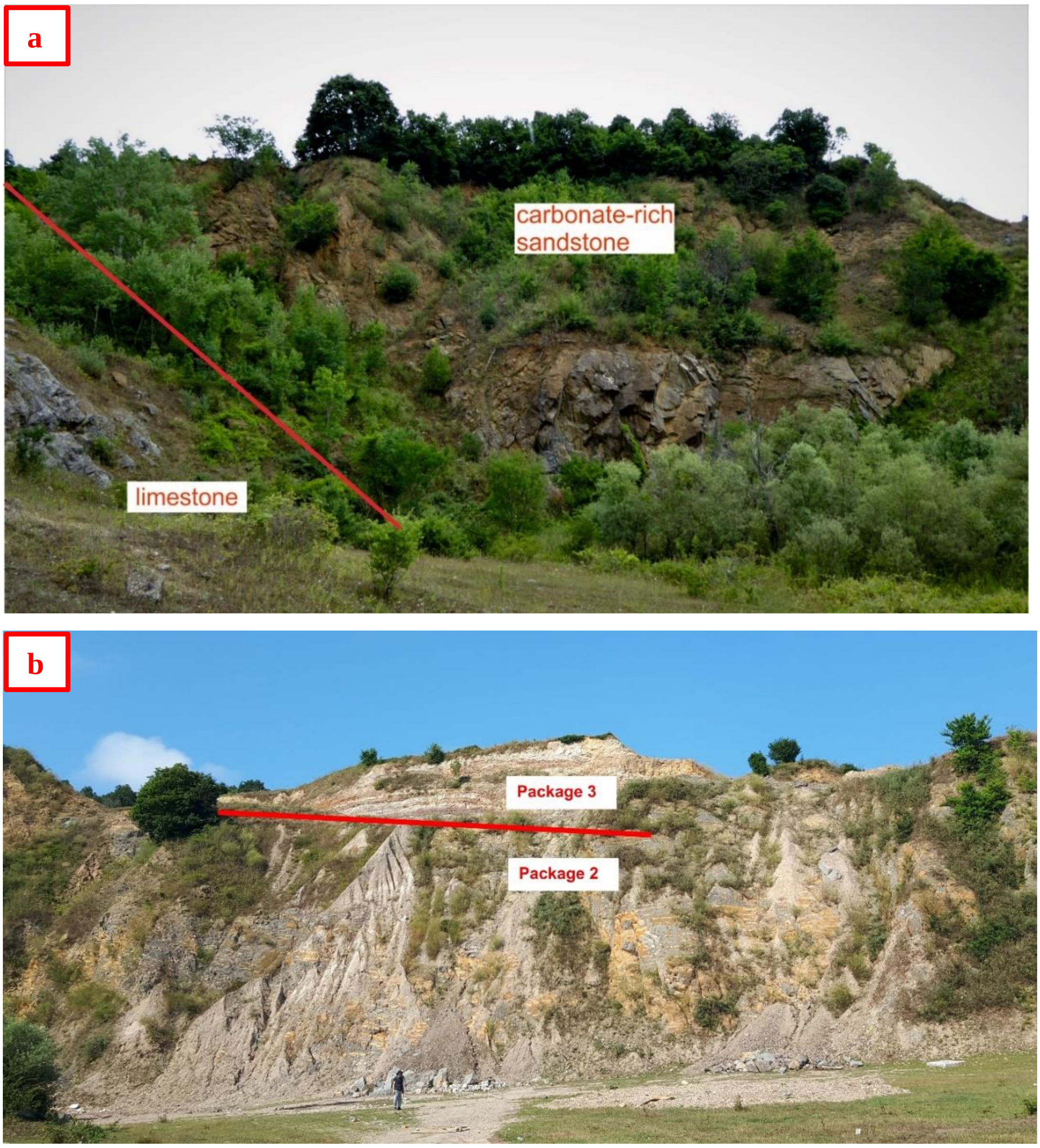

Figure 2.6 : Panoramic views showing the sedimentary packages 1, 2 and, 3. a) Limestone and carbonate-rich sandstone of the sedimentary package 1. b) Marl interbedded with calcareous siltstone in the sedimentary package 2, and radiolarian siltstone in the sedimentary package 3.

2.3.1.1 Sedimentary package 1

The sedimentary sequence starts with shallow marine limestone (Figure 2.7a) which are massive or very thickly bedded so that the orientation of the bedding cannot be measured. They have grey color, lots of calcite veins in various orientations and, are approximately 10 m thick. Arca (2012) identified a rudist fauna within the upper levels of the limestone, including *Eoradilites* cf. *murgensis* Torre, 1965, *Eoradilites* sp., *Radiolites* sp., Radiolitidae and, Requienidae. and stated that the age of this unit is Albian based on these rudist fragments. This first sedimentary package continues upwards with 20 m thick dark grey, carbonate-rich sandstone (Figure 2.7b). They are very thickly bedded and step faulting is observed. The sandstone unit is coarse grained at the bottom but, the grain size becomes finer upwards indicating deepening upwards. Pamir and Baykal (1947) provided the age data for this unit by using foraminifera *Orbitolina concava* as Cenomanian and Senonian, respectively. Arca (2012) found *Orbitolina minuta* within the sandstone layers and determined the age as Albian.

Figure 2.7 : Field photographs of the sedimentary package 1 from location 4 and 5, respectively. a) Rudist-bearing shallow marine limestone at the base of the İğneada Group b) Orbitolina-bearing carbonate-rich sandstone.

2.3.1.2 Sedimentary package 2

The second sedimentary package is composed of marl and calcareous silt/claystone (Figure 2.8). The alteration and oxidation has caused brown outcrops, but their fresh surface color is grey. They are medium bedded with approximately 30 cm beds and the total thickness of this package is 25 m. There are some oxidized dark layers up to 10 cm thick within the package. The cleavage surfaces are observed in the claystone beds. Çağlayan and Yurtsever (1998) identified *Orbitolina* sp., *Dictyoconus* sp., *Textularia* sp., and *Lithophillum* sp. within this package and determined the age as Cenomanian. Arca (2012) found thin shelled bivalvia, some benthic and planktonic foraminifera, which are *Orbitolina* sp., Verneuillinidae, Textulariidae, and the algea *Actinoporella* sp. The ages of foraminifera and algea are given between Albian and Cenomanian.

Figure 2.8 : Field photo of marl and calcareous silt/claystone from location 6 in the sedimentary package 2.

2.3.1.3 Sedimentary package 3

The third package is composed of laminated radiolarian silt/claystone at the bottom and carbonate-rich sand/siltstone at the top (Figure 2.9). The laminated radiolarian silt/claystone, which have reddish grey to reddish brown color, is 20 m thick. The gradual decrease in grain size in the sedimentary sequence up to this unit indicates that the sequence is transgressive. At the top of this unit, the carbonate-rich sand/siltstone is present with approximately 8 m thickness. Although the carbonate-rich sand/siltstone indicates a grain size increase contradicting with transgressive sequence, there may be a tectonic reason for this unit overlying laminated siltstone. The sedimentary package 3 is also seen at the contact between sedimentary rocks and volcanic-volcaniclastic rocks of İğneada Group.

Figure 2.9 : Field photos of the laminated radiolarian calcareous siltstone from location 7 in the sedimentary package 3. a) The outcrop view of the radiolarian calcareous siltstone b) The close up view showing the reddish dark brown oxidized laminations within siltstone.

2.3.2 Volcanic and volcaniclastic sequence in İğneada Group

The sequence containing volcanic and volcaniclastic rocks is firstly defined by Pamir and Baykal (1947). According to their study, the volcanic-volcaniclastic rocks are deposited concordantly on the sedimentary sequence. The andesitic tuffs are mentioned as intercalations within flysch layers and the andesite is mentioned as veins cutting the flysch layers. Çağlayan and Yurtsever (1998) described the "Limanköy Formation" which includes tuff and spilite members. At the bottom, this formation includes tuff, ignimbrite, agglomerate, shale and pyroclastic sandstone intercalations and andesitic rocks. The spilitic basalts are found above these andesitic and volcaniclastic rocks. In this study, the volcanogenic sedimentary rocks such as sand/siltstone are also observed (Location 42, 75, 99, 100; see App-A) as it will be mentioned in the following sections. They are important due to their fossil content which helps understanding the age of the initiation of the volcanism.

The volcanic and volcaniclastic rocks are very well exposed along the coast from Limanköy Beach to Beğendik Village. The thickness of the volcanic and volcaniclastic units of İğneada Group is approximately 4,3 km according to cross-sections made throughout the coast. Their continuation along Bulgarian Black Sea coasts can be observed well from Beğendik Village. The stratigraphic section of these volcanic-volcaniclastic sequence is conducted starting from the Limanköy beach continuing to Beğendik Village. The sequence is locally disrupted by faulting and other structural elements as it is explained in the structural geology chapter. Therefore, 3 separate volcanic-volcaniclastic domains can be defined and they are indicated on the map as D1, D2, and D3 (Figure 2.1). Each of the volcanic-volcaniclastic domains can be divided into parts in themselves based on the depositional and compositional changes in rocks. This chapter explains the domains of the volcanic-volcaniclastic sequence and the parts within these domains in detail. The generalized stratigraphic section showing the entire volcanic-volcaniclastic sequence is presented in Figure 2.10 and the legend for the section is given in Figure 2.11. The detailed stratigraphic section for each part of the domains are given in the following parts.

The classification of Fisher (1966) is used for the definition of the volcaniclastic rocks. Based on this classification, the terms are used according to the sizes of pyroclastic fragments. The fragment sizes of ash, lapilli and blocks & bombs are determined as < 2 mm, 2 – 64 mm, and > 64 mm, respectively (Fisher, 1966).

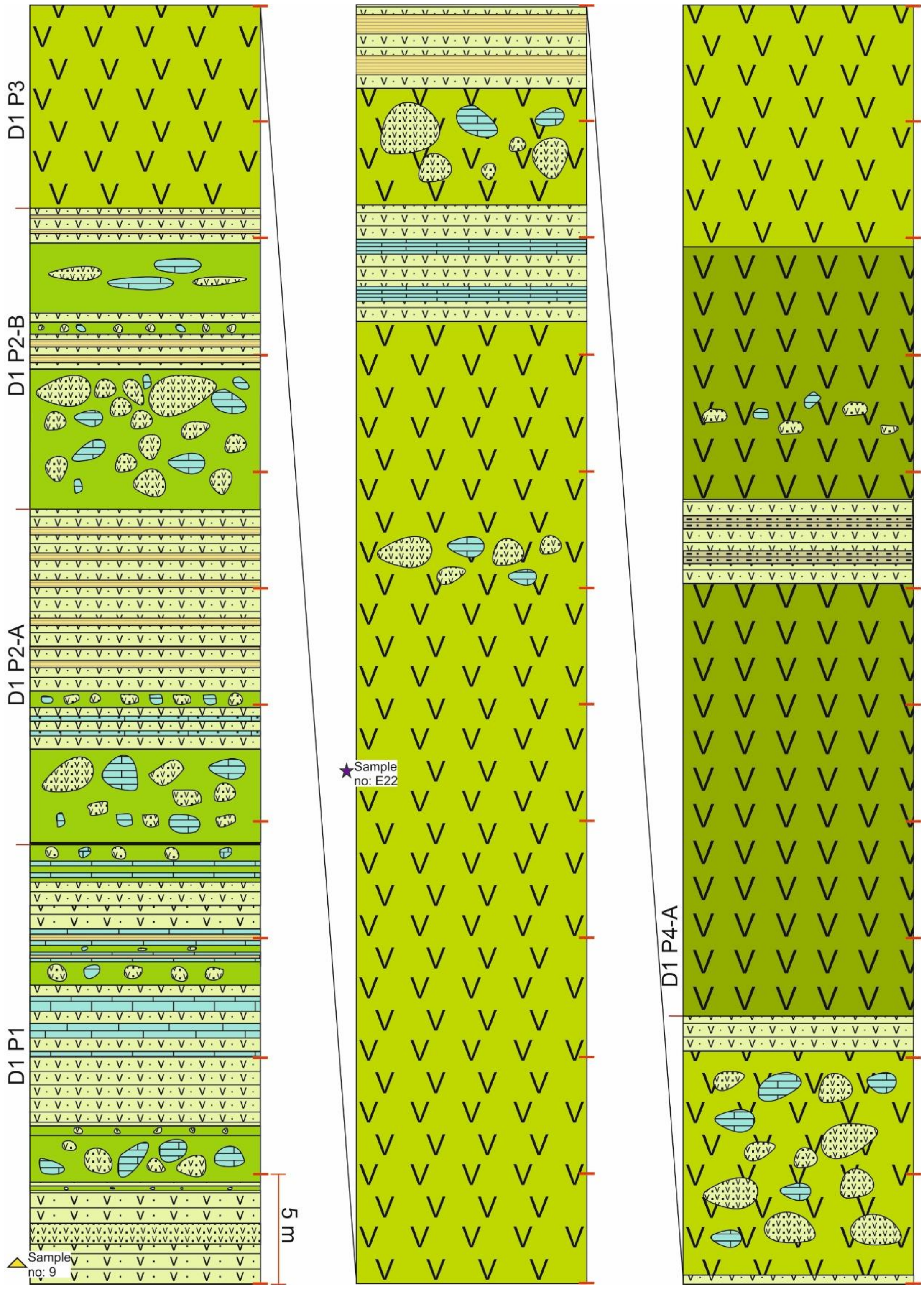

Figure 2.10 : The generalized section of three domains of the volcanic-volcaniclastic sequence from Limanköy to Beğendik. The parts of the domains are indicated on the left side of the columns.

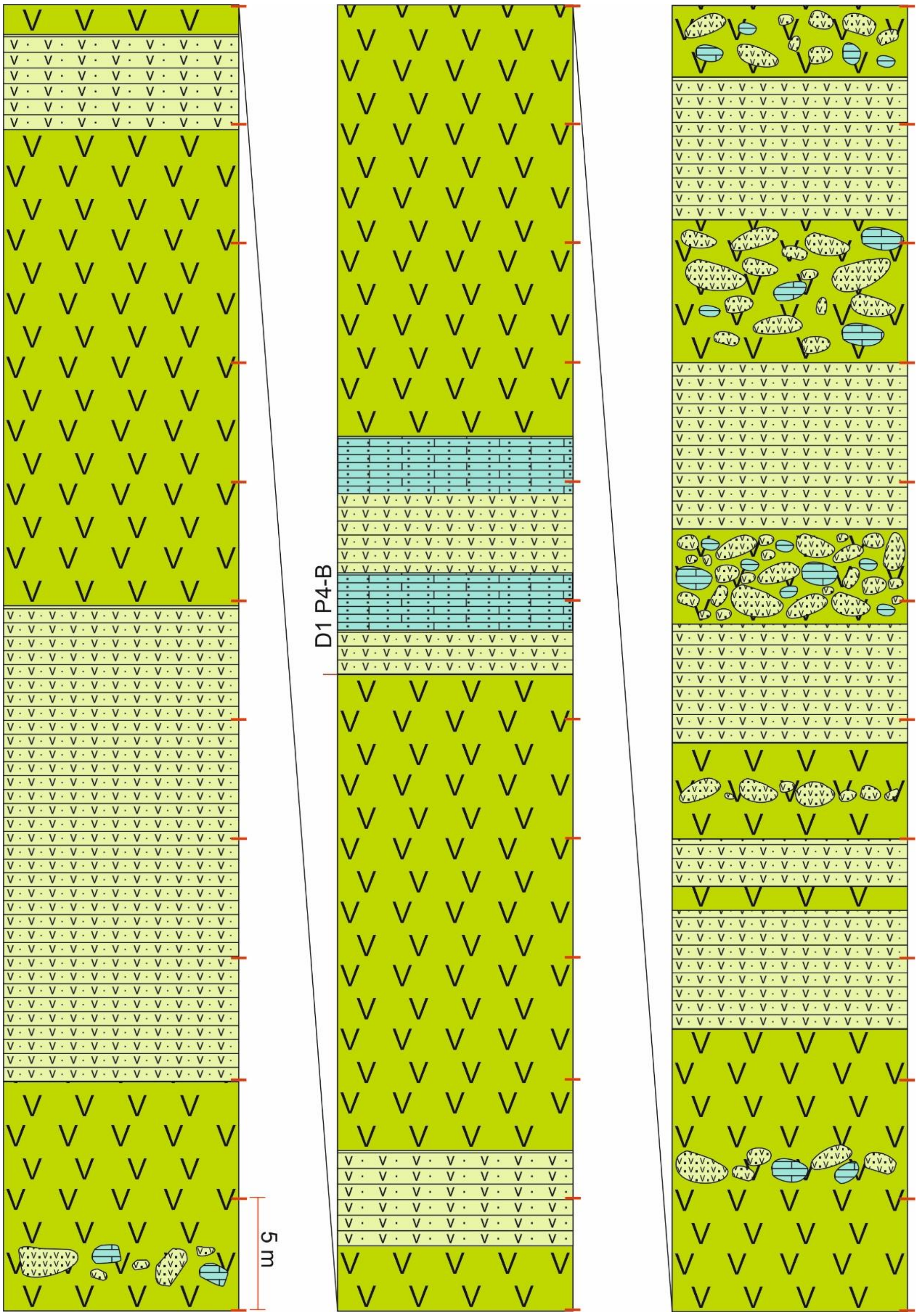

Figure 2.10 (continued) : The generalized section of three domains of the volcanic-volcaniclastic sequence from Limanköy to Beğendik.

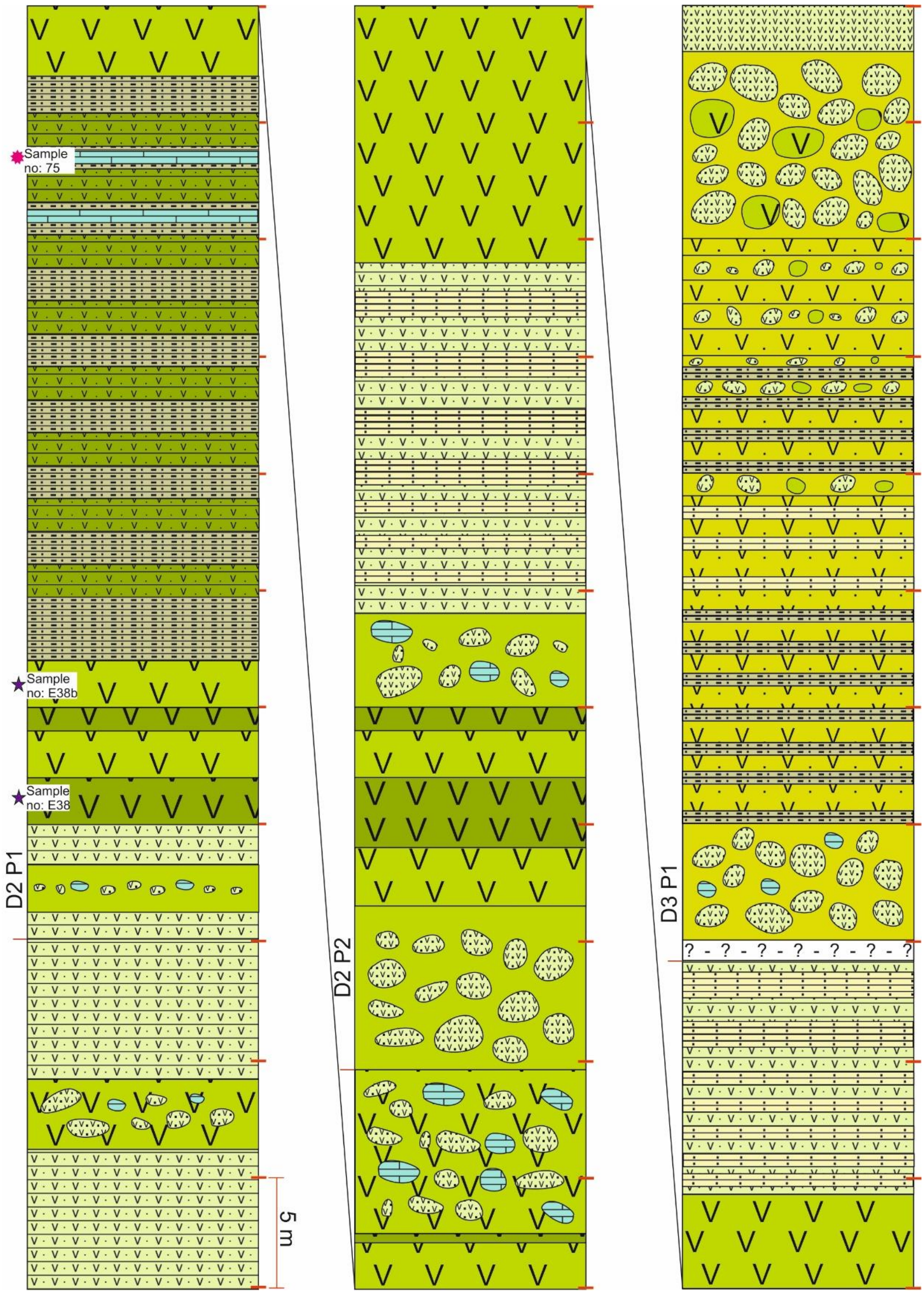

Figure 2.10 (continued) : The generalized section of three domains of the volcanic-volcaniclastic sequence from Limanköy to Beğendik.

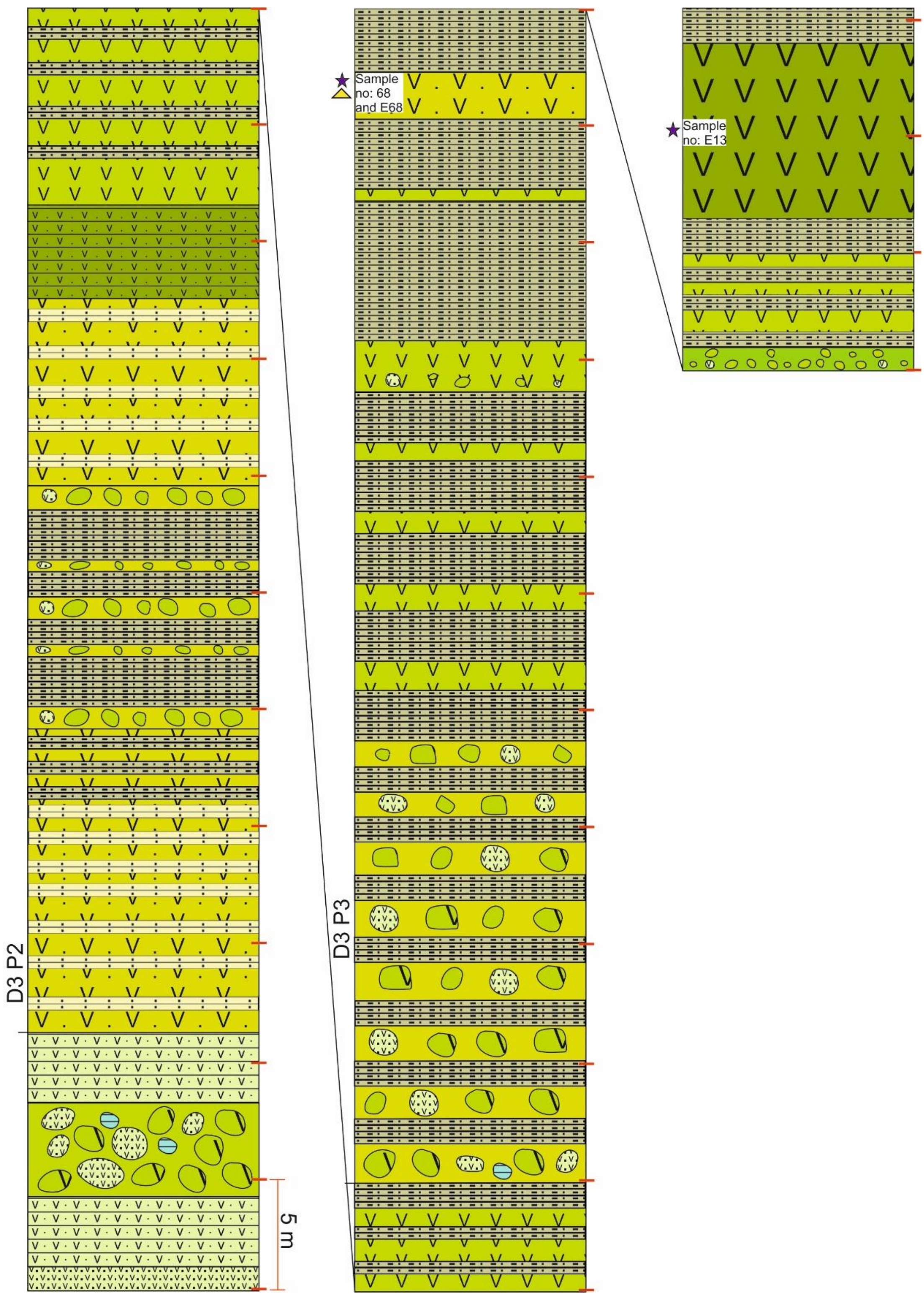

Figure 2.10 (continued) : The generalized section of three domains of the volcanic-volcaniclastic sequence from Limanköy to Beğendik.

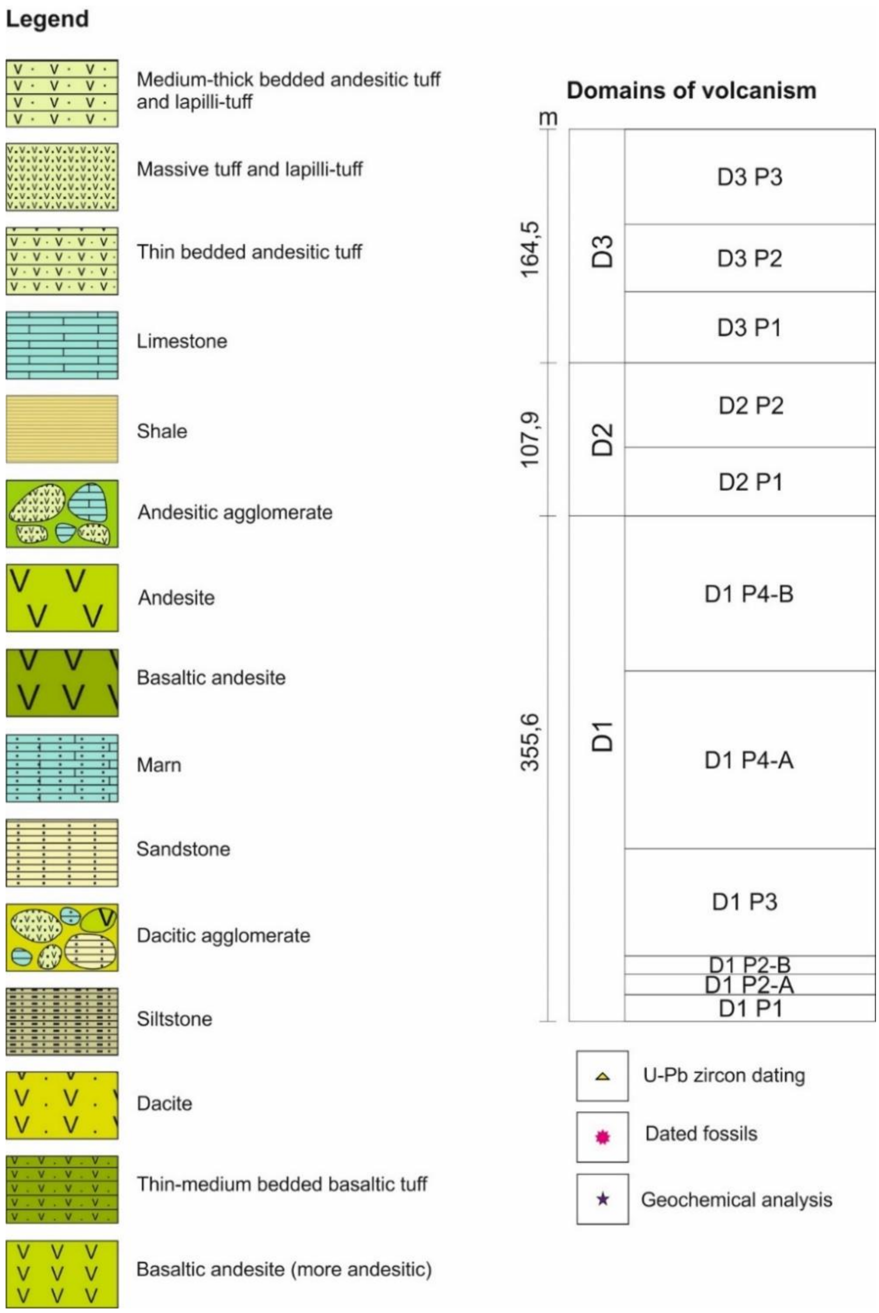

Figure 2.11 : The legend for the generalized volcanic-volcaniclastic sequence from Limanköy to Beğendik.

2.3.2.1 D1 Domain

The first volcanic-volcaniclastic domain, which constitutes the basement of the volcanic-volcanoclastic sequence, starts from Limanköy Beach (Location 9) and ends at the location 36 (Figure 2.2). The beginning of the volcanism can be observed with the volcaniclastic rocks which are deposited conformably on calcareous radiolarian siltstones. The total thickness of the D1 domain is about 350 m. The volcanism in the D1 domain can be examined under 4 parts.

The first part of the D1 domain (D1 P1)

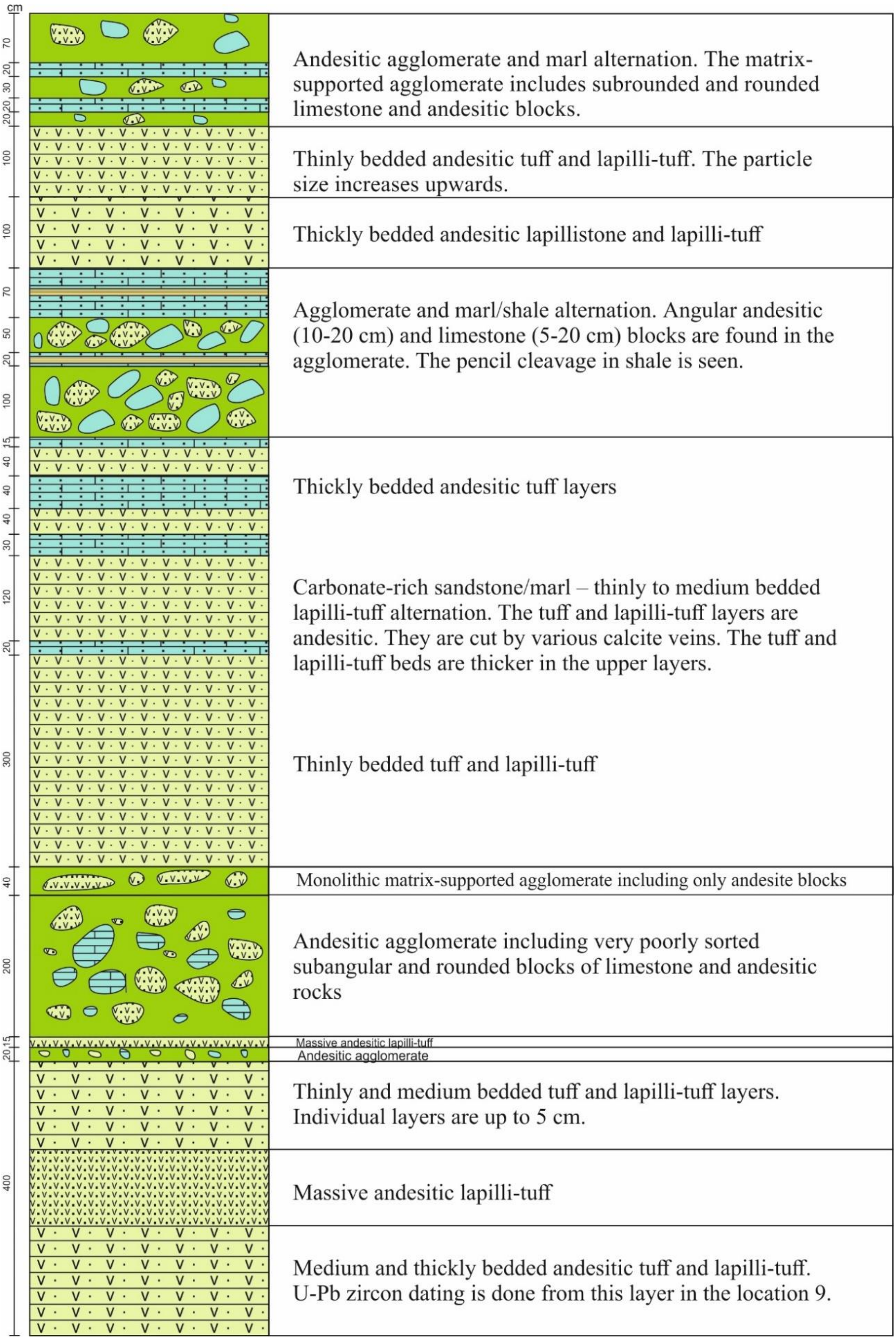

Figure 2.12 : The stratigraphic section of the first part of the D1 domain (D1 P1).

The first part of the D1 domain starts with andesitic tuff, lapilli-tuff layers and agglomerates. The tuff layers which are at the base of the domain are medium to thickly bedded with maximum 30 cm beds. As it is seen in the petrographic investigation for the sample from location 9 (Figure 2.13), the lithic tuff sample is moderately sorted and composed of 70 % lithic fragments. The crystals of quartz and plagioclase constitute 20 % of the sample. The rest of the sample is comprised of an intersertal groundmass, that is calcitized and chloritized due to alteration. The euhedral rectangular plagioclase crystals show simple and lamellar twinning. The quartz crystals show undulose extinction. The lithic fragments are mostly composed of andesitic rocks and the plagioclase phenocrysts are observable within some of the volcanic fragments. They show poorly-developed sieve texture due to resorption. There is no mafic mineral observed in the andesitic fragments. There is secondary calcite, which have perfect cleavage intersecting at 120^{o}, as a filling material on volcanic glass and as crystal. There are also some clay minerals, which have brown and brownish green color, formed due to the alteration of feldspars.

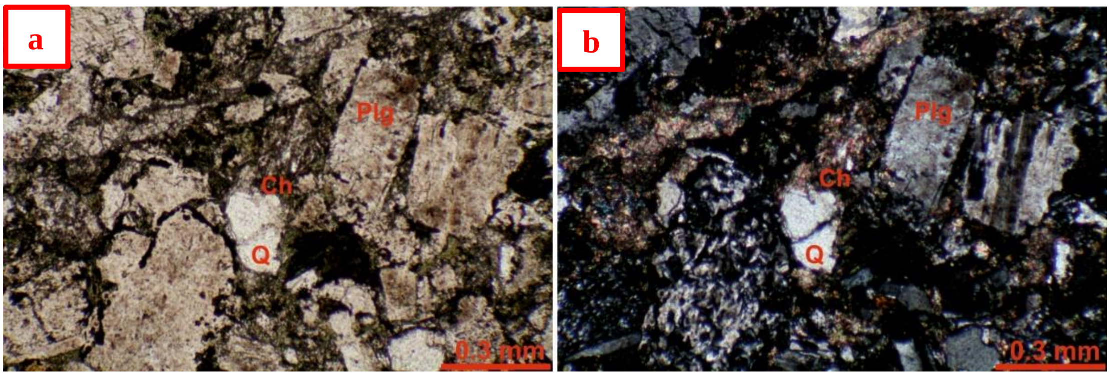

Figure 2.13 : Photomicrographs showing plagioclase (Plg), quartz (Q), calcitized and chloritized (Ch) intersertal groundmass in the andesitic lithic tuff sample from location 9. a) plane-polarized light b) cross-polarized light (Sample no: 9).

The relationship between the sedimentary rocks of İğneada Group and the volcanic-volcaniclastic rocks is well observed at the location 9. Since the volcaniclastic rocks conformably overlie the sedimentary sequence, this location is considered to be represented the beginning of the volcanism in İğneada. Therefore, U-Pb zircon dating is done for andesitic tuff sample which is taken from location 9. Its petrographic properties are explained above and shown in Figure 2.13. A total of 26 analyses were made on 20 zircon grains which are seen in the cathodoluminescence image (Figure 2.14a). Only two analyses from a single zircon grain (11th and 12th spot analyses in Figure 2.14a) gave a Campanian (80.6 ±1.5 Ma) age. The rest of the zircons gave Permian age and older zircon ages derived as xenocrysts from the Strandja Massif (Figure 2.14c).

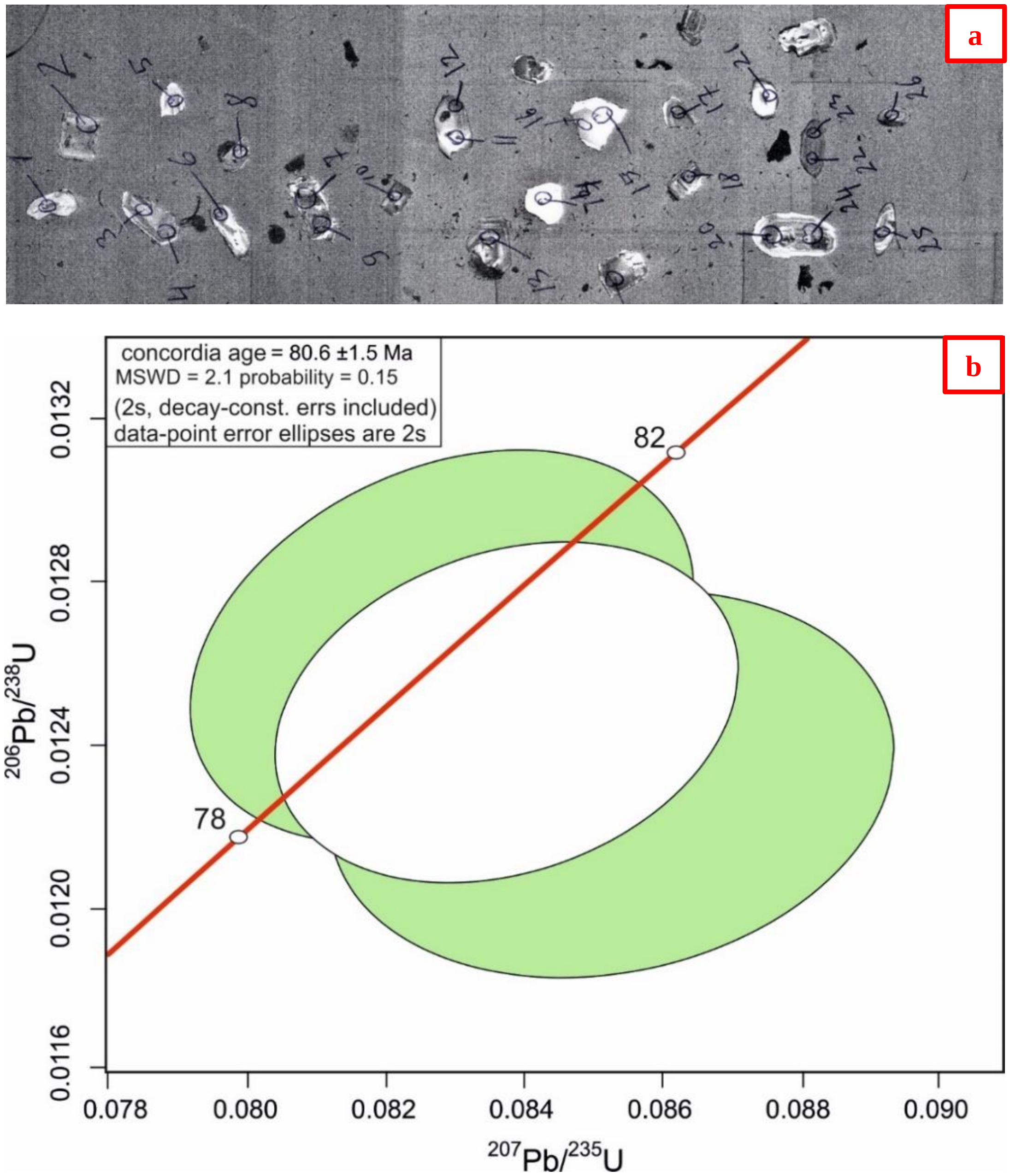

Figure 2.14 : a) Cathodoluminescence images of zircon crystals from the andesitic tuff taken from sample 9 in location 9 b) U-Pb concordia diagram for LA-ICP-MS zircon data from sample 9.

Table 2.1 : Zircon LA-ICP-MS data of sample 9.

			Isotopic ratios														
Spots	U (ppm)	Th (ppm)	$^{207}Pb/^{235}U$	2s	$^{206}Pb/^{238}U$	2s	rho	$^{238}U/^{206}Pb$	2s	$^{207}Pb/^{206}Pb$	2s	rho	$^{208}Pb/^{232}Th$	2s	Best Age (Ma)	2s	Concordance
1	217	151	0,551	0,019	0,07	0,00	0,79	14,28	0,45	0,057	0,001	0,24	0,022	0,001	436	13	0,98
2	226	173	0,302	0,015	0,04	0,00	0,32	25,16	0,77	0,055	0,003	0,17	0,013	0,000	250	8	0,94
3	301	152	0,349	0,011	0,05	0,00	0,46	20,79	0,64	0,052	0,001	0,61	0,015	0,000	303	9	1,00
4	448	212	0,349	0,011	0,05	0,00	0,52	20,68	0,63	0,052	0,001	0,27	0,015	0,000	305	9	1,00
5	306	45	0,567	0,017	0,07	0,00	0,46	13,78	0,42	0,057	0,001	0,34	0,023	0,001	451	13	0,99
6	125	4	0,446	0,020	0,06	0,00	0,94	16,72	0,65	0,054	0,001	0,36	0,030	0,008	374	14	1,00
7	288	272	0,286	0,009	0,04	0,00	0,66	24,88	0,77	0,052	0,001	0,43	0,012	0,000	254	8	0,99
8	412	313	0,750	0,162	0,05	0,00	0,99	19,19	0,80	0,102	0,017	0,21	0,026	0,004	307	15	0,58
9	429	330	0,288	0,010	0,04	0,00	0,84	24,57	0,77	0,051	0,001	0,39	0,013	0,000	257	8	1,00
10	321	253	0,304	0,013	0,04	0,00	-0,40	25,50	0,78	0,055	0,002	0,52	0,012	0,000	247	7	0,92
11	115	115	0,085	0,003	0,01	0,00	0,18	81,30	2,56	0,050	0,002	0,26	0,004	0,000	79	2	0,95
12	340	302	0,083	0,003	0,01	0,00	0,31	79,11	2,47	0,047	0,001	0,43	0,004	0,000	81	3	1,00
13	293	265	0,275	0,009	0,04	0,00	0,80	25,44	0,79	0,051	0,001	0,41	0,012	0,000	249	8	1,01
14	36	22	0,834	0,028	0,10	0,00	0,41	10,30	0,33	0,062	0,002	0,34	0,029	0,001	596	19	0,97
15	58	52	0,886	0,036	0,10	0,00	0,92	9,62	0,34	0,062	0,001	0,48	0,030	0,001	637	22	0,99
16	78	86	0,918	0,030	0,11	0,00	0,51	9,37	0,30	0,062	0,001	0,55	0,031	0,001	653	20	0,99
17	411	65	0,560	0,017	0,07	0,00	0,52	14,00	0,43	0,057	0,001	0,38	0,021	0,001	444	13	0,99
18	279	274	0,293	0,010	0,04	0,00	0,84	25,43	0,78	0,054	0,001	0,37	0,011	0,000	248	8	0,95
19	244	225	0,283	0,009	0,04	0,00	0,69	25,34	0,79	0,052	0,001	0,39	0,012	0,000	249	8	0,99
20	482	103	0,537	0,017	0,07	0,00	0,56	14,49	0,44	0,056	0,001	0,44	0,020	0,000	430	13	0,99
21	20	25	0,889	0,032	0,10	0,00	0,55	9,73	0,34	0,062	0,002	0,23	0,030	0,001	630	21	0,98
22	308	306	0,743	0,024	0,09	0,00	0,77	10,97	0,34	0,059	0,001	0,43	0,026	0,001	562	17	1,00
23	352	80	0,597	0,018	0,08	0,00	0,21	13,30	0,41	0,058	0,001	0,36	0,023	0,001	467	14	0,98
24	393	80	0,562	0,018	0,07	0,00	0,78	13,90	0,43	0,056	0,001	0,42	0,022	0,001	447	13	0,99
25	155	173	10,647	0,329	0,45	0,01	0,96	2,24	0,07	0,173	0,003	0,43	0,113	0,003	2302	80	0,95
26	238	400	10,050	0,618	0,17	0,01	0,99	5,86	0,23	0,425	0,015	0,34	0,131	0,007	553	43	0,42

The thickness of beds decreases to 10 cm while going upwards. The lapilli-tuff beds which have thickness up to 2 m are seen between medium-thickly bedded and thinly-medium bedded tuff layers (Figure 2.15). Then, the thinly bedded tuffs are overlain by agglomerates which include blocks of andesitic rocks and pelagic limestone up to 40 cm (Figure 2.16). The outcrops have greenish color due to the andesitic composition of the matrix. The blocks are very poorly sorted and have various angularity.

Figure 2.15 : Field photo of the tuff and lapilli-tuff layers from location 9, which is at the beginning of the first domain of the volcanic-volcaniclastic sequence.

Figure 2.16 : Field photo of the poorly sorted andesitic and limestone blocks in the agglomerate from location 10.

Carbonate-rich sandstone, marl and shale layers with pencil cleavage are observed within the first part. They alternate with tuff layers and agglomerates and there are oxidized levels up to 1 cm between them. They have brownish grey color due to seawater alteration and thicknesses between 15 and 70 cm (Figure 2.17).

Figure 2.17 : Field photo showing the alternation of volcanogenic carbonate-rich sandstone and tuff layers.

In the upper level of the first part, the clasts in the andesitic tuff layers grow larger and this unit can be called as lapillistone. The andesitic and pelagic limestone blocks in agglomerates become rounded and they start to get sparse compared to the agglomerate at the bottom of this part.

The second part of the D1 domain (D1 P2)

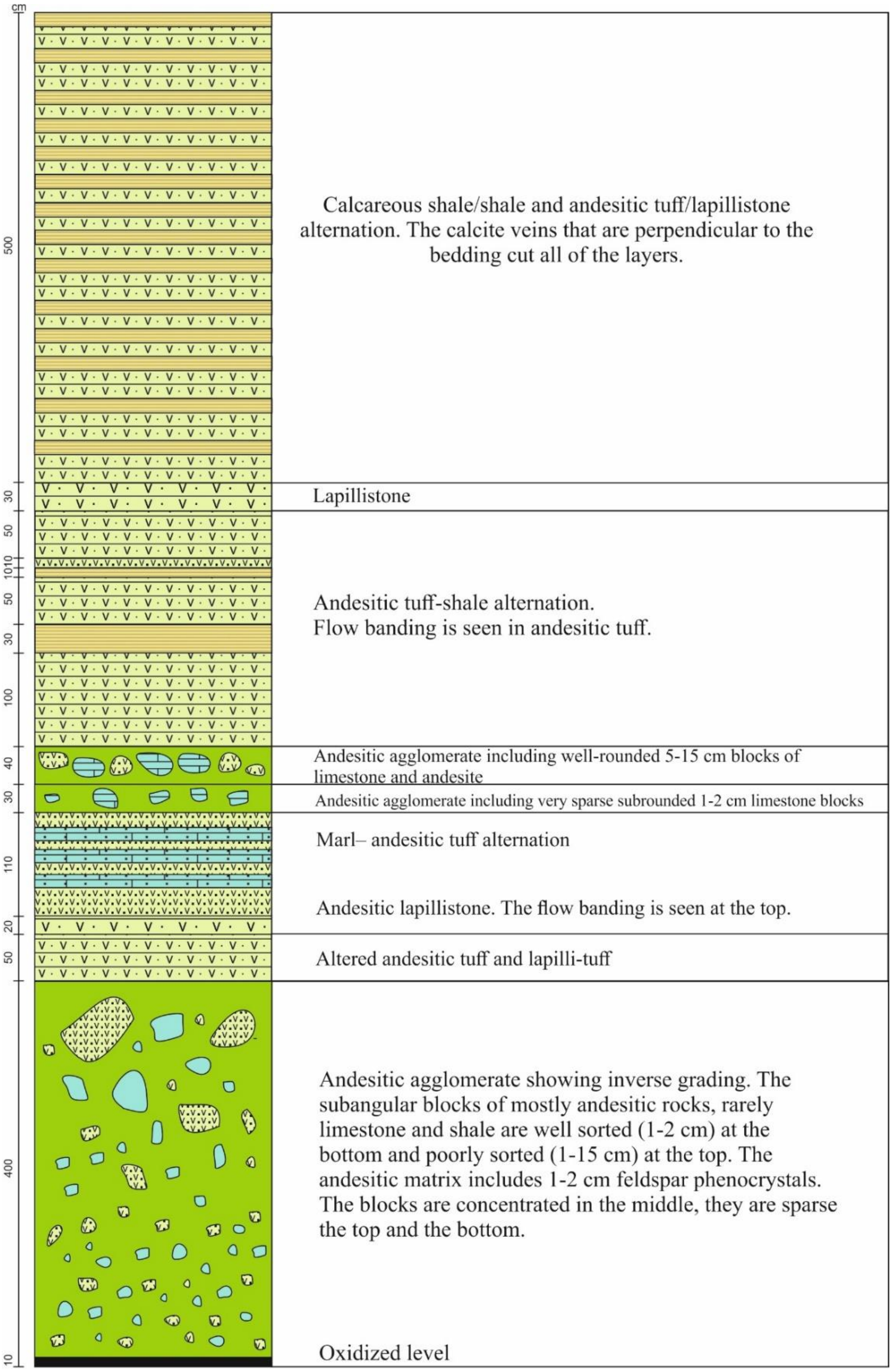

Figure 2.18 : The stratigraphic section of the second part of the D1 domain (D1 P2-A).

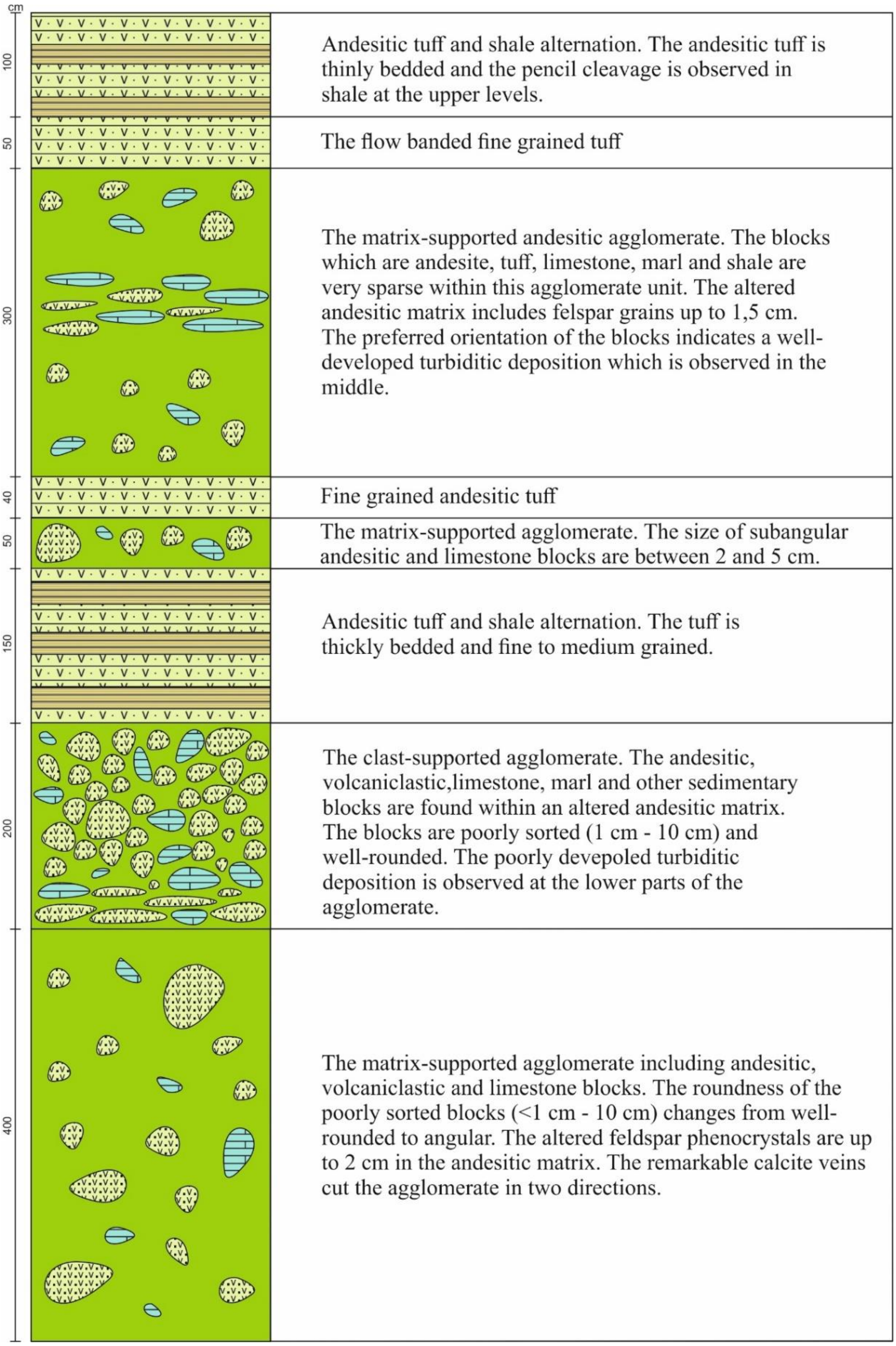

Figure 2.19 : The continuation of the stratigraphic section of the second part of the D1 domain (D1 P2-B).

The second part of the D1 domain starts with nearly 10 cm oxidized layer and continues with 4 m of andesitic agglomerate. The blocks in agglomerate are sparse within the second part of the D1 domain and mostly composed of andesitic rocks with big phenocrysts and rarely limestone and shale. They are well sorted at the base, but poorly sorted at the top (Figure 2.20a). Their size ranges from 1 cm to 15 cm. This part continues with the very altered, light green massive andesitic tuff and lapilli-tuff (Figure 2.20b). It is followed by marl-andesitic tuff alternation and andesitic agglomerate. The middle parts are mainly represented by the alternation of shale/calcareous shale and andesitic tuff/lapillistone layers (Figure 2.21). The alternation continues for approximately 7 m. The tuff and lapilli-tuff layers also alternate in themselves from very fine grained to coarser grained tuff layers.

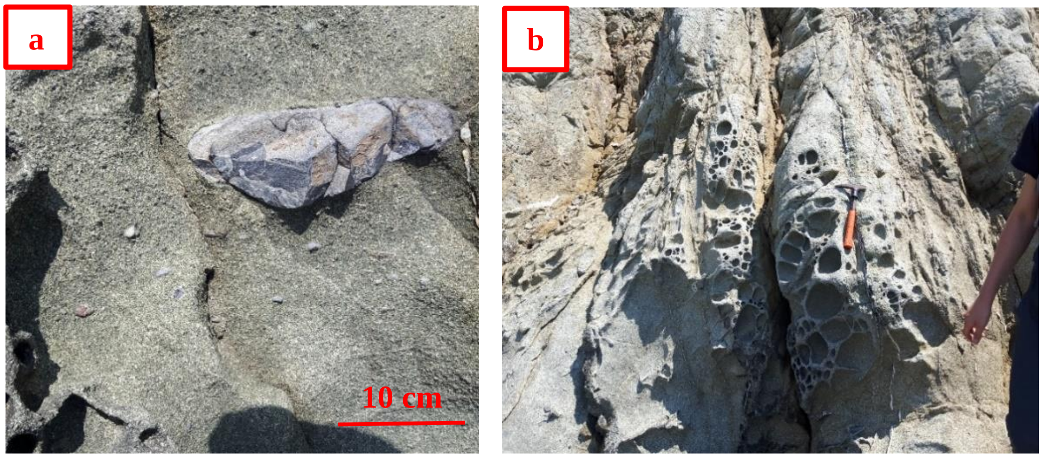

Figure 2.20 : Field photos showing the andesitic volcaniclastic rocks. a) The very poorly sorted subrounded blocks in the andesitic agglomerate b) Altered andesitic tuff.

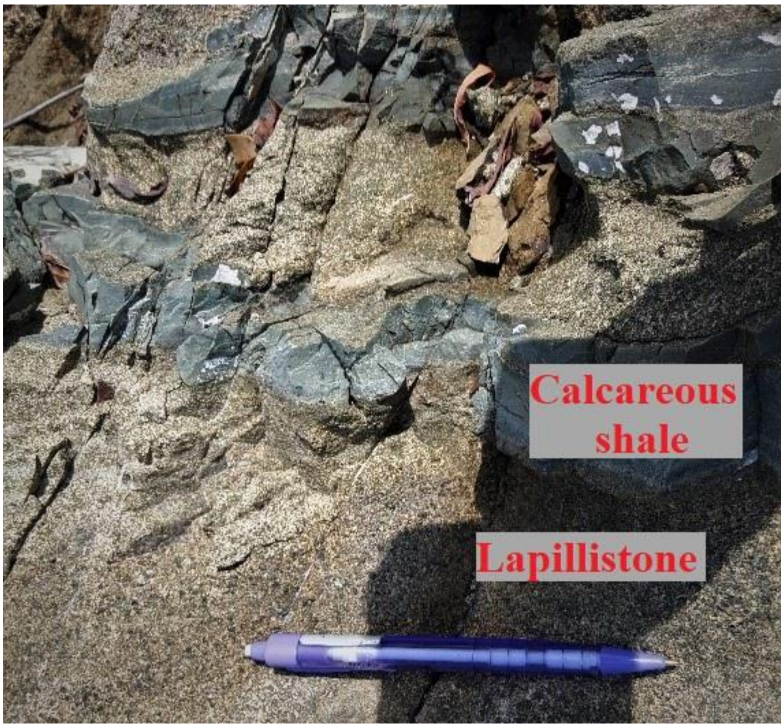

Figure 2.21 : The outcrop photo of the alternation of the calcareous shale and massive lapillistone from location 28.

Above this alternation, the second part continues with the agglomerate units which have a total thickness of 10 m. As distinct from the previously mentioned agglomerates, the agglomerate starts to exhibit turbiditic characteristics here (Figure 2.19). The preferred orientation of poorly sorted blocks indicates deep marine turbiditic deposition. Firstly, the agglomerate is matrix-supported. Then, it becomes clast-supported in the middle and, again matrix-supported at the top. The blocks are mostly composed of andesite, tuff and limestone and they are mostly poorly sorted. There are andesitic tuff and shale alternations between agglomerate levels and the fine grained tuff layers show banded texture.

The third part of the D1 domain (D1 P3)

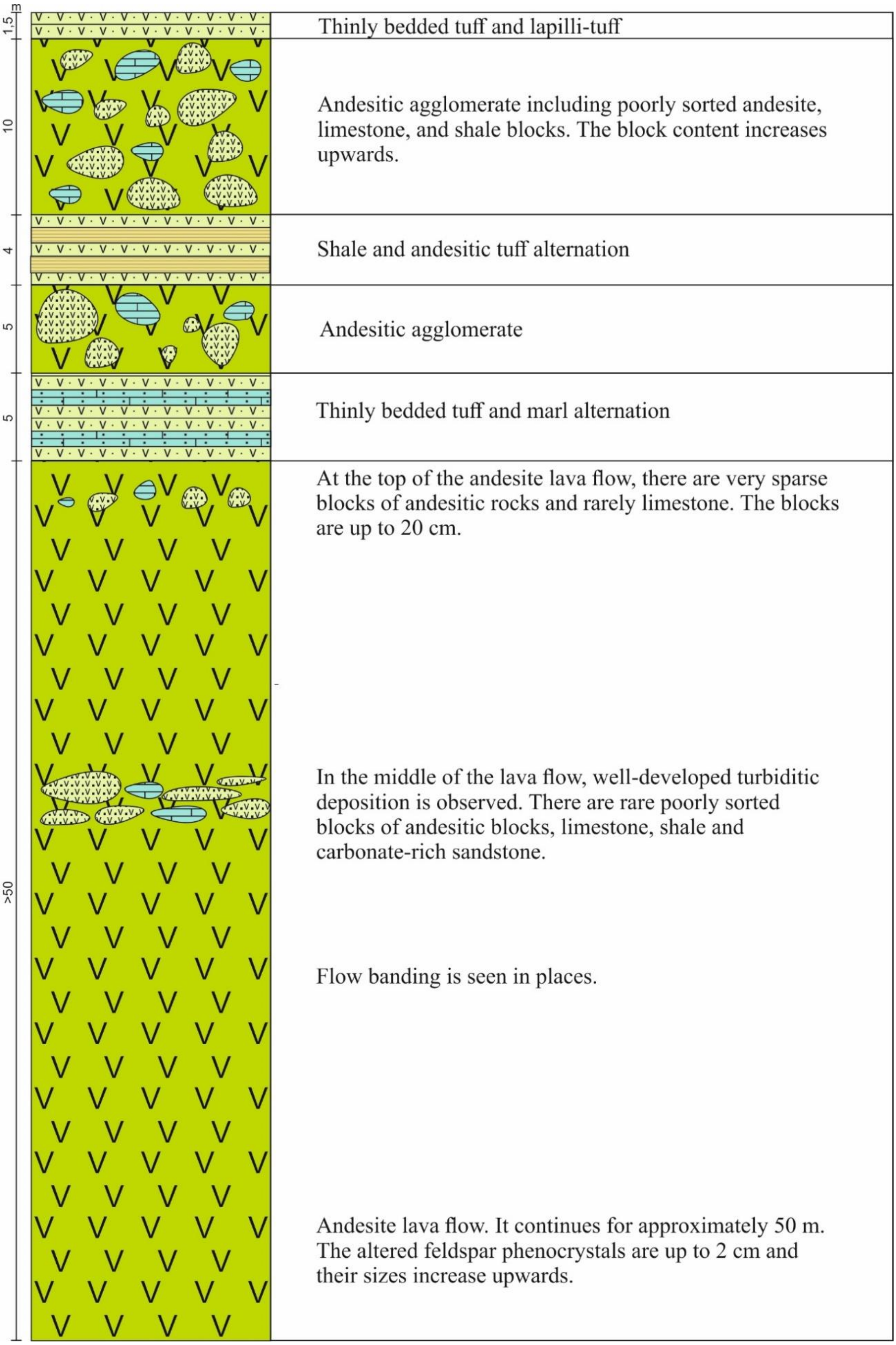

Figure 2.22 : The stratigraphic section of the third part of the D1 domain (D1 P3).

The third part of the D1 domain is characterized by massive andesite and basaltic andesite which are formed by lava flow continuing for at least 50 m (Figure 2.22). Therefore, the orientation of the bedding is not clear within D1 P3 domain. In some places, there are at most 30 cm thick greenish fine grained tuff beds between andesitic lava flow layers. The rocks at the bottom of this part are andesite with big feldspar phenocrysts (Figure 2.23b).

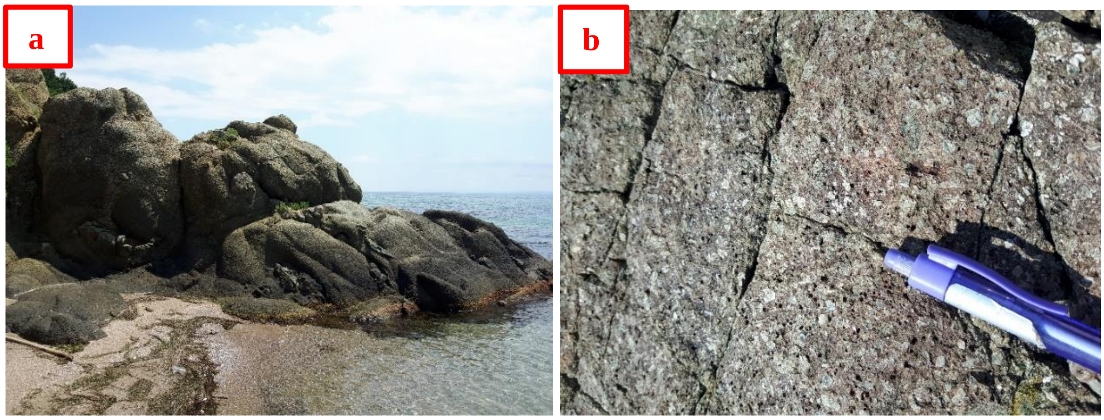

Figure 2.23 : The outcrop views of andesite from location 22 a) The dark color at the bottom of the andesite is a result of the seawater alteration. b) The feldspar phenocrysts in light green andesite.

The thin section of the coarse grained andesite from location 22 is seen in Figure 2.24. The feldspar phenocrysts and microlitic chloritized groundmass are present. There is no mafic mineral observed. The lamellar and deformational twinnings are observed in plagioclase. The oscillatory zoning in the feldspars indicate changes in the magma chemistry. The poorly-developed sieve texture is observed in some feldspars. It indicates that they have undergone the resorption due to temperature decrease during the magmatic crystallization or assimilation (Shaw, 2006). The calcite is seen as alteration on the other crystals or as filling material in the vesicles.

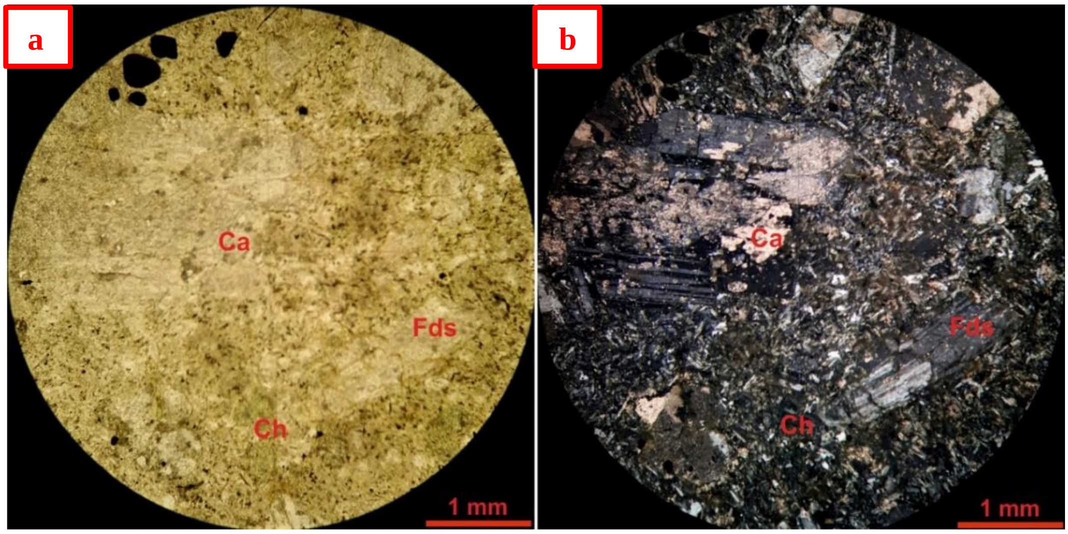

Figure 2.24 : Photomicrographs of the andesite from location 22 in which the feldspar (Fds), chloritized (Ch) groundmass and calcite (Ca) are observed. a) plane-polarized light b) cross-polarized light (Sample no: 22).

There are some levels that indicate well-developed turbiditic deposition between the andesitic lava flow. They have sparse blocks, which have size between 0.5 cm and 20 cm. The blocks are composed of mostly greenish andesitic rocks and rarely limestone, shales and carbonate-rich sandstone (Figure 2.25).

Figure 2.25 : Field photo of the turbiditic deposition indicated by preferably oriented blocks of limestone, shale and andesite from location 16.

The fourth part of the D1 domain (D1 P4)

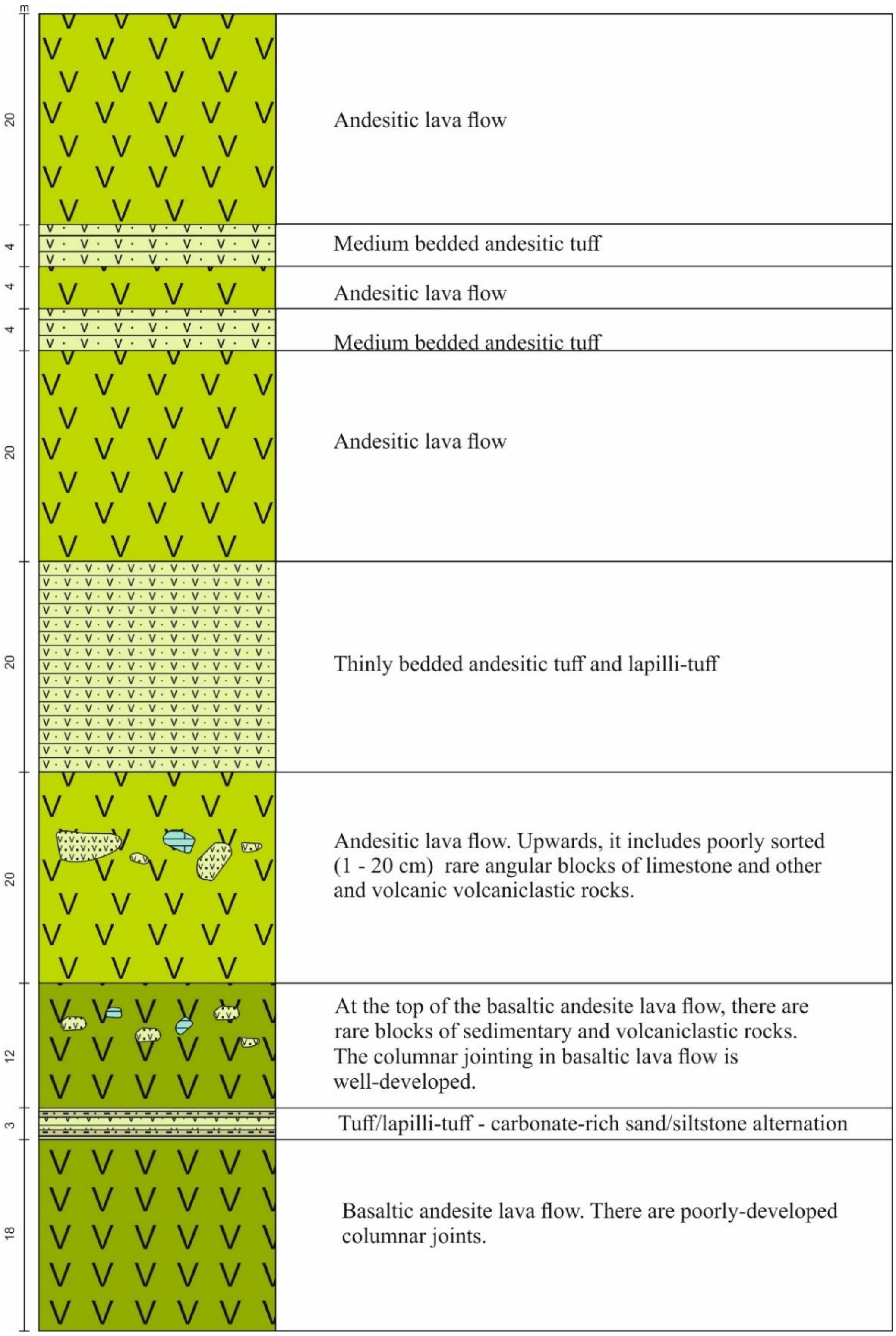

Figure 2.26 : The stratigraphic section of the fourth part of the D1 domain (D1 P4-A).

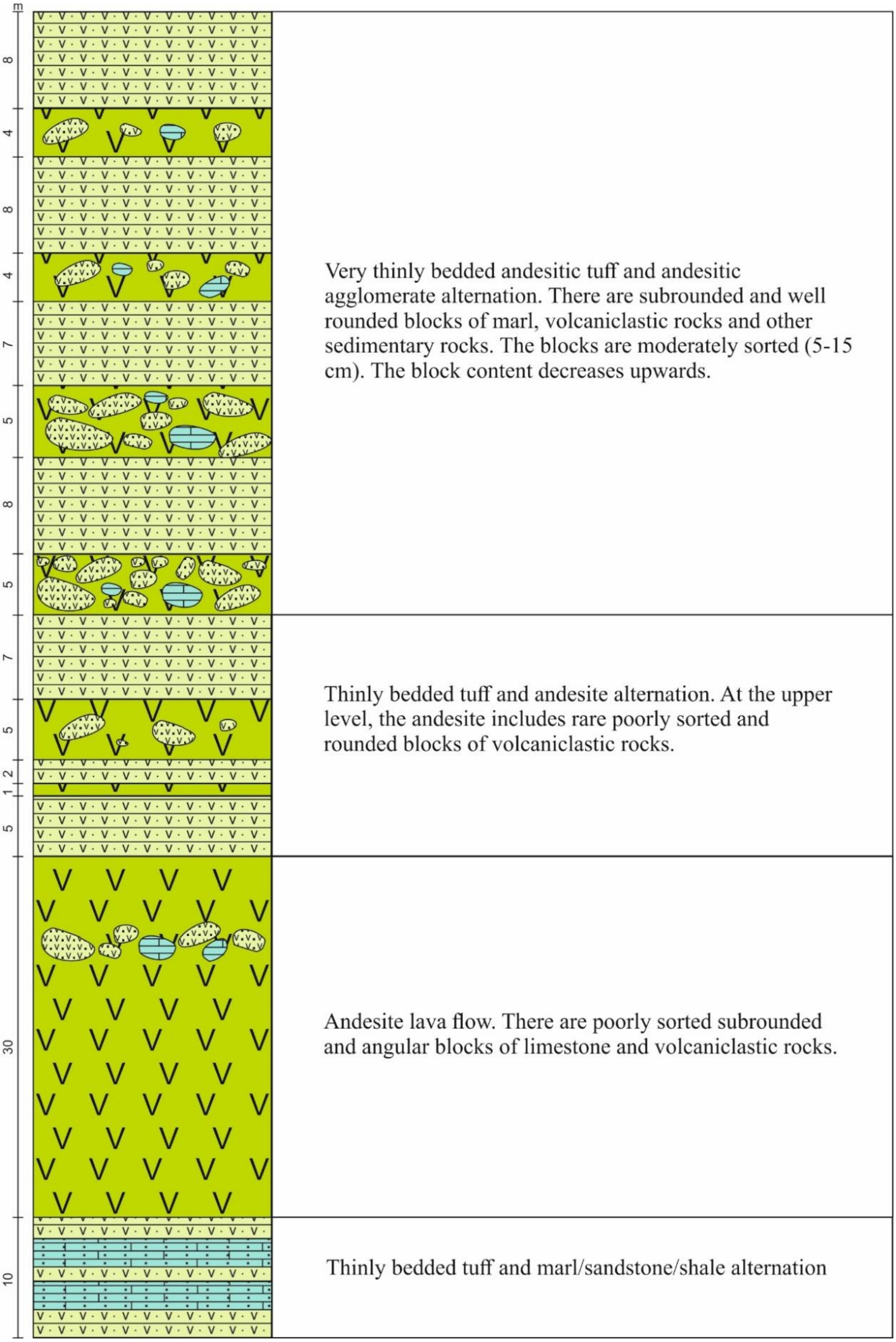

Figure 2.27 : The continuation of the stratigraphic section of the fourth part of the D1 domain (D1 P4-B).

The fourth part of the D1 domain comprises of rocks which have more basaltic composition. The basaltic andesitic lava flow continues for approximately 30 m. The columnar jointed basalts are observed for at least 6 m (Figure 2.28). Although the columnar joints are well-developed in some places, they are poorly-developed in most of the outcrops. The color of the altered outcrops is black or brownish black due to seawater. There are no observable blocks in basaltic andesitic rocks in lower levels. After approximately 18 m, the thinly and medium bedded tuff and lapilli-tuff layers start to alternate with carbonate-rich sand and siltstone. This alternation is followed by basaltic andesite in which well-developed columnar jointed basalts are seen. Then, the andesitic lava flow is started to be seen and thinly bedded andesitic tuff layers, which continue for 20 m, are found above this lava flow.

Figure 2.28 : Field examples of the columnar jointed basaltic andesite from location 33 a) The columnar joints are well-developed here and it is possible to see the internal angles are 120° from this outcrop. b) The poorly-developed columnar jointed basaltic andesite.

It is followed by andesitic lava flow and medium bedded andesitic tuff alternation for approximately 60 m. Above this, the alternation of thinly bedded tuff and marl/sandstone/shale is observed for 10 m. They are followed by andesite lava flow for 30 m. After 30 m, andesite starts to alternate with thinly bedded tuff. Above them, the alternation of very thinly bedded andesitic tuff and andesitic agglomerate is seen (Figure 2.29a). The blocks in agglomerate are marl, volcaniclastic rocks and other sedimentary rocks which are subrounded and well-rounded. The blocks are moderately sorted (5 - 15 cm) and their number decrease upwards. At the end of the fourth part of the first domain, the sequence cannot be followed due to the change in the bedding plane orientation. The steeply dipping beds of tuff and agglomerate layers continue to be observed along the shore (Figure 2.29b).

Figure 2.29 : The outcrop photos of tuff layers and agglomerate from location 36 a) The thinly bedded light green andesitic tuff layers b) The beddings of tuff become almost steep. The red arrow shows the younging direction.

2.3.2.2 D2 Domain

The second volcanic-volcaniclastic domain, that can be followed from older to younger, is located in the east of the study area, between Limanköy and Beğendik villages. The volcanic rocks have more basaltic composition within this domain. The thickness of the D2 domain is about 110 m. The D2 domain has 2 parts based on the rock type.

The first part of the D2 Domain (D2 P1)

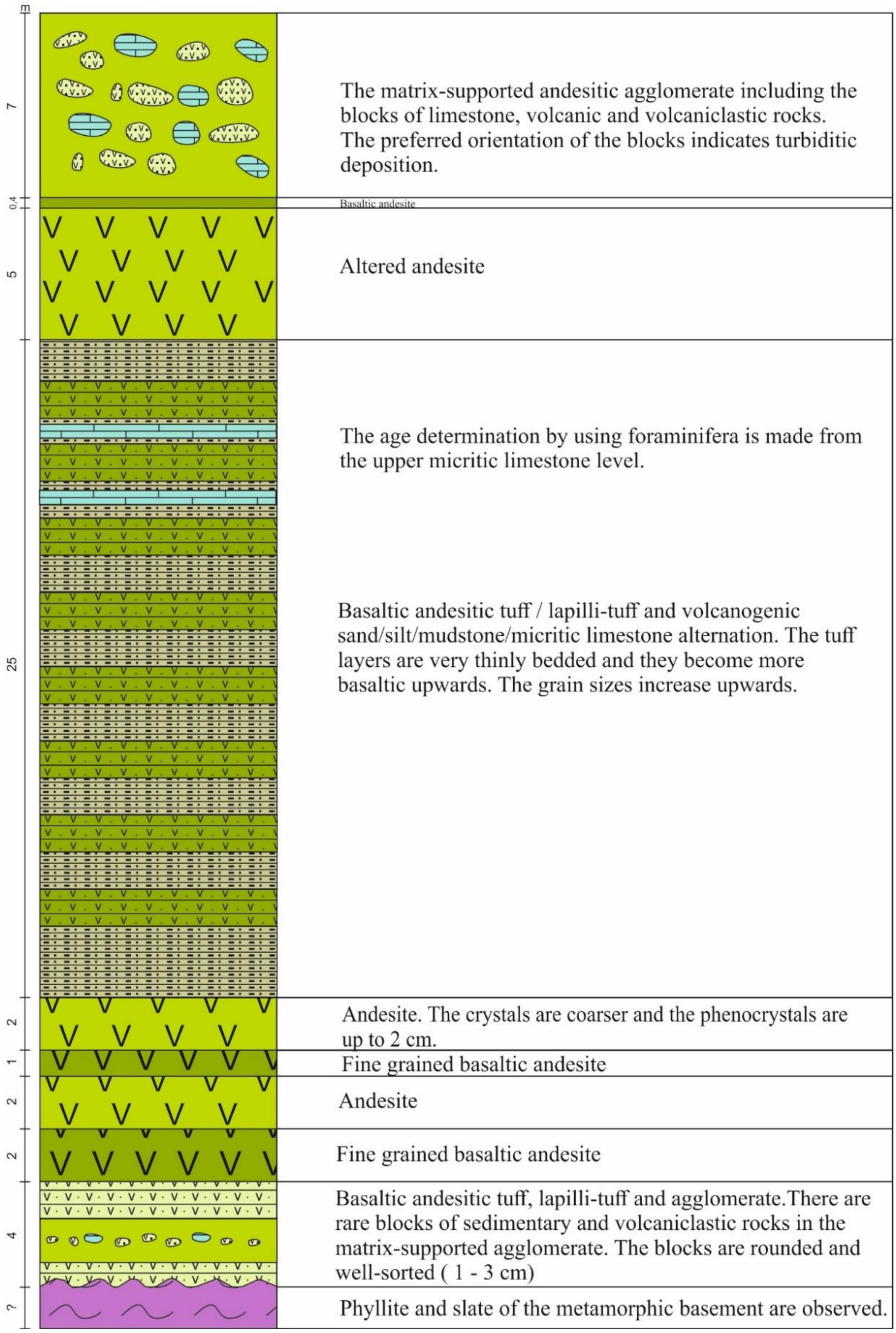

Figure 2.30 : The stratigraphic section of the first part of the D2 domain (D2 P1).

In the beginning of the first part, there are very altered slate and phyllite which means that the metamorphic basement is observed here again. Then, the basaltic andesitic tuff, lapilli-tuff and matrix-supported agglomerate with 1 – 3 cm, mostly rounded andesitic blocks are found above this basement, possibly indicating the beginning of the volcanism. The contact between them is partly covered. It may be tectonic since several step faults are observed in the outcrops near the contact. Thin beds of tuff and lapilli-tuff are followed by basaltic andesitic and andesitic lava flows for 7 m (Figure 2.31). The basaltic andesite (Figure 2.32) is fine grained at the bottom and the sizes of both felsic and mafic phenocrysts increases upwards. The thin section views of the fine grained basaltic andesite are seen in Figure 2.33. The abundant plagioclase crystals and the other chloritized crystals are observed. The fine grained microlitic groundmass is almost completely composed of plagioclase crystals. The plagioclase crystals show patchy and oscillatory zoning and, simple and albite twinnings. Some of the plagioclase phenocrysts show glomeroporphyritic texture and the cluster of the phenocrysts all show primary oscillatory zoning. The oscillatory zoning indicate that the chemistry of the magma has changed during the crystallization or the crystal growth within convection currents in the magma chamber. The acicular plagioclase microlites show simple twinning. The calcite probably replaced some of the feldspar crystals. The abundant green chlorite minerals are found as a result of the sea floor alteration.

Figure 2.31 : Field photo from location 90 showing the thinly layering of greenish brown andesitic tuff and lapilli-tuff layers in the SW and the grey/dark grey fine grained andesite/basaltic andesite lava flow in the NE. The red line separates these two units.

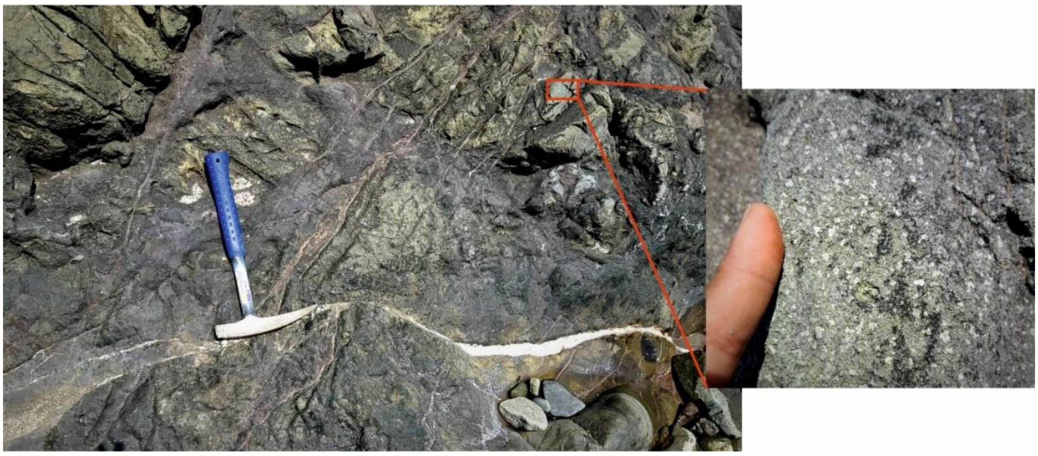

Figure 2.32 : Field photo and close up view of the dark greenish grey basaltic andesite from location 38.

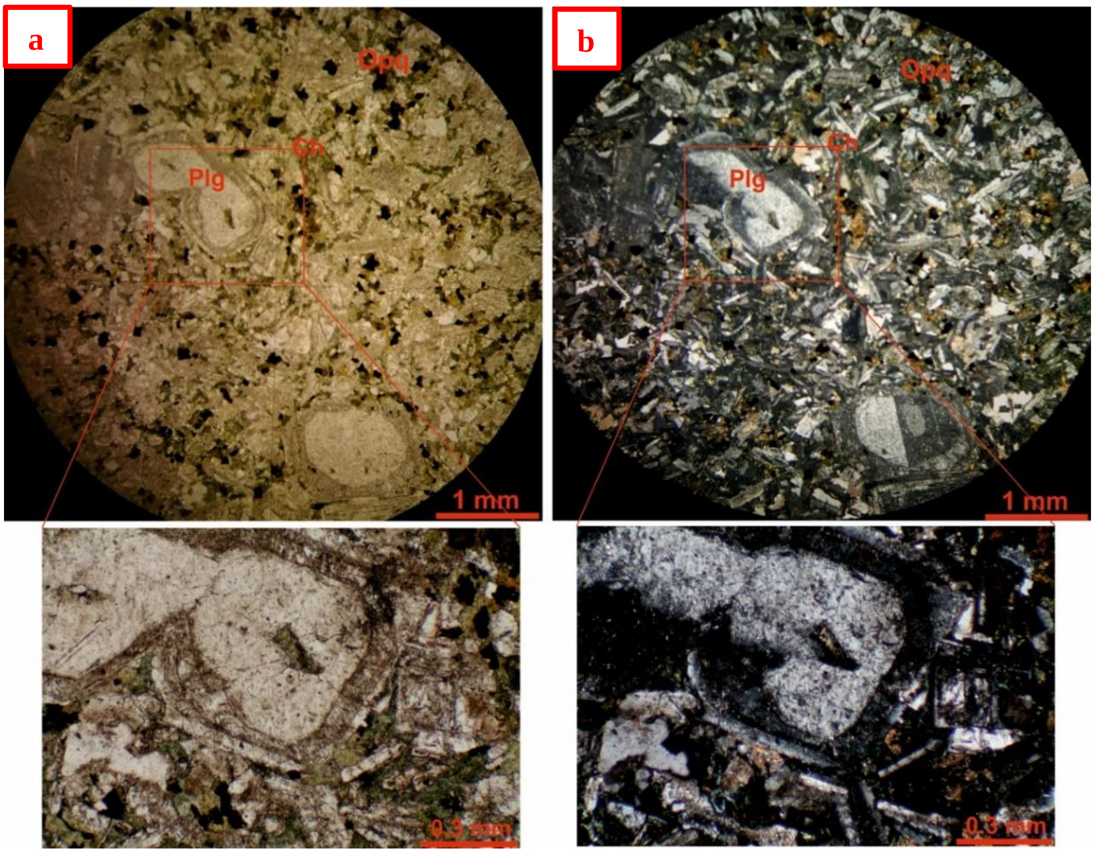

Figure 2.33 : Photomicrographs of the fine grained basaltic andesite from location 38. The abundant plagioclase (Plg) crystals, chlorite (Ch), the other chloritized crystals and the opaque minerals (Opq) are seen. The close up views show the glomeroporphyritic texture of the plagioclase phenocrystals. a) plane-polarized light b) cross-polarized light (Sample no: 38b).

Above them, the alternation of basaltic andesitic tuff/lapilli-tuff and volcanogenic sand/silt/mudstone-micritic limestone (Figure 2.34) begins and continues for 25 m. The grain size in both of these units increases upwards. The thinly bedded tuff layers become more basaltic upwards. The thin section of the biomicritic limestone from location 75 (Figures 2.1, 2.35) shows that it contains abundant radiolaria and Turonian foraminifera, which are *Marginotruncana pseudolinneana*, *Marginotruncana marginata*, Whitenella sp., *Whitenella praehelvetica*, *Muricohedbergella* sp., and ?*Helvetoglobotruncana* cf. *Helvetica*, as identified by Prof. Dr. Demir Altıner.

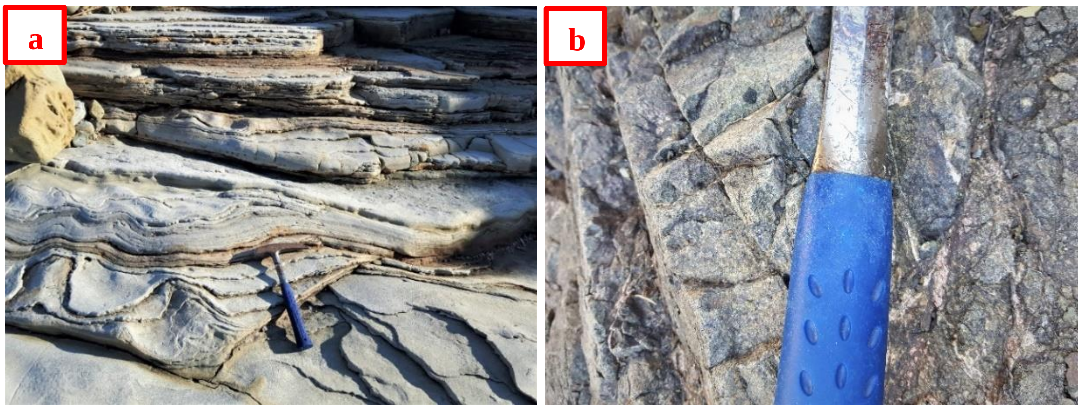

Figure 2.34 : Field photos from location 75 a) Exfoliation of volcanogenic laminated silt/mudstone within tuff and sand/silt/mudstone alternation b) The close up view of the biomicrite level including the Turonian aged planktonic foraminifera.

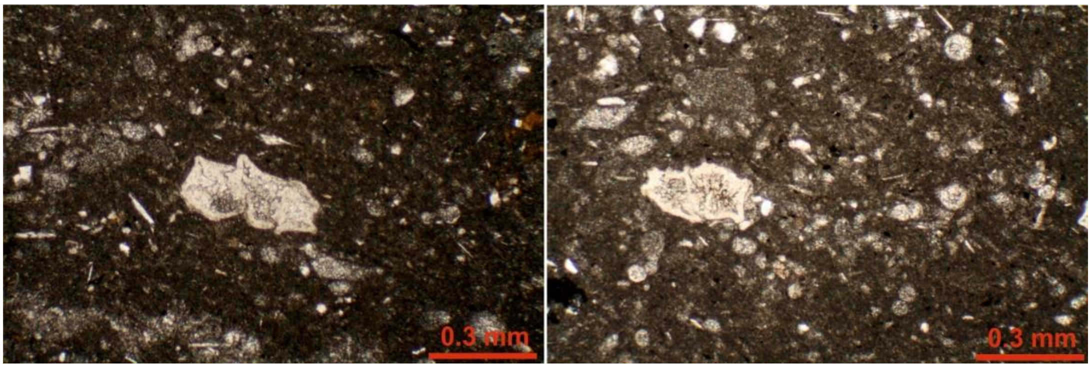

Figure 2.35 : Photomicrographs showing the biomicrite from location 75 including radiolaria, which are rounded, and the fragments of Turonian planktonic foraminifera *Marginotruncana pseudolinneana* and *Marginotruncana marginata* (Sample no: 75).

Then, the sequence is followed by 5 m thick altered andesite. The feldspar phenocrystals in andesite are up to 1 cm. They look like white round spots since they have lost their euhedral rectangular shapes due to alteration. It is followed by 40 cm thick basaltic andesite level. The matrix-supported agglomerate with an andesitic matrix is found above the basaltic andesite. The agglomerate continues for at least 7 m. It has very sparse blocks which are andesite, basaltic andesite, limestone and volcaniclastic rocks. The blocks in the agglomerate are accumulated densely in some places and they are preferably oriented remarking the turbiditic deposition. The D2 domain is interrupted by a long beach and therefore, the first part of D2 domain ends here.

Although it is not included in this part or any parts of the other domains, there is biomicrite level which is found in the location 100 (App-A), which can be correlated with the biomicrite level in the location 75. It can be accepted that the biomicrite level belongs to the volcanic-volcaniclastic sequence, since it is found between the andesitic tuff and agglomerate. The thin section of the biomicrite from location 100 is seen in Figure 2.36. The planktonic foraminifera *Marginotruncana pseudolinneana, Marginotruncana coronate* and *Muricohedbergella flanderini* are identified in the thin section and their age range is defined between uppermost Turonian and Santonian by Prof. Dr. Demir Altıner. There are also radiolaria in the sample.

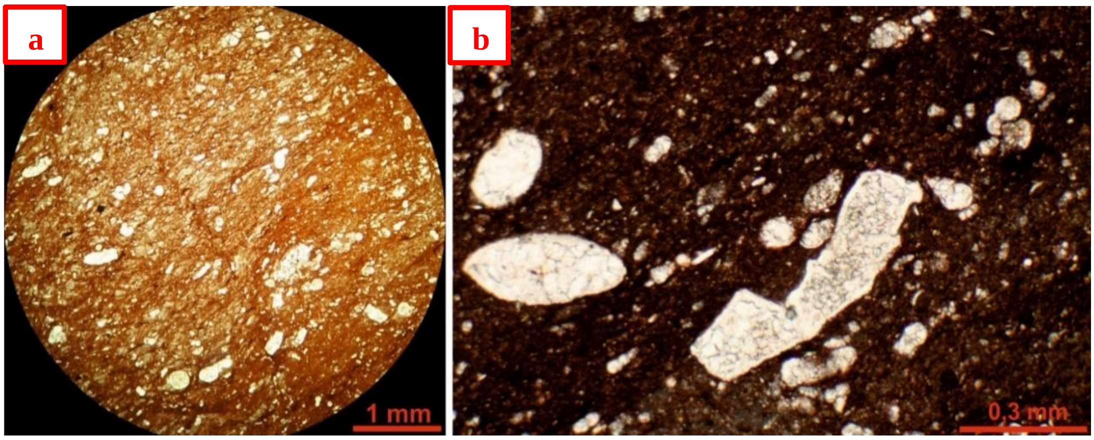

Figure 2.36 : Photomicrographs showing the biomicrite from location 100. a) The general view of the biomicrite including uppermost Turonian and Santonian aged planktonic foraminifera fragments b) *Marginotruncana coronate* are seen on the right. The rounded radiolaria are also observed. (Sample no: 100).

The second part of the D2 Domain (D2 P2)

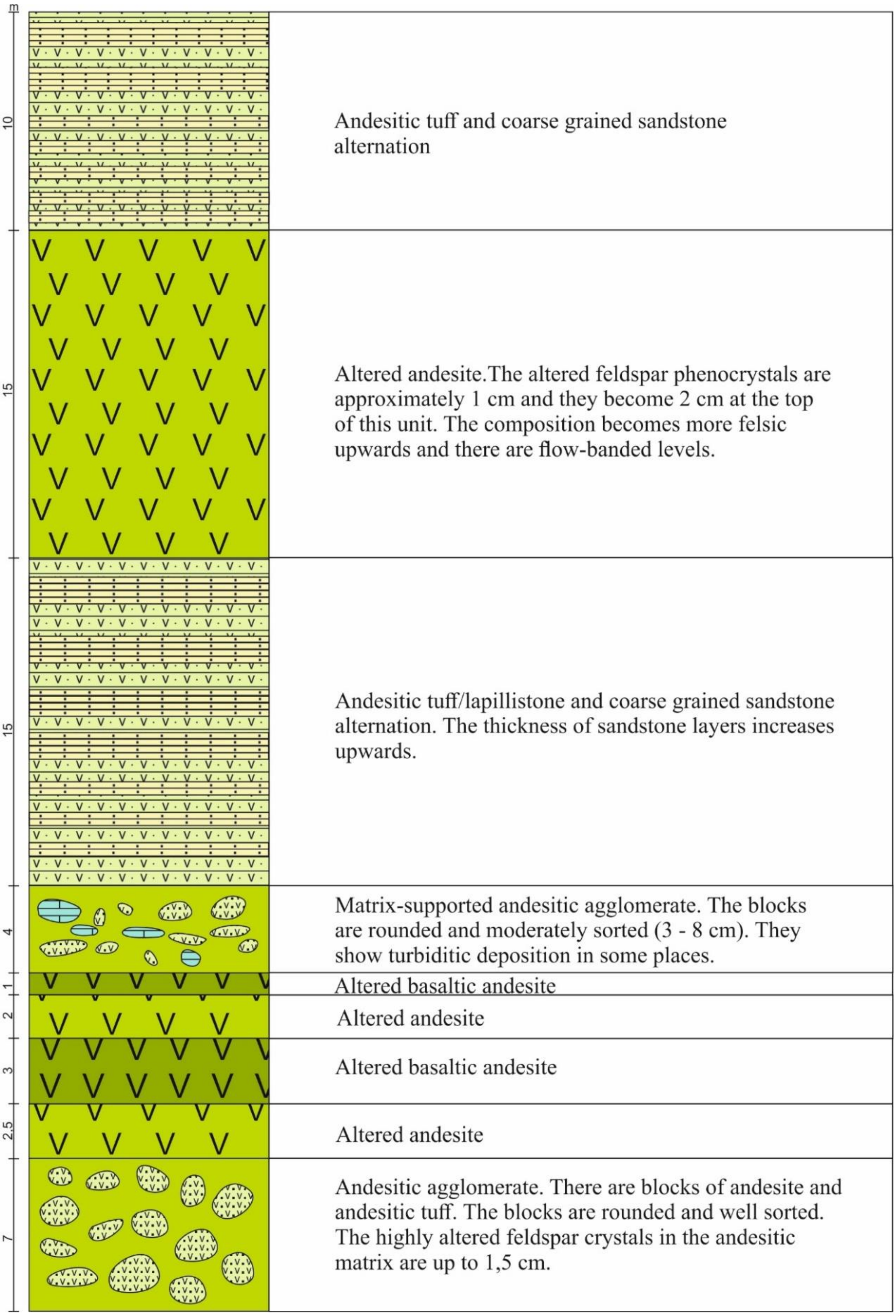

Figure 2.37 : The stratigraphic section of the second part of the D2 domain (D2 P2).

The second part of the D2 domain is mainly represented by the massive andesitic rocks and the alternation of sandstone and tuff/lapillistone. The composition of the volcanic and volcaniclastic rocks varies within this part of the domain. It starts with andesitic agglomerate which includes only the blocks of andesitic rocks and tuff. Then, the light greenish grey massive andesitic rocks (Figure 2.38a), which have more felsic composition compared to the andesitic matrix of the agglomerate below, are observed. The alteration of feldspar phenocrysts is seen again and the sizes of feldspars get bigger up to 2 cm. The altered and exfoliated basaltic andesitic rocks are found above the altered andesite. They are followed by the andesitic agglomerate (Figure 2.38b) which includes sparse blocks of green andesite and dark grey shale blocks. But, the blocks in the agglomerate become denser and they are preferentially oriented in some places indicating the turbiditic deposition. Then, the andesitic tuff/lapillistone and the coarse grained sandstone alternation is observed and, it continues for 15 m. At the beginning of this alternation, the composition of the andesitic tuff and lapillistone layers is more felsic (Figure 2.38c). The sizes of the feldspar phenocrysts are up to 1 cm. The thin section from the andesitic tuff layer at the beginning of the alternation is seen in Figure 2.39. It includes plagioclase crystals showing oscillatory zoning, lithic grains, prehnite with anomalous interference colors, chloritized volcanic glass and some accessory minerals. The prehnite and chlorite formation indicates the sea floor alteration.

This alternation is continued by altered green andesite for 15 m (Figure 2.40). The composition of andesite becomes more felsic as it continues upwards and the phenocrysts get larger up to 2 cm. It shows flow banding in some places (Figure 2.38d). The levels which have more felsic composition are observed with its lighter green color compared to andesite. Above the altered andesite, the alternation of andesitic tuff and coarse grained sandstone is observed for 10 m. After the alternation, the second domain ends since it cannot be followed along the shore anymore.

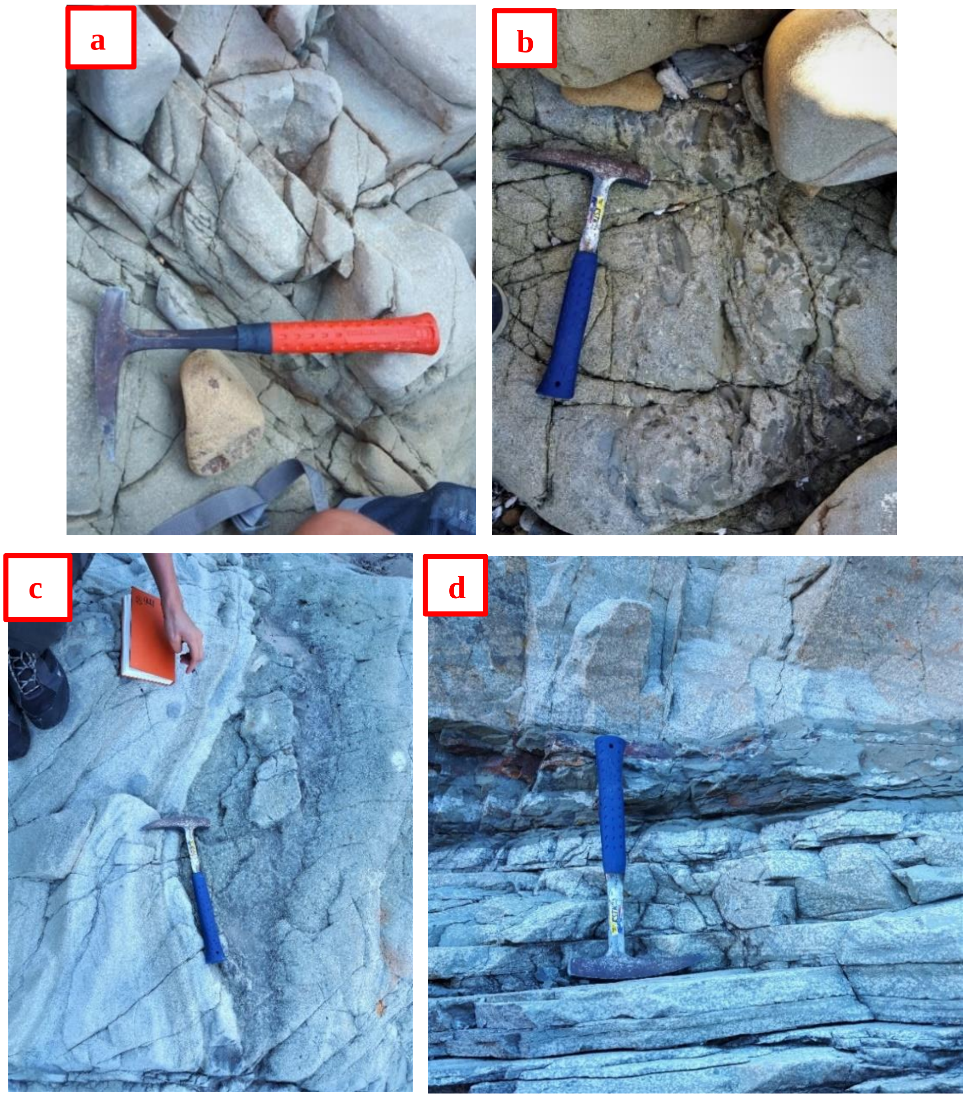

Figure 2.38 : Field photos showing andesitic rocks from location 89, 89, 88 and 86, respectively a) The light greenish grey andesite with white phenocrysts of feldspar b) The green andesite and dark colored shale blocks which are accumulated densely in the agglomerate. c) The compositional change from more felsic andesitic to andesitic tuff layers is seen. d) The flow banding in andesite is seen above the lapillistone layers.

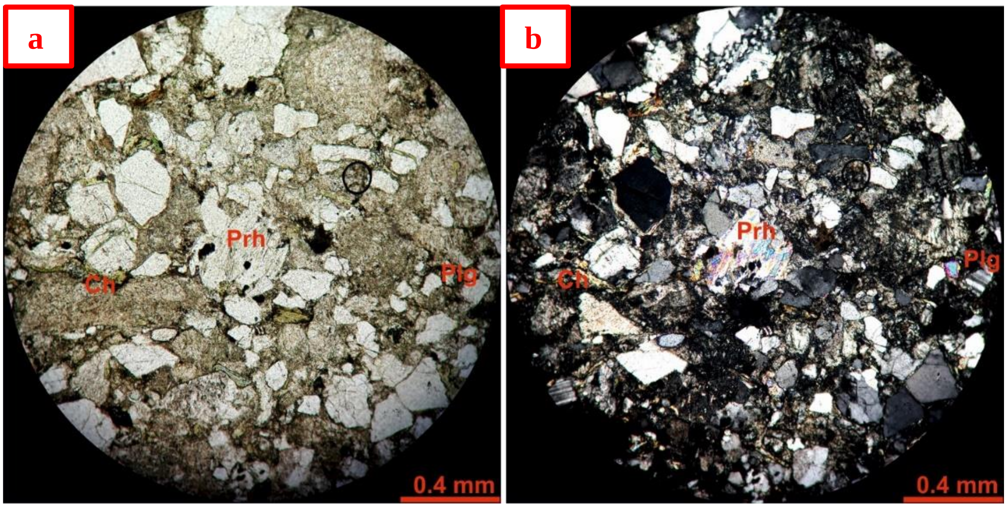

Figure 2.39 : Photomicrographs showing the andesitic tuff from location 89 including plagioclase (Plg), prehnite (Prh), chloritized volcanic glass (Ch). The anomalous interference colors of prehnite is observed. a) plane-polarized light b) cross-polarized light (Sample no: 89).

Figure 2.40 : Field photo from location 94 showing the alternation of the andesitic tuff/lapillistone/sandstone in the SW and the light green massive andesitic rocks in the NE. The red line separates these two units.

2.3.2.3 D3 Domain

The third volcanic-volcaniclastic domain is located in the northeast of the study area. The continuation of the volcanic and volcaniclastic rocks towards Bulgaria is observed. The thickness of D3 domain is about 170 m. The dacitic composition of the rocks start to be seen in this domain. Additionally, the andesitic rocks mostly have more felsic composition within D3 domain. All of the rock units in the second part of the D3 domain are cut by calcite veins in two or three different orientations. The D3 domain can be examined as three separate parts.

The first part of the D3 Domain (D3 P1)

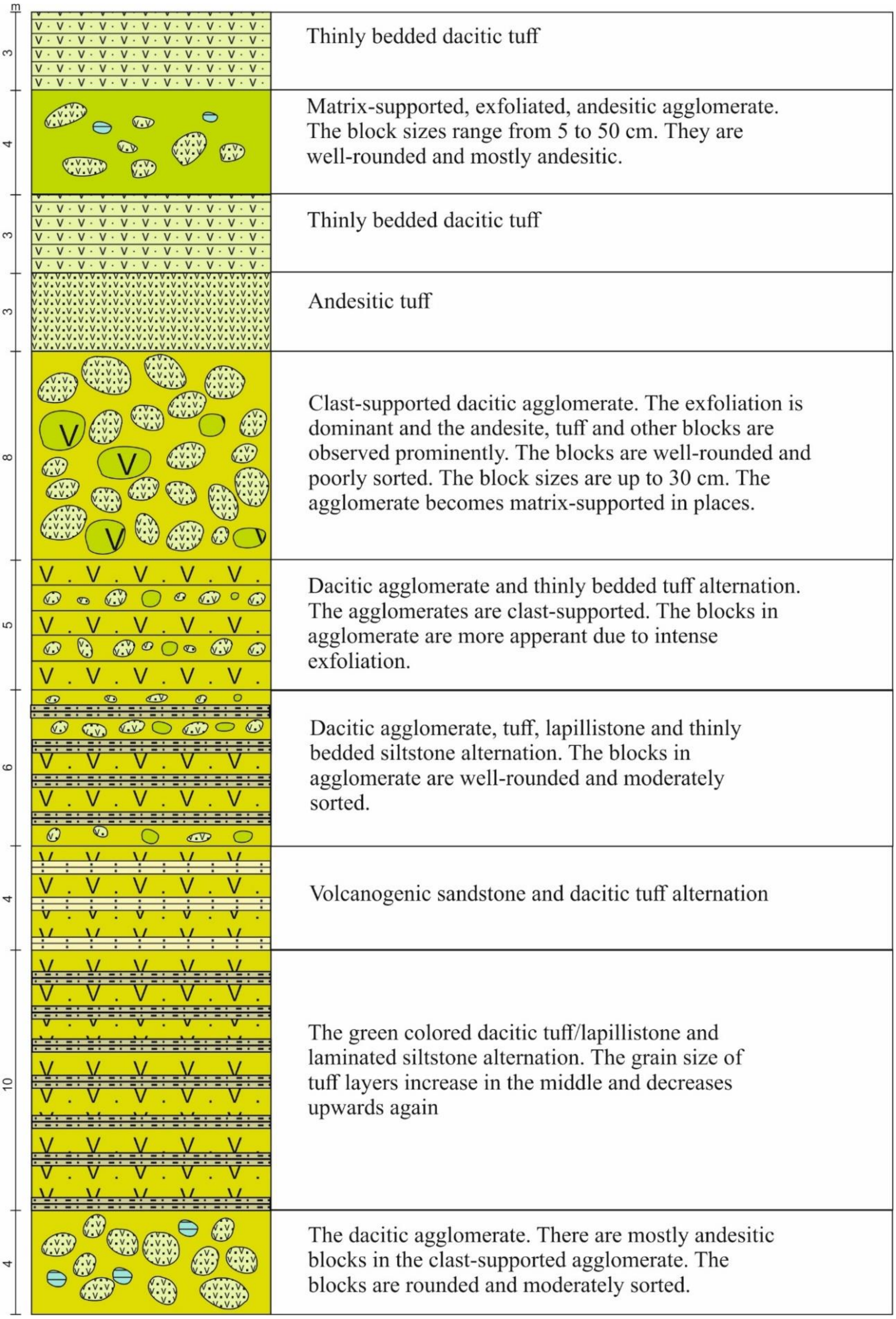

Figure 2.41 : The stratigraphic section of the first part of the D3 Domain (D3 P1).

The first part of the D3 domain starts with dacitic agglomerate including blocks of mostly andesitic rocks. The dacitic matrix is remarkable with its light green color. The dacitic agglomerate is followed by green dacitic tuff/lapillistone and laminated siltstone. The grain size of tuff layers increases in the middle and decreases upwards again. After 25 m alternation, dacitic clast-supported agglomerate is observed. The agglomerate is exposed to exfoliation and its well-rounded and poorly sorted blocks have become apparent. The block sizes are up to 30 cm. The dacitic agglomerate becomes matrix-supported in places. The appearance of the exfoliated agglomerate can be mistaken for the pillow lava flow. However, the block content of the agglomerate indicates that they are volcaniclastic rocks. The agglomerate continues for at least 8 m and then the thinly bedded andesitic and dacitic tuff layers are observed for 6 m. Then, there is matrix-supported andesitic agglomerate and they are followed by thinly bedded dacitic tuff layers again (Figure 2.42).

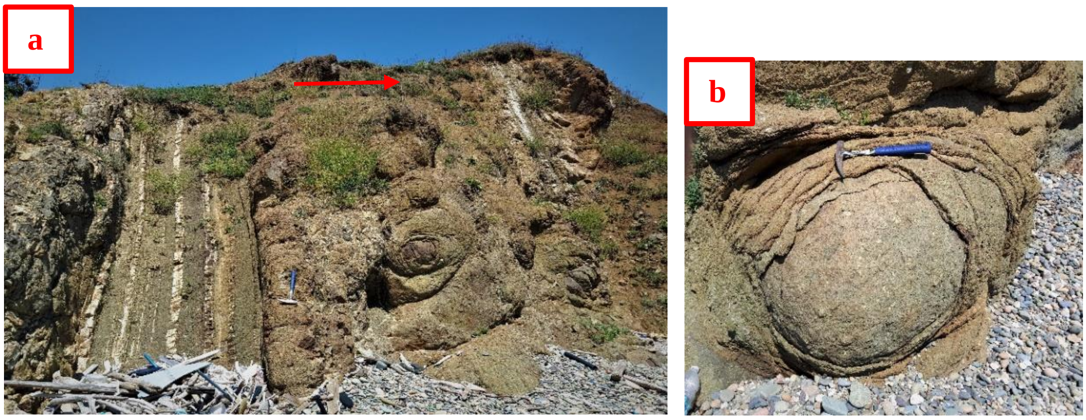

Figure 2.42 : Field photos showing the dacitic rocks from location 64. a) The outcrop view showing the thinly bedded dacitic tuff layers and exfoliated dacitic agglomerate. The red arrow indicates the younging direction. b) The close up view of the exfoliated dacitic agglomerate.

The second part of the D3 Domain (D3 P2)

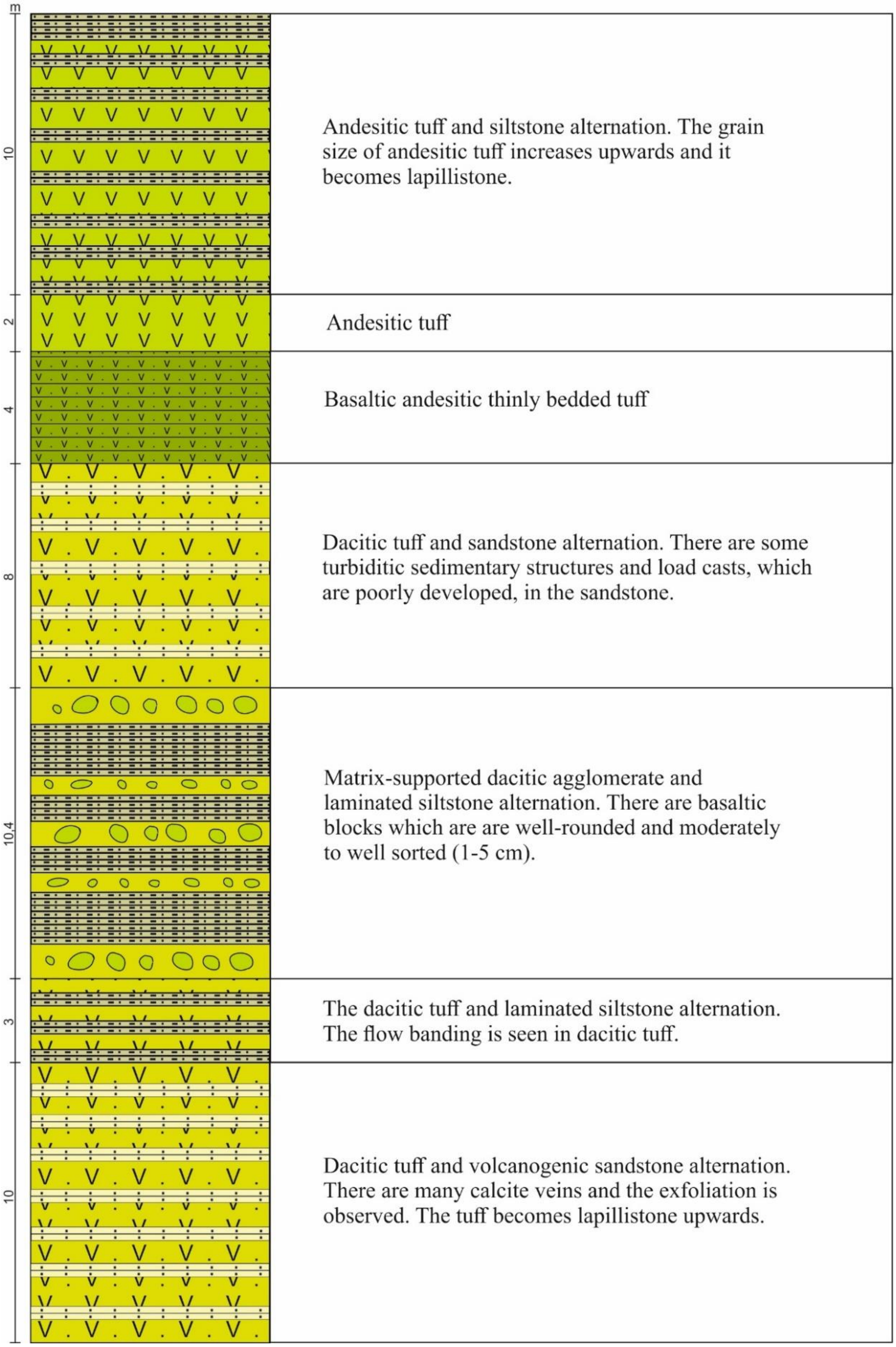

Figure 2.43 : The stratigraphic section of the second part of the D3 domain (D3 P2).

The second part of the D3 domain can be represented by the alternation of the dacitic/andesitic tuff and sand/siltstone. It starts with dacitic tuff and volcanogenic sandstone alternation. It is followed by dacitic matrix-supported agglomerate and laminated siltstone alternation. The dacitic agglomerate includes dark grey basaltic blocks (Figure 2.44a) which are well-rounded and moderately to well sorted (1- 5 cm). However, the source for the basaltic blocks in the agglomerate is not observed along the whole volcanic-volcaniclastic sequence. There are some poorly-developed sedimentary structures which are load casts and turbiditic structures within sand/siltstone layers. These alternations continue approximately for 30 m. Then, there are grey tuff layers which have basaltic andesitic composition. These fine grained basaltic andesitic rocks start to show the alternation of mineralogically unlike layers due to flow banding (Figure 2.44b). The flow banding is observed in all basaltic andesitic and andesitic rocks after this location until the end of the D3 domain. The second part of the D3 domain ends with the andesitic tuff and siltstone alternation for 10 m.

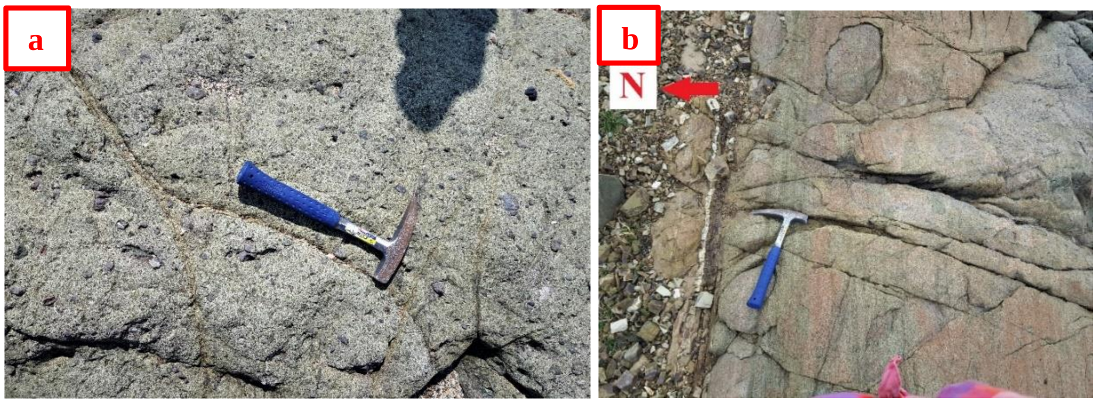

Figure 2.44 : Field photos showing the dacitic and basaltic andesitic rocks from location 58 and 51, respectively a) The dark grey basaltic blocks in dacitic agglomerate. b) The flow banding in basaltic andesitic tuff.

The third part of the D3 Domain (D3 P3)

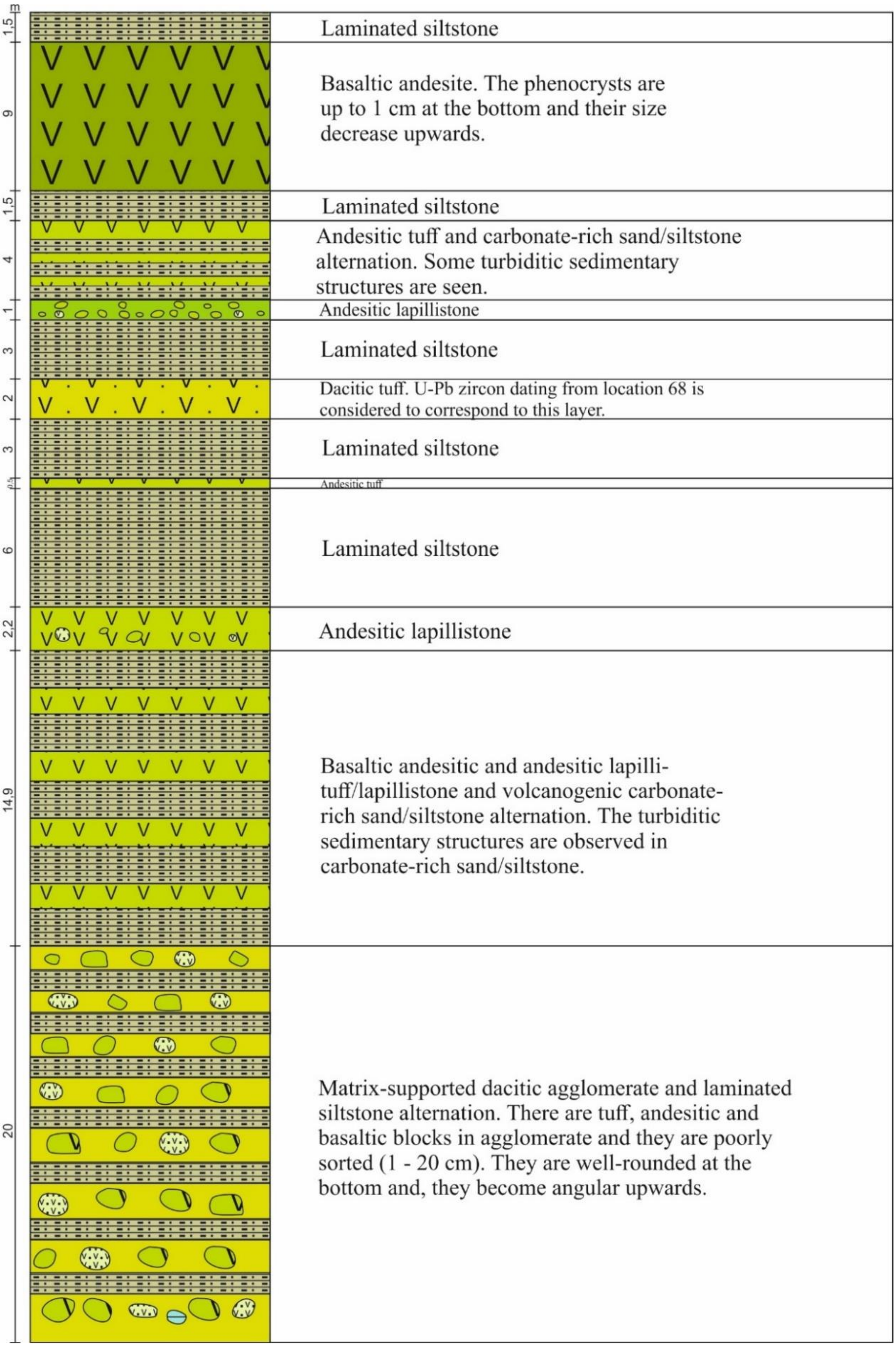

Figure 2.45 : The stratigraphic section of the third part of the D3 domain. (D3 P3).

The third part of the D3 domain includes dacitic, andesitic, and basaltic andesitic rocks. The composition of volcanic and volcaniclastic rocks becomes basaltic upwards. At the base, the matrix-supported dacitic agglomerate and laminated siltstone alternate. Then, the alternation of the basaltic andesitic/andesitic lapilli-tuff/lapillistone and volcanogenic sand/siltstone (Figure 2.46) is observed for approximately 15 m.

The thin section of the basaltic andesitic lithic tuff is seen in Figure 2.47. The poorly sorted tuff has basaltic andesitic fragments in which plagioclase and pyroxene phenocrysts are present. Some of the euhedral pyroxene crystals have cleavages intersecting at 90^{o}. There are sieve-textured plagioclase crystals that have deformational twinning. The chlorite and calcite are present as secondary minerals. The fine grained glassy matrix constitutes 10 % of the basaltic andesitic tuff sample. Additionally, the thin section of the andesitic tuff sample (Figure 2.48), which is found above the basaltic andesitic tuff, shows that the sample is a vitric-crystal tuff based on its glassy matrix that constituting 50 % of the sample. The euhedral pyroxene crystals, plagioclase and chlorite and few angular lithic fragments are present.

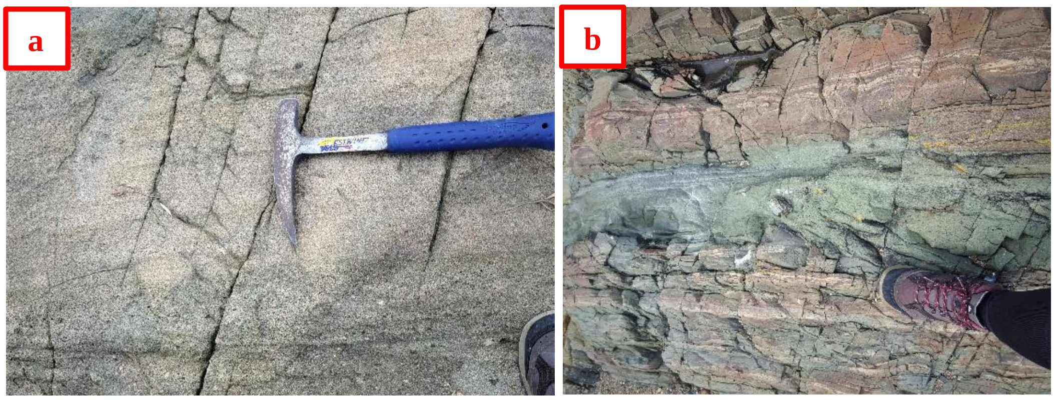

Figure 2.46 : Field photos showing the basaltic andesitic lapillistone and the alternation of the siltstone and andesitic tuff from location 50 and 49, respectively. a) The basaltic andesitic lapillistone has mafic mineral fragments. b) The alternation of brown – light brown volcanogenic sand/siltstone and green andesitic lapilli-tuff is observed.

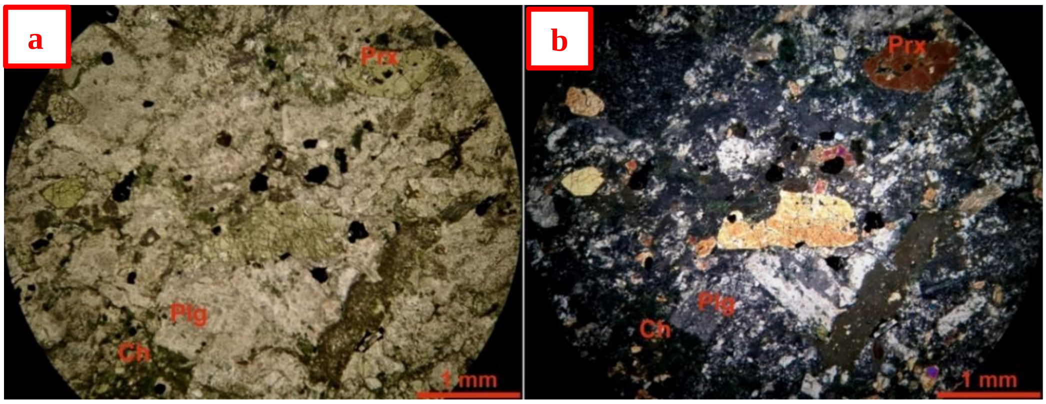

Figure 2.47 : Photomicrographs showing the basaltic andesitic lithic tuff from location 50. The plagioclase (Plg), pyroxene (Prx) and chlorite (Ch) are observed in a fine grained glassy matrix. a) plane-polarized light b) cross-polarized light (Sample no: 50).

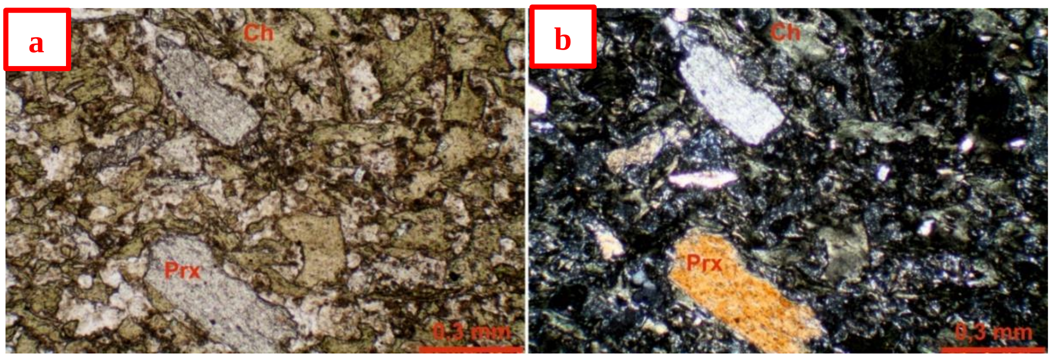

Figure 2.48 : Photomicrographs showing the andesitic vitric-crystal tuff from location 47. It includes the crystals pyroxene (Prx) and chloritized volcanic glass (Ch) a) plane-polarized light b) cross-polarized light (Sample no: 47).

As it is seen in the thin section of the altered basaltic andesite in Figure 2.49, it is more basaltic than the previous basaltic andesites with its pyroxene content. The altered and chloritized feldspars, the oscillatory zoning in pyroxene and the prehnite formation due to hydrothermal alteration are seen. The euhedral pyroxene phenocrysts may be clinopyroxene based on their inclined extinction and medium to high birefringence with the 2nd order interference color. The chlorite alteration is mostly observed around grain boundaries and the opaque minerals have grown on the pyroxene and feldspar phenocrysts. The prehnite is observed with its anomalous interference colors. They are mostly formed around the pyroxene crystals. The release of CaO to the system during the alteration of pyroxene can lead to prehnite formation. However, the prehnite may be formed due to the hydrothermal fluid activity. The temperature for prehnite formation is between 300 – 450 ^{o}C (Azer et al., 2018). The calcite is also observed filling the vesicles.

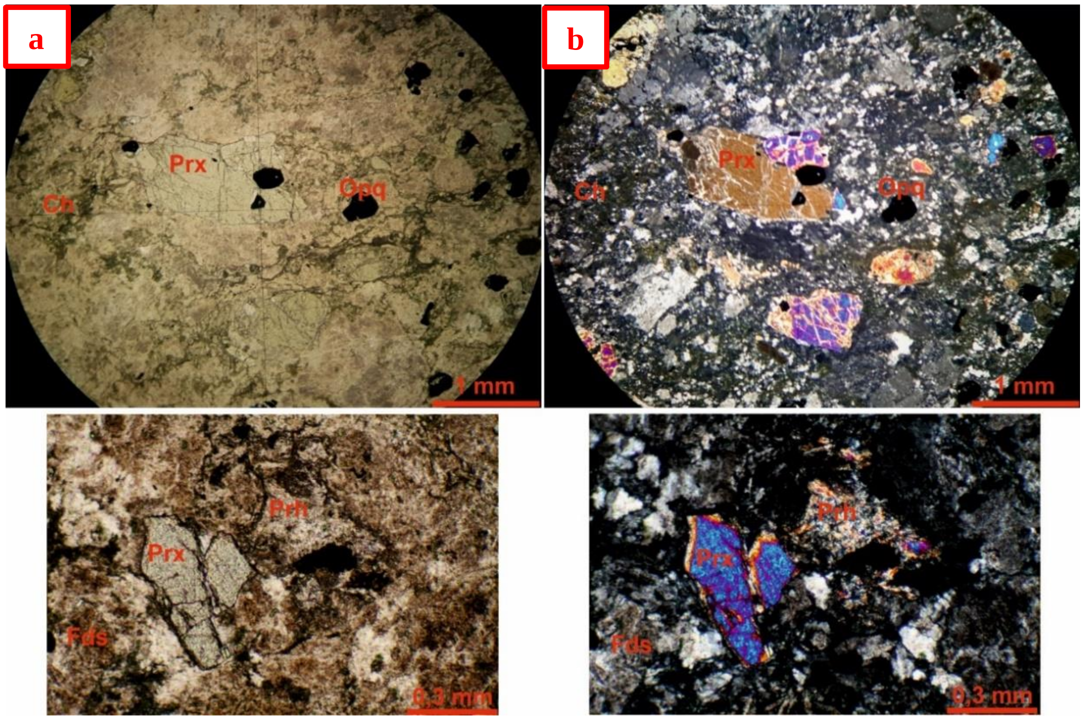

Figure 2.49 : Photomicrographs of the basaltic andesite from location 13. The pyroxene (Prx), feldspar (Fds), chlorite (Ch), prehnite (Prh) and opaque minerals (Opq) are seen. The anomalous interference colors of the prehnite is seen in the close up view. a) plane-polarized light b) cross-polarized light (Sample no: 13).

The third part of the D3 domain continues with laminated siltstone and andesitic/dacitic tuff alternation. As it is seen in the thin section (Figure 2.50) of the dacitic tuff sample from location 68, the sample can be defined as lithic-crystal fine grained tuff, which contains quartz, plagioclase, chlorite and lithic fragments. Some of the quartz crystals have rounded and corroded grain boundaries indicating partial dissolution after the crystallization from magma, before the solidification of the matrix. The rectangular plagioclase crystals show lamellar twinning. Also, there are fragments of other andesitic rocks which are well and moderately-rounded. The secondary chlorite is seen with its green color under plane polarized light. The fine grained matrix is mostly composed of microlitic plagioclase.

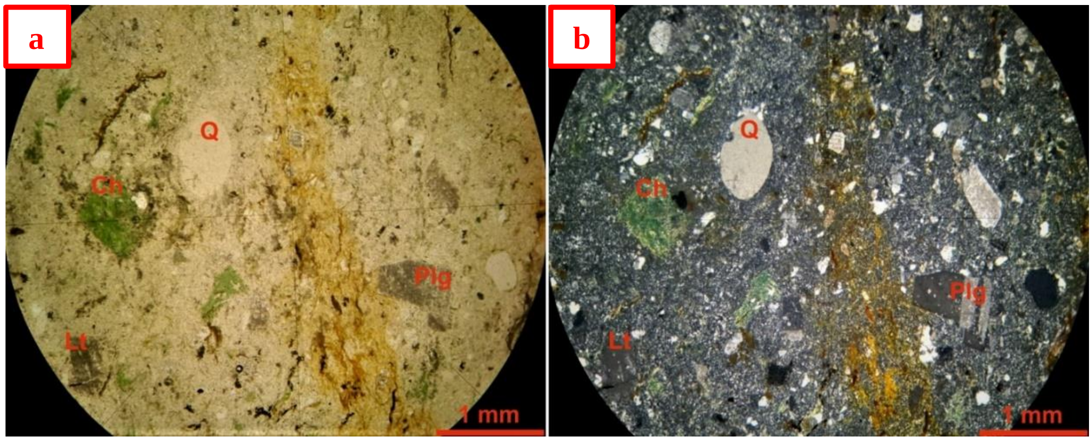

Figure 2.50 : Photomicrographs of the dacitic tuff from location 68 including the crystals of quartz (Q), plagioclase (Plg), some lithic fragments (Lt) and secondary chlorite (Ch). a) plane-polarized light b) cross-polarized light (Sample no: 68).

The age of the dacitic tuff layers, which are found in the upper levels of the volcanic-volcaniclastic sequence in İğneada, is important for geochronology of Upper Cretaceous volcanism in İğneada. This layer can be considered as the end of the volcanism in the region. Therefore, the zircons taken from sample 68 which is taken from location 68 are dated. The petrographic properties of sample 68, which is a dacitic tuff, is explained above in Figure 2.50. This dacitic tuff layer corresponds to the indicated layer in the stratigraphic section (Figure 2.45). A total of 30 analyses were made on 30 zircon grains which are seen in the cathodoluminescence image (Figure 2.51a). As a result of the U-Pb zircon dating, Santonian (84.85 ± 0.42 Ma) ages are obtained as it is shown in the U/Pb concordia diagram (Figure 2.51b). 22 zircons give U-Pb ages between 76 and 90 Ma, whereas 8 zircons are xenocrystic zircons from the Strandja Massif as it is given in zircon LA-ICP-MS data (Table 2.2).

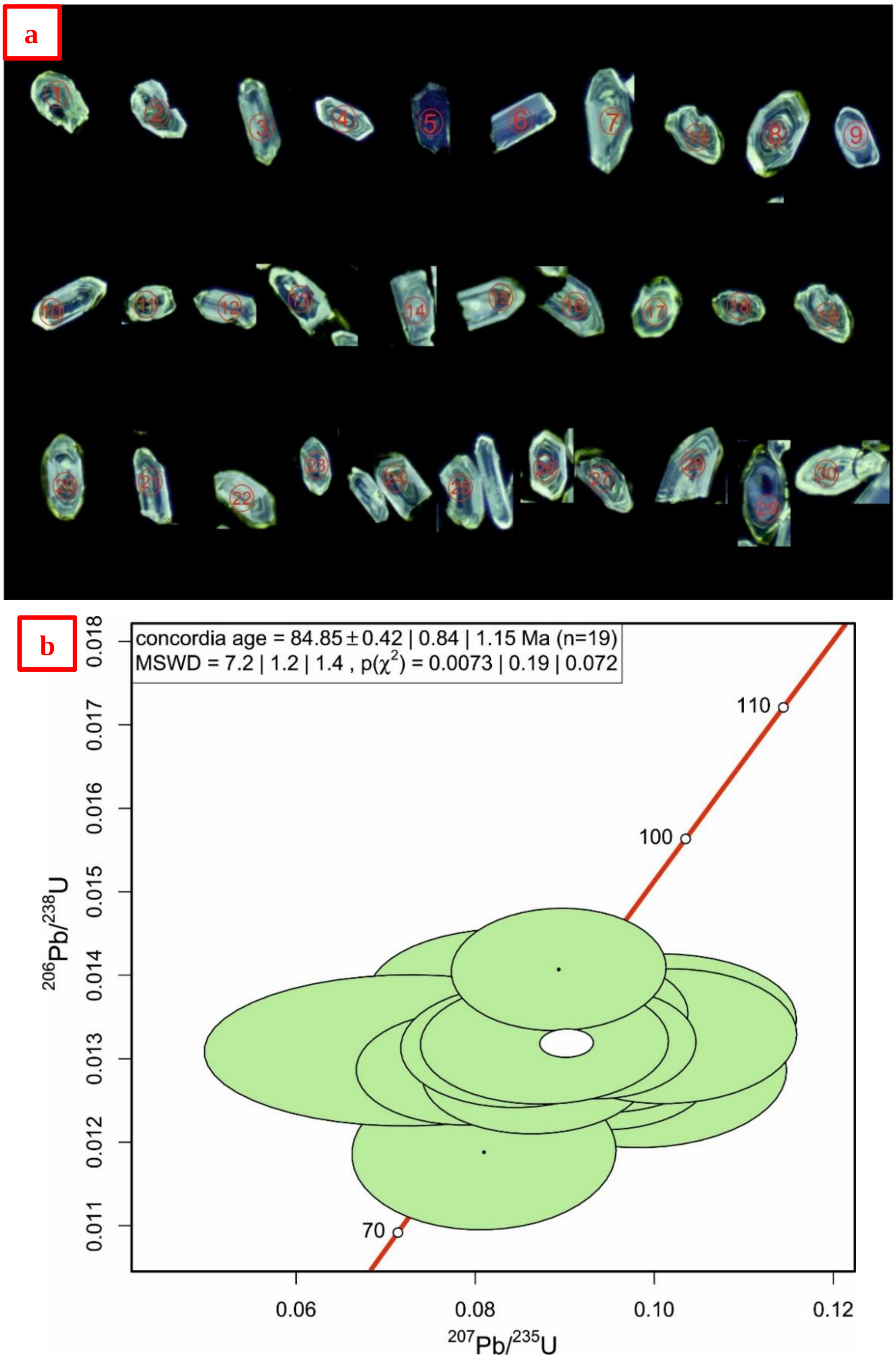

Figure 2.51 : a) Cathodoluminescence images of zircon crystals from the dacitic tuff taken from sample 68 in location 68 b) U-Pb concordia diagram showing LA-ICP-MS zircon data from sample 68.

Table 2.2 : Zircon LA-ICP-MS data of sample 68.

	Isotopic ratios: 1 sigma uncertainty							Age estimates (Ma)		Age estimates: 1 sigma uncertainty (Ma)			
Spots	$^{208}Pb/^{235}U$	$^{207}Pb/^{235}U$	$^{206}Pb/^{238}U$	$^{206}Pb/^{238}U$	$^{207}Pb/^{206}Pb$	$^{208}Pb/^{232}Th$	Corcordance	Spots	$^{207}Pb/^{206}Pb$	$^{206}Pb/^{238}U$	$^{206}Pb/^{238}U$	$^{207}Pb/^{235}U$	$^{207}Pb/^{235}U$
1	0,36984	0,01158	0,052	0,00082	0,05159	0,01583	1,02	1	267,2	326,8	5,02	319,5	8,58
2	0,08542	0,00476	0,0129	0,0003	0,04802	0,00385	0,99	2	99,1	82,6	1,93	83,2	4,45
3	0,09691	0,00686	0,01312	0,00034	0,05356	0,00432	0,9	3	352,4	84,1	2,15	93,9	6,35
4	0,09861	0,00661	0,01284	0,00037	0,05572	0,00452	0,86	4	440,8	82,2	2,38	95,5	6,11
5	0,80486	0,01214	0,09372	0,00113	0,0623	0,0294	0,96	5	684,4	577,5	6,65	599,6	6,83
6	0,70366	0,02006	0,09366	0,00152	0,0545	0,02868	1,07	6	391,7	577,1	8,98	541	11,95
7	0,08695	0,00568	0,01317	0,00034	0,04791	0,00455	1	7	93,6	84,3	2,18	84,7	5,3
8	0,09507	0,00466	0,01281	0,00027	0,05385	0,00407	0,89	8	364,7	82	1,69	92,2	4,32
9	0,79758	0,06003	0,09668	0,00348	0,05984	0,03131	1	9	597,9	594,9	20,46	595,5	33,91
10	0,08638	0,00537	0,01298	0,00032	0,04829	0,00448	0,99	10	113,5	83,1	2,04	84,1	5,02
11	0,85817	0,03492	0,10031	0,00211	0,06206	0,03018	0,98	11	676,1	616,2	12,37	629,1	19,08
12	0,10022	0,0064	0,01345	0,00033	0,05404	0,00458	0,89	12	372,6	86,1	2,13	97	5,9
13	0,29991	0,00944	0,0397	0,00065	0,0548	0,01408	0,94	13	404,2	251	4,04	266,3	7,37
14	0,60912	0,03073	0,07454	0,00197	0,05928	0,02712	0,96	14	577,3	463,4	11,84	483	19,39
15	0,08098	0,00603	0,01188	0,00038	0,04946	0,00474	0,96	15	169,6	76,1	2,4	79,1	5,66
16	0,08328	0,00621	0,0138	0,00031	0,04377	0,00475	1,09	16	0,1	88,4	1,94	81,2	5,82
17	0,07243	0,00927	0,0131	0,00037	0,04011	0,00418	1,18	17	0,1	83,9	2,39	71	8,77
18	0,07929	0,00514	0,01289	0,00028	0,04461	0,00441	1,07	18	0,1	82,6	1,77	77,5	4,84
19	0,08752	0,00629	0,01312	0,00032	0,04838	0,00473	0,99	19	118	84	2,01	85,2	5,87
20	0,09028	0,00432	0,01331	0,00027	0,04919	0,00413	0,97	20	156,8	85,3	1,69	87,8	4,02
21	0,09491	0,00505	0,01304	0,00028	0,0528	0,00467	0,91	21	320,3	83,5	1,76	92,1	4,68
22	0,08672	0,00516	0,01281	0,00029	0,0491	0,00457	0,97	22	152,7	82,1	1,84	84,4	4,82
23	0,10148	0,0059	0,01327	0,00033	0,05547	0,00449	0,87	23	431,1	85	2,12	98,1	5,44
24	0,08482	0,00537	0,01315	0,0003	0,0468	0,00429	1,02	24	38,7	84,2	1,91	82,7	5,03
25	0,09085	0,00528	0,01352	0,00029	0,04876	0,0046	0,98	25	136,2	86,5	1,86	88,3	4,91
26	0,09395	0,00438	0,01318	0,00027	0,05171	0,00439	0,93	26	272,7	84,4	1,75	91,2	4,07
27	0,08774	0,00566	0,01319	0,0003	0,04826	0,00462	0,99	27	112,1	84,5	1,93	85,4	5,29
28	0,08933	0,0049	0,01407	0,0003	0,04604	0,00476	1,04	28	0,1	90,1	1,92	86,9	4,57
29	0,56538	0,01453	0,07555	0,0011	0,05429	0,02289	1,03	29	382,8	469,5	6,61	455	9,43
30	0,36017	0,01218	0,04914	0,00084	0,05316	0,0168	0,99	30	335,7	309,3	5,15	312,3	9,09

In the upper parts of the third part of the D3 domain, the laminated siltstone is observed indicating a deep marine depositional environment. The thin section of the laminated siltstone is seen in Figure 2.52. The angular clasts of the coarse grained siltstone are poorly sorted. The clasts are mostly calcitized and they are made up of lithic grains, feldspar, quartz, and pyroxene. The presence of pyroxene and the pieces of other minerals show that some clasts come from a volcanic source. The matrix is composed of clay-sized grains.

There are well-developed sedimentary structures within sand/siltstone (Figure 2. 53). In addition to the mentioned radiolaria content of the siltstone, these sedimentary structures exhibiting turbiditic characteristics with preferably oriented poorly sorted blocks and convolute bedding. The flow direction can be determined as top to NW from these turbiditic carbonate-rich sandstones. The laminated siltstone is followed by andesitic tuff and lapillistone. Then, the turbiditic carbonate-rich sand/siltstone and flow-banded basaltic andesitic rocks are continued to be observed. They are followed by basaltic andesite which is observed for 9 m. The D3 domain ends with laminated siltstone which is found above basaltic andesite. It ends at the Turkish – Bulgarian border. However, the continuation of volcanic and volcaniclastic units in Bulgarian shores can be observed from Beğendik Village.

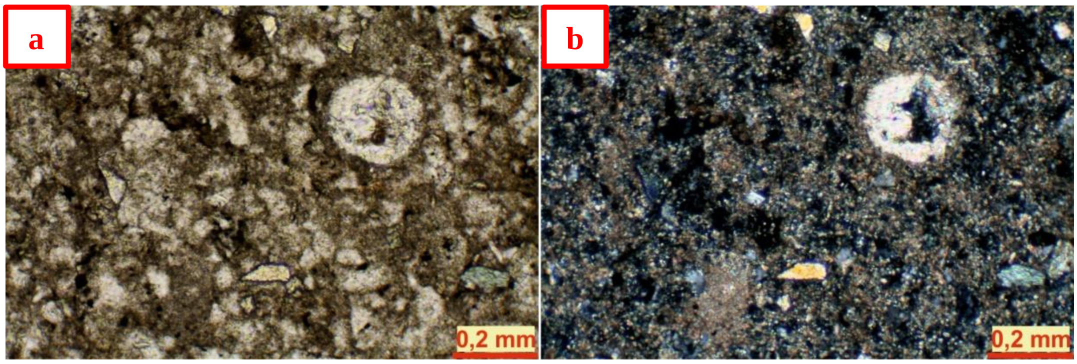

Figure 2.52 : Photomicrographs of the radiolarian siltstone from location 42. The calcitized radiolaria and other calcitized grains are observed. a) plane-polarized light b) cross-polarized light (Sample no: 42).

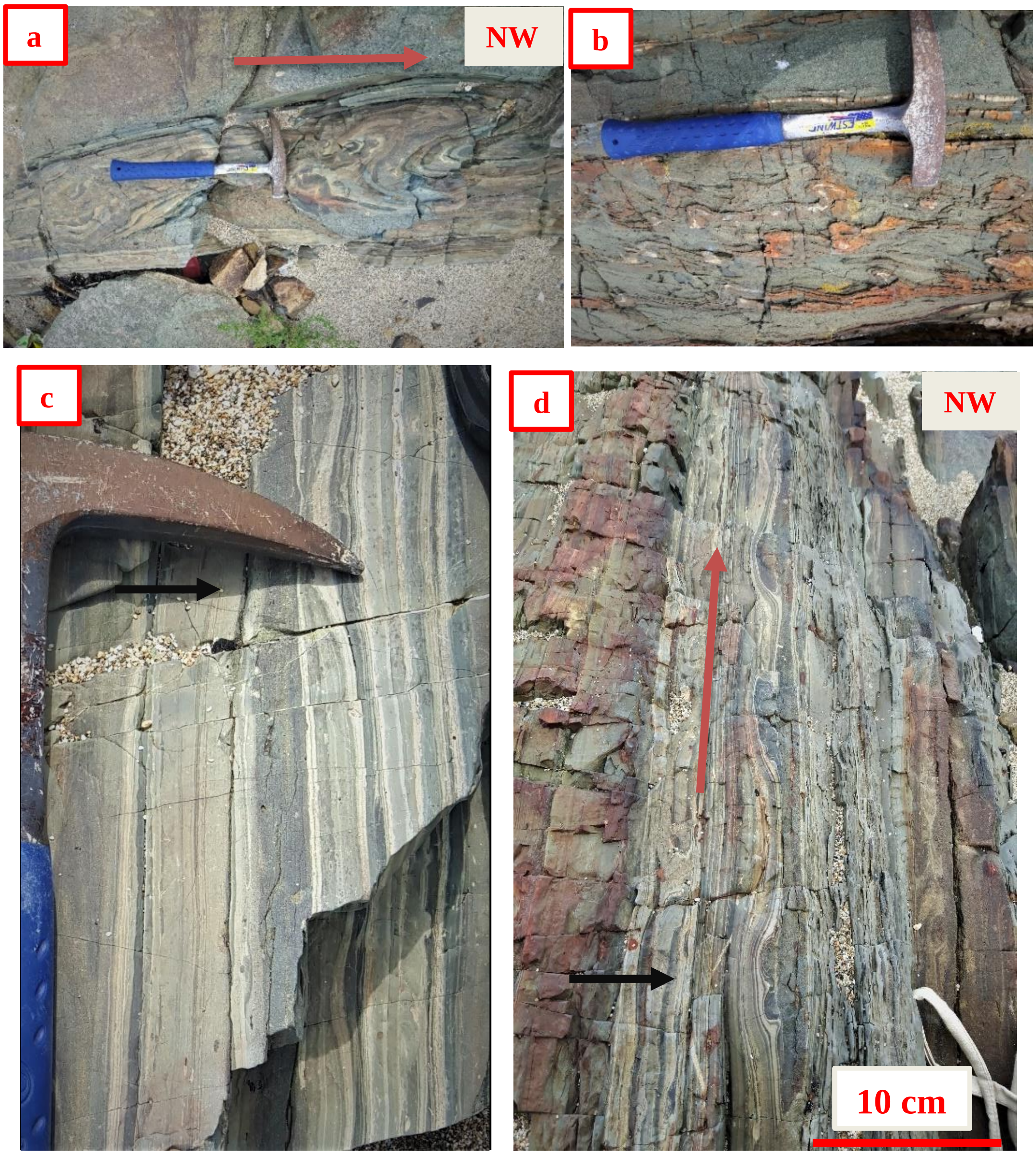

Figure 2.53 : Field examples of the turbiditic sedimentary structures in sand/siltstone from location 42, 44, 43, and 45, respectively. The possible turbidity current directions are indicated by red arrows. a) The convolute bedding in the volcanogenic siltstone indicating the current direction is observed within the coarse siltstone. b) The convolute bedding in the volcanogenic fine grained sandstone interbedded with fine grained silt/mudstone is seen. c) The poorly-developed load cast, whose younging direction is indicated by black arrow, is seen in the coarse grained siltstone. d) The well-developed load casts within sand/siltstone layers. The black arrow indicates the younging direction.

3. STRUCTURAL GEOLOGY

3.1 Introduction to the Structural Geology of the Study Area

The observation points in the study area are mostly located along the shore as it is seen in the geological map (App-A). In order to analyze the sequence properly from older to younger, the orientation of the bedding planes should be same throughout the sequence. Therefore, it is necessary to separate the volcanic-volcaniclastic sequence into domains, which are D1, D2 and D3 in which the bedding plane orientations do not change. This chapter explains the change in bedding plane orientations, faults, folds and fractures in the study area. The cross-sections display the relationship between rock units (App-B).

3.2 Bedding Planes, Faults and Folds

The faulting and folding are the main reasons for change in the orientations. It is seen that the volcaniclastic rocks overlie sedimentary rocks conformably at the beginning of the volcanic rocks in the Limanköy harbour. They can be traced until location 36 where the orientation of the bedding planes changes. After this location, there are different bedding plane orientations in the study area. The poles of the bedding planes for each domain are indicated in the stereographic projection (Figure 3.1a).

There are lots of low and high-angle normal faults in the study area. The largest scale normal faults are observed mostly within D2 and D3 domains, where step faulting creates the pocket beaches. Additionally, small-scale normal faults are abundantly observed in the study area (Figure 3.2). The poles of fault planes are plotted on stereonet separately for three domains (Figure 3.1b). According to orientation of fault planes, a NNW-SSE, NE-SW and NW-SE, NW-SE extensions caused the formation of the faults in D1, D2 and D3 domains, respectively.

Pamir and Baykal (1947) mentioned about prevalent large-scale Alpine-type N-vergent folding seen in İğneada and Limanköy regions. According to their study, these folds are observed in a W-E cross-section from Rezve to Limanköy. In the study area of this thesis, there is a syncline which has an interlimb angle of 60° as it is seen in the Y-Y' cross-section (App-B). The orientation of the fold axis is determined as 142/25 (dip direction/dip angle) and it is shown with green point in Figure 3.1a.

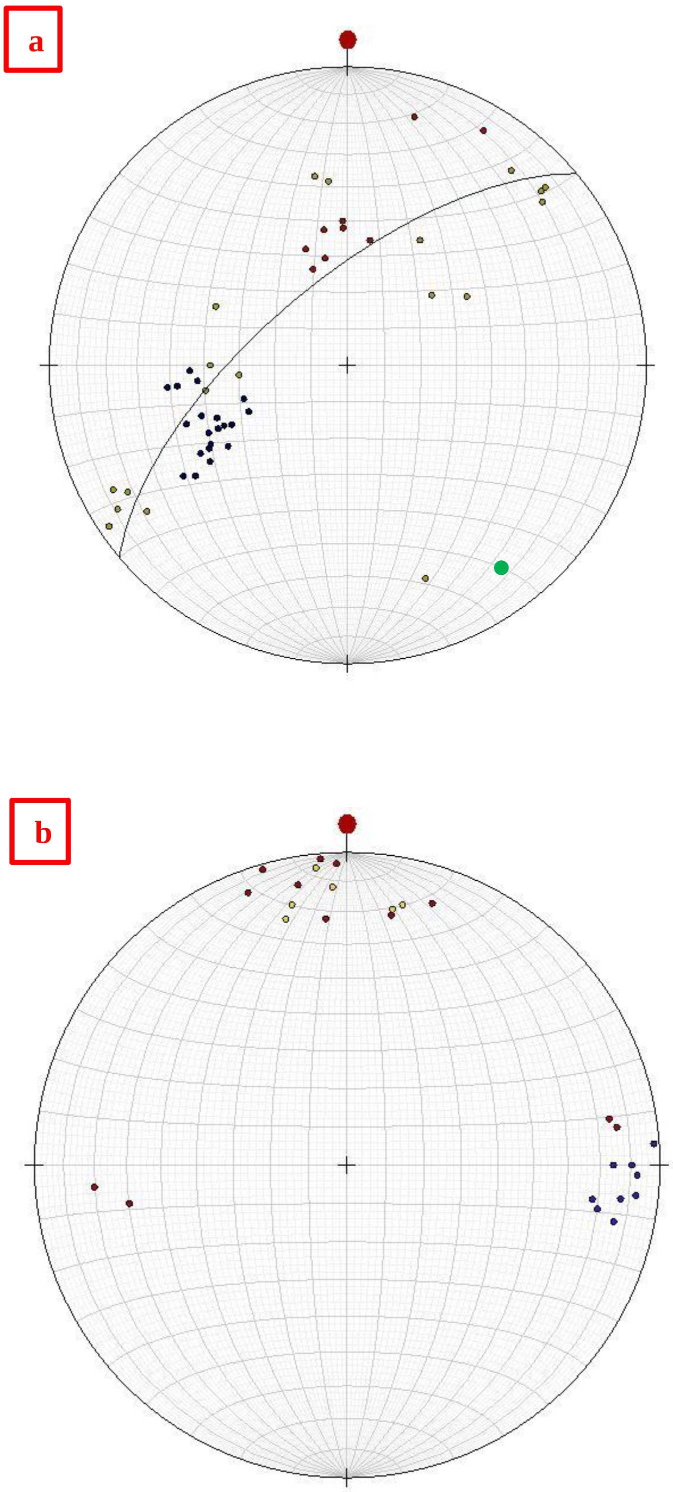

Figure 3.1 : Stereographic projections showing the poles for D1, D2 and D3 domains with blue, red and yellow, respectively. The lower hemisphere is used in the equal-area stereographic projection. a) Plots of bedding planes. The green point indicates the fold axis. b) Plots of fault planes.

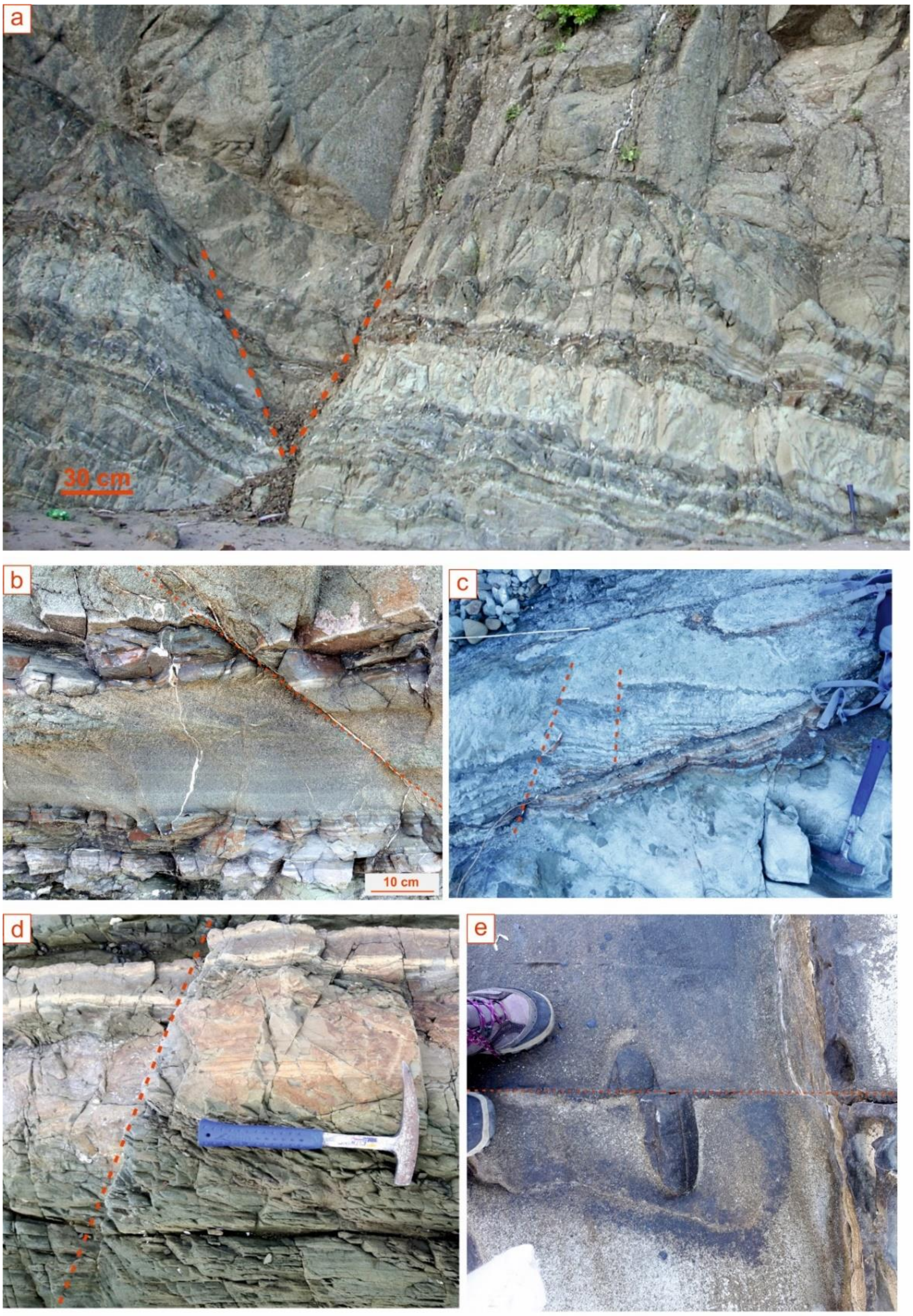

Figure 3.2 : Field examples of normal faults a) A graben in volcaniclastic rocks b) The low-angle normal fault cutting the limestone-volcaniclastic rock altermation c) Small-scale faulting in volcanogenic siltstone d) The high-angle normal fault cutting volcanogenic sandstone e) The left-lateral slip of the trace of block due to normal faulting.

3.3 Fractures

Although the fractures are seen dominantly within the volcanic-volcaniclastic sequence, they are abundant in all units in the study area (Figure 3.4). They are mostly systematic fractures which can be observed as one, two or three fracture sets. The distribution of the fractures is shown in the rose diagrams (Figure 3.3). The directional trends of fractures are NW and SSE-ENE according to rose diagrams of D1 and D2-D3 domains, respectively.

The shear fractures, which are produced by shear stress, create the parallel surfaces of the fracture planes (Figure 3.4d). The tensile fractures which have uneven fracture plane surfaces, are formed due to tensile stress (Figure 3.4b).

The fractures are mostly filled with calcite and quartz. The fractures in the metamorphic and sedimentary rocks are mostly filled with quartz veins, whereas all of the fractures in the volcanic and volcaniclastic rocks are filled with calcite veins.

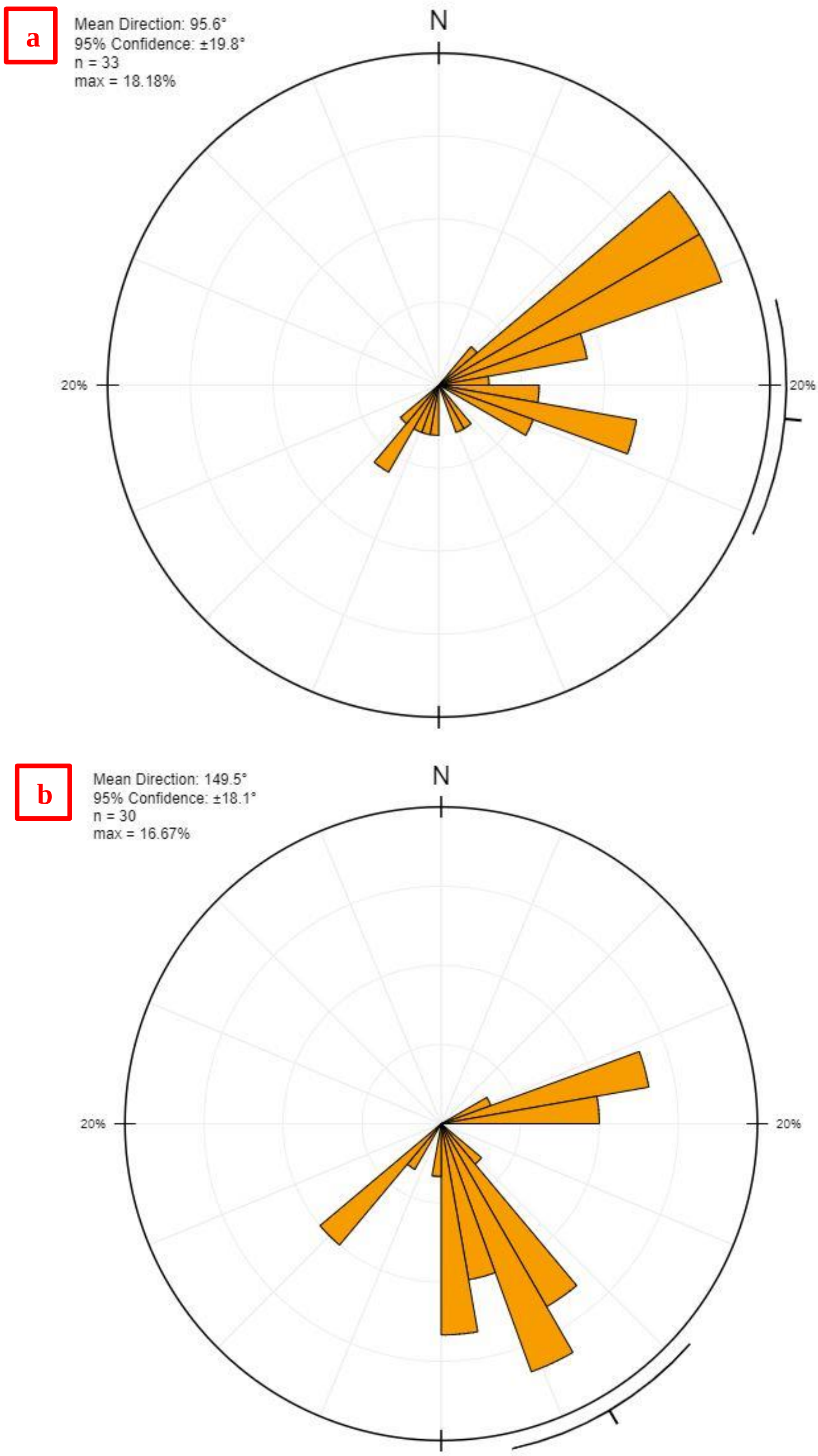

Figure 3.3 : Rose diagrams showing the distribution of the fractures. a) Rose diagram for D1 domain b) Rose diagram for D2 and D3 domains together.

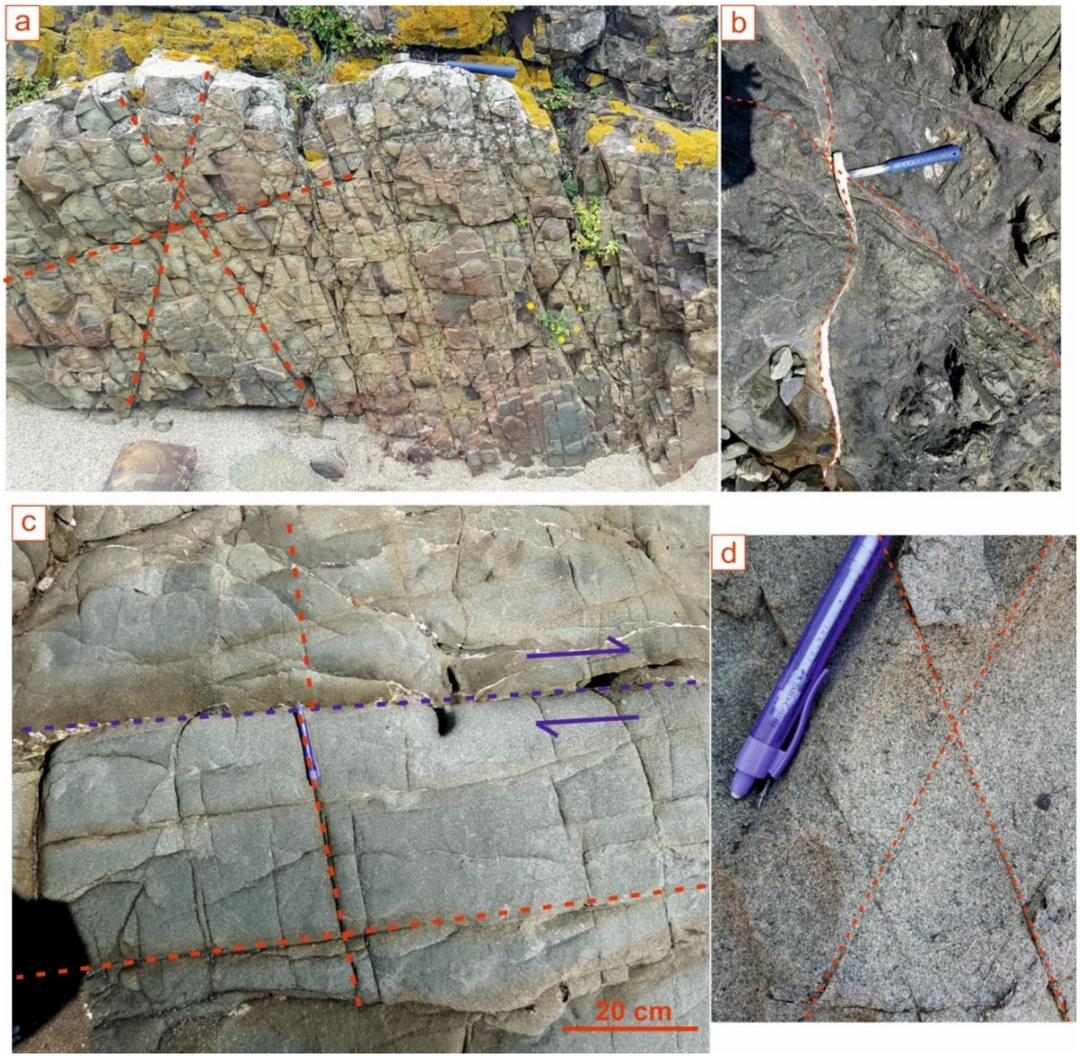

Figure 3.4 : Field examples of joint sets within the volcanic-volcaniclastic domains. a) Three conjugate sets of joints are seen in volcanogenic sandstone. b) Uneven fracture surface in basaltic andesite indicating tensile stress. The fractures are filled with calcite. c) The orthogonal joint sets with 90^0 dihedral angle. The right-lateral slip as a result of normal faulting is also observed. d) Conjugate joint sets which have parallel fracture surfaces indicating shear stress.

4. GEOCHEMISTRY

4.1 Interpretation of Geochemical Data

Five samples are selected for whole rock geochemical analyses. Selected five samples, which are E13, E22, E38, E38b, E68, are volcanic rocks. Their rock types are defined as basaltic andesite, andesite or dacite based on petrographical investigations and their thin sections are shown in previous chapters. Their locations are indicated in geological map (App-A).

The calculated loss on ignition (LOI) ranges from 2.1 % to 4.9 %. As it can be understood from the high LOI values and altered rock samples, the alteration is widely effective on all of the rock units. It is also consistent with the observed intense alteration in thin sections in which calcite, chlorite, prehnite, other clay and opaque minerals are found. Due to this alteration and various LOI values, major elements are normalized to 100 % on a LOI -free basis. Since the alteration affects the mobility of elements, immobile elements, that are REEs (rare earth elements) and high field strength elements (HFSEs), are important to interpret the source of the volcanic rocks and the tectonic setting in which they form. Whole rock geochemistry data for major and trace elements are given in Table 4.1. After normalization to 100 % on LOI-free basis, the comparison can be made for major oxide values in samples. SiO_2 % values range from 56 % to 77 %. But, if the sample E68, which has 77.18 SiO_2 %, is excluded, the average SiO_2 % is 57.7. It is clear that E68 sample has more acidic composition compared to other four samples. The SiO_2 values decrease towards north meaning that the volcanism becomes more acidic from older to younger. But, E13 sample, which is from the uppermost level, shows that the sequence becomes basaltic andesitic again.
The average values of Al_2O_3 %, Fe_2O_3 %, MgO %, CaO % and Na_2O % for the four samples except E68 are 17.77, 7.5, 3.22, 4.99 and 4.65, respectively. Al_2O_3 %, Fe_2O_3 %, MgO %, CaO % and Na_2O % values for E68 are 13.79, 1.59, 0.42, 0.33 and 4.20, respectively. Except E68 sample, the major oxides values vary within a narrow range for all samples. The average value of total amounts of REEs for all samples is 117,502 ppm.

Magnesium numbers (Mg# = (MgO wt % / MgO mol wt.) x 100 / (MgO wt % / MgO mol wt.) + (FeO wt % / FeO mol wt.)) are calculated for all samples to see how much the samples are differentiated. The magnesium numbers for E13, E22, E38, E38b and E68 samples are 41 , 43.5 , 47 , 41 and 32, respectively. All Mg#s are lower than 65 indicating that the melts were highly differentiated. The magnesium number for E68 sample is lower than the others as expected from a more acidic sample.

All samples have more sodic composition rather than potassic as it is understood from Na_2O % values which are higher than K_2O % values. Aluminium Saturation Index (ASI) (ASI = molar Al_2O_3 / (CaO + Na_2O + K_2O)) is calculated to see aluminum saturation degrees of samples. The ASI values for samples E13, E22, E38, E38b, E68 are 0.84, 0.88, 0.93, 0.94 and 1.39, respectively. The ASI values for andesite and basaltic andesite samples are less than 1 indicating that they are metaluminous, whereas the dacite sample E68 has ASI value greater than 1 indicating its peraluminous characteristics. It should be considered that alteration may be effective on the ASI values. The high chlorite content in E68 may be the reason for increased ASI value.

Table 4.1 : Geochemical data obtained from whole-rock analyses (Major oxides are normalized on a LOI-free basis.).

Sample	**E13**	**E22**	**E38**	**E38b**	**E68**
Oxides (wt%)					
SiO_2	58,89	56,14	56,44	59,35	77,18
Al_2O_3	17,88	18,16	18,43	16,63	13,79
Fe_2O_3	6,22	8,08	7,75	7,93	1,59
MgO	2,44	3,49	3,85	3,13	0,42
CaO	4,11	6,1	5,95	3,82	0,33
Na_2O	6,36	3,79	3,92	4,52	4,2
K_2O	3,05	3	2,24	3,01	2,22
TiO_2	0,61	0,77	0,91	1,01	0,23
P_2O_5	0,27	0,25	0,25	0,32	0,03
MnO	0,13	0,14	0,36	0,26	0,03
Total	100	100	100	100	100
LOI	2,1	4,4	4,9	4,4	2,3
Trace elements (ppm)					
Cs	0,1	1,2	1,1	1,1	1,2
Rb	61,8	86,2	45,7	69,4	84,7

Table 4.1 (continued) : Geochemical data obtained from whole-rock analyses (Major oxides are normalized on a LOI-free basis.).

Ba	184	422	456	518	351
Sr	496,8	370,2	452,7	390,5	270,5
Pb	13,4	5	91,4	15,1	12,7
Th	6,9	8	6,2	6,9	11,4
U	1,8	2,1	1,4	1,6	2,7
Zr	112,7	106,4	84,3	99	101,5
Hf	2,8	2,9	2,6	2,7	2,9
Ta	0,4	0,2	0,1	0,1	0,3
Nb	5,6	4,1	2,8	2,9	3,7
Ni	<20	<20	<20	<20	<20
Co	15,8	21,9	21,8	16,3	1,8
V	168	208	201	172	35
W	0,6	0,6	1	1,3	0,9
Ga	15,8	16,9	17,8	17	9,8
Zn	72	54	101	106	11
Cu	65,8	118,9	171,7	191,6	8,2
As	1,1	2,2	20,3	16,2	0,5
Mo	0,5	0,4	0,9	0,9	<0,1
Sc	11	19	19	16	3
Y	20,5	19,9	20,9	27,8	13,1
Rare earth elements (ppm)					
La	22,3	24,3	17,6	24,1	32,9
Ce	45,2	50,6	35,4	49,1	47,6
Pr	5,5	5,89	4,53	6,05	5,51
Nd	21,5	23,1	19,7	26,5	18,8
Sm	4,9	4,65	4,36	5,77	3,03
Eu	1,4	1,25	1,2	1,65	0,69
Gd	4,3	4,43	4,23	5,68	2,49
Tb	0,64	0,64	0,66	0,84	0,37
Dy	3,45	3,72	4,1	5	2,13
Ho	0,72	0,74	0,87	1	0,43
Er	2,14	2,2	2,5	3,07	1,4
Tm	0,33	0,31	0,38	0,45	0,22
Yb	2,39	2,04	2,38	2,86	1,5
Lu	0,37	0,33	0,38	0,47	0,27

4.2 Discrimination Diagrams

The discrimination diagrams, which are conducted by using abundances of major and trace elements in volcanic rock samples, are used to specify rock type, determine volcanic series and tectonic setting.

Total Alkali versus Silica diagram (TAS: Le Bas et al., 1986) is shown in Figure 4.1a. According to this diagram, volcanic rocks have intermediate composition, excluding E68 sample which has acidic composition. Intermediate rocks plot in the field trachy-andesite and basaltic trachy-andesite. The acidic sample is located in the field of rhyolite. The four samples which have intermediate composition are found in the border area between alkaline and subalkaline/tholeiitic series. However, the acidic sample E68 plots in the field of subalkaline/tholeiitic series.

The validity of TAS diagram should be evaluated by constructing alternative diagrams in which immobile elements are used. The Nb/Y-Zr/Ti diagram, which is formed by Winchester and Floyd (1977) and later modified by Pearce (1996), makes the discrimination considering the ratios of immobile elements. As it is seen in Figure 4.1b, all samples except E68 sample plot in the field of andesite / basaltic andesite. E68 sample plots in rhyolite/dacite field.

According to the K_2O-SiO_2 diagram (Figure 4.2a) of Peccerillo and Taylor (1976) for the classification of volcanic arc lavas, four samples E13, E22, E38 and E38b plot in the field of high-K calc-alkaline series. E22 sample is located close to the field of shoshonite and E68 sample plots in the field of calc-alkaline series.

Another diagram based on immobile elements Th and Co, is conducted by Hastie et al. (2007) to classify altered volcanic arc lavas. The diagram is designed by replacing K_2O and SiO_2 in the diagram of Peccerillo and Taylor (1976) by Th and Co, respectively. In accordance with the Nb/Y-Zr/Ti diagram, according to Th-Co diagram, four samples plot in basaltic andesite/andesite field whereas one sample plots in the field of dacite/rhyolite.

It is indicated in the diagram (Figure 4.2b) that three basaltic andesite/andesite samples, that are E13, E38 and E38b, are located on the border between calc-alkaline series and high-K calc-alkaline/shoshonite series. The rhyolite/dacite sample E68 and the other basaltic andesite/andesite sample E22 are found in the field of high-K calc-alkaline/shoshonite series. As it is seen in the diagram, the plot of E22 in Th-Co diagram is compatible with the K_2O-SiO_2 diagram. However, E68 plots in high-K calc-alkaline/shoshonite series field in the Th-Co diagram whereas it plots in the field of calc-alkaline series in the K_2O-SİO_2 diagram.

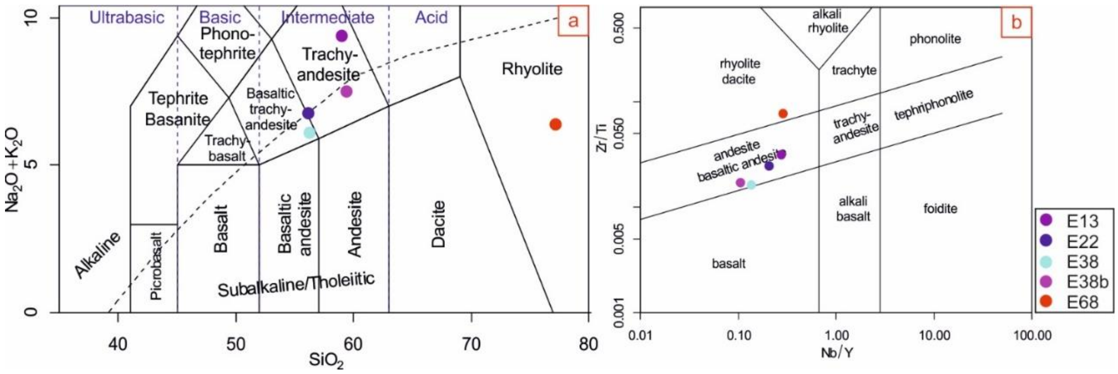

Figure 4.1 : Discrimination diagrams for determination of rock types a) Total alkali versus silica diagram (TAS) after Le Bas et al. (1986) b) Nb/Y-Zr/Ti diagram of Pearce (1996) modified after Winchester and Floyd (1977).

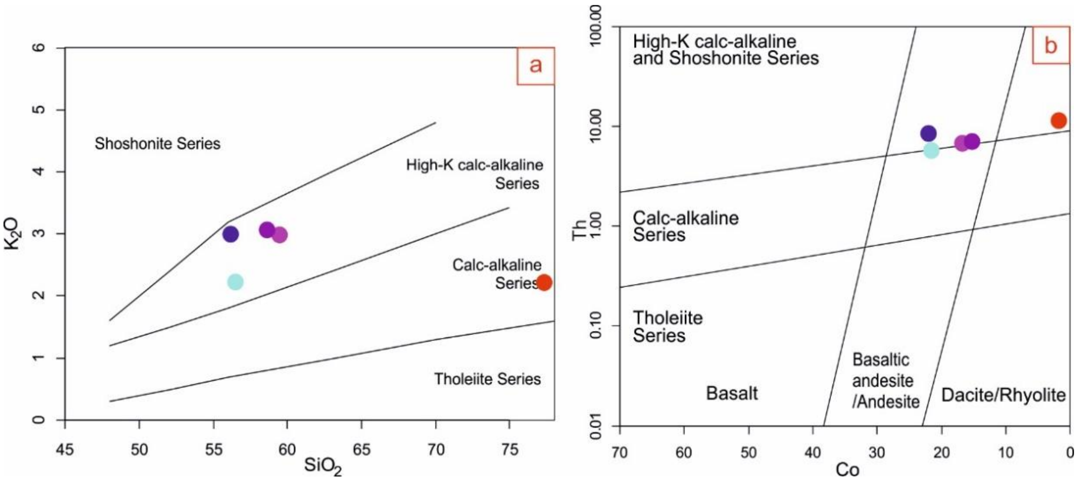

Figure 4.2 : Discrimination diagrams showing magmatic series a) K_2O-SİO_2 diagram after Peccerillo and Taylor (1976) b) Th-Co diagram for rock type and volcanic series after Hastie et al. (2007).

The Ta/Yb-Th/Yb diagram which is conducted by Pearce (1982) is shown in Figure 4.3. According to this diagram, all samples plot in the field of volcanic arc magmas indicating that there is no anorogenic source. Additionally, E22 and E68 samples plot in the field of shoshonitic series compatibly with the Th-Co diagram. E13, E38 and E38b samples plot in calc-alkaline field in Ta/Yb-Th/Yb diagram whereas they are located in between calc-alkaline/high-K calc-alkaline and shoshonite series in Th-Co diagram.

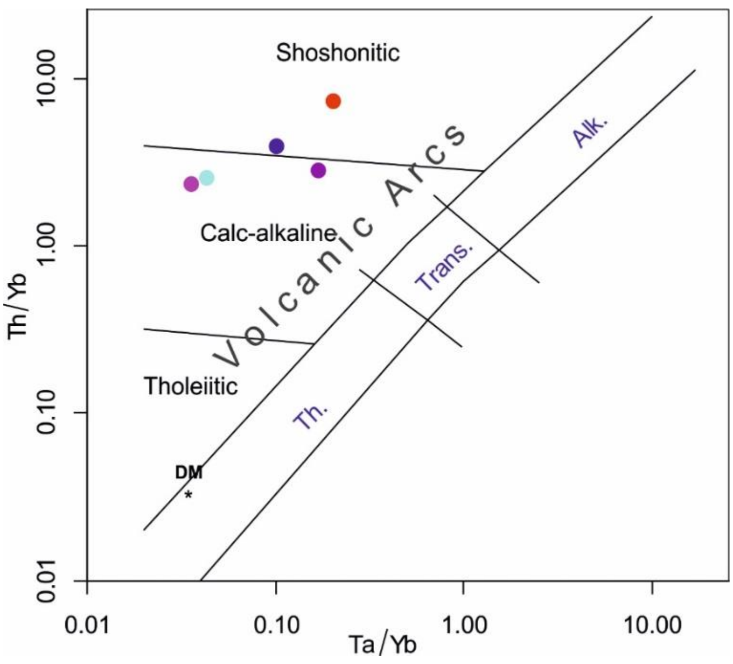

Figure 4.3 : Ta/Yb-Th/Yb diagram after Pearce (1982) showing that all samples plot in volcanic arc field.

Chondrite-normalized REE patterns and primitive mantle-normalized trace element spider diagrams are shown in figures 5.4 and 5.5. These diagrams are conducted separately for andesite/basaltic andesite samples and dacitic sample. High field strength elements, which are Th, Ce, Zr, Hf, Ti, Nb, Ta, U, are relatively immobile and therefore, they are more resistant against alteration. Their patterns are important for interpretation of altered samples.

According to chondrite-normalized REE patterns (Figure 4.4), the La/Yb ratio is approximately 7 for andesite/basaltic andesite samples and, 12.5 for dacitic sample. High La/Yb ratios indicate that heavy REEs are incorporated by a mineral or some minerals leaving light REEs in the melt. The reason for slight negative anomaly in Eu may be limited plagioclase fractionation. Steep light REE pattern, almost flat heavy REE pattern and the slight rise in the end of heavy REE pattern indicate fractionation of a melt including hornblende.

According to primitive mantle-normalized trace element spider diagrams (Figure 4.5), distinct negative Nb-Ta anomaly, which is typical for volcanic arc basalts, is seen for all samples. Large-ion lithophile elements (LILE) which are Sr, K, Rb and Th are relatively enriched whereas high field strength elements (HFSE) which are Nb, Ta, Ti are relatively depleted indicating the subduction-related signature of the volcanism. The reason for the negative anomaly in Ba may be fractionation of a feldspar or mica mineral. Negative anomaly in Ti may be explained with fractionation of rutile or ilmenite. Zr also shows negative anomaly indicating that a mineral including Zr is fractionated. The slight negative anomaly in Eu is also observed here. Positive anomaly in Pb may be seen because of hydrothermal alteration.

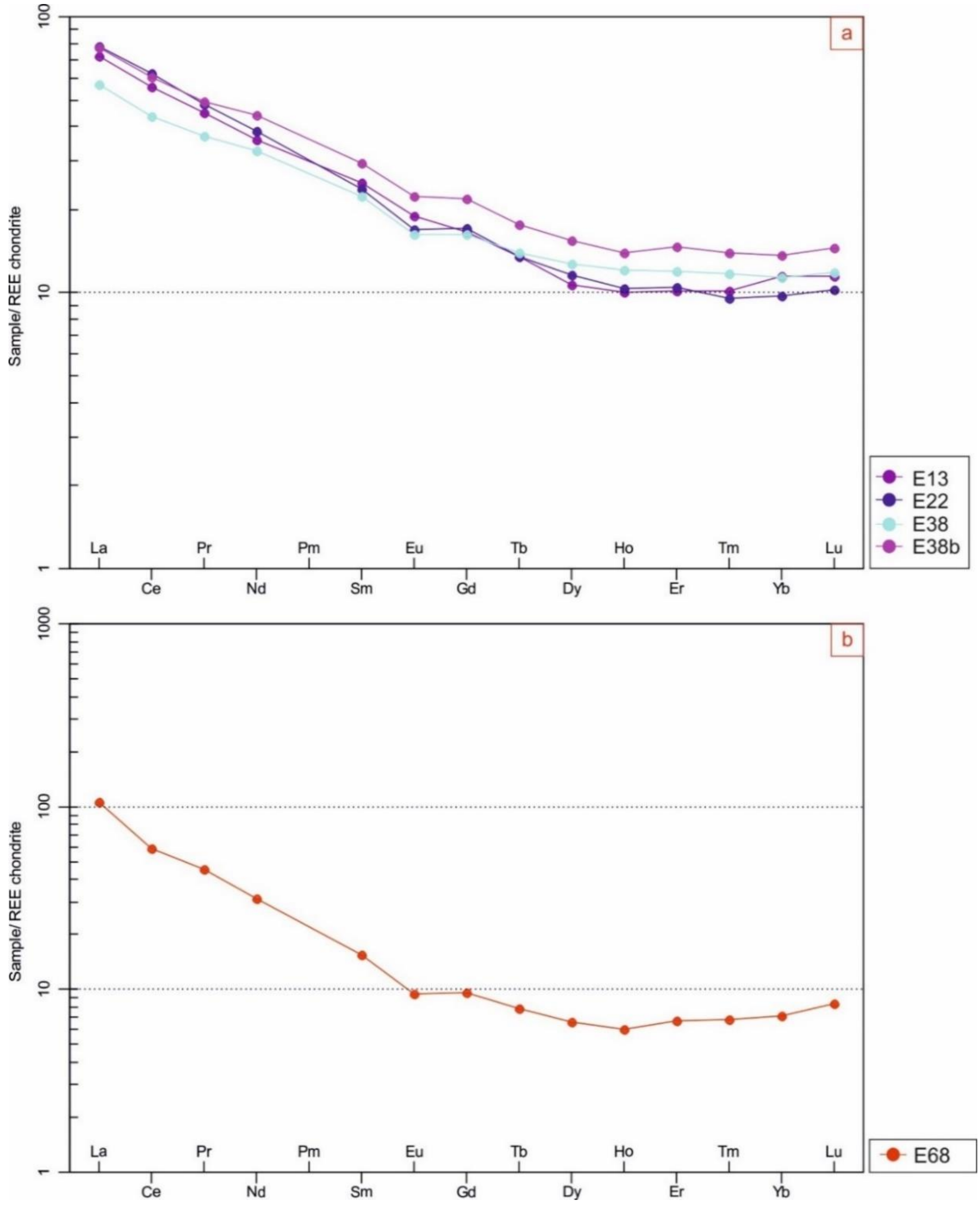

Figure 4.4 : Chondrite-normalized REE diagrams after Boynton (1984) a) For andesite and basaltic andesite samples b) For dacitic sample.

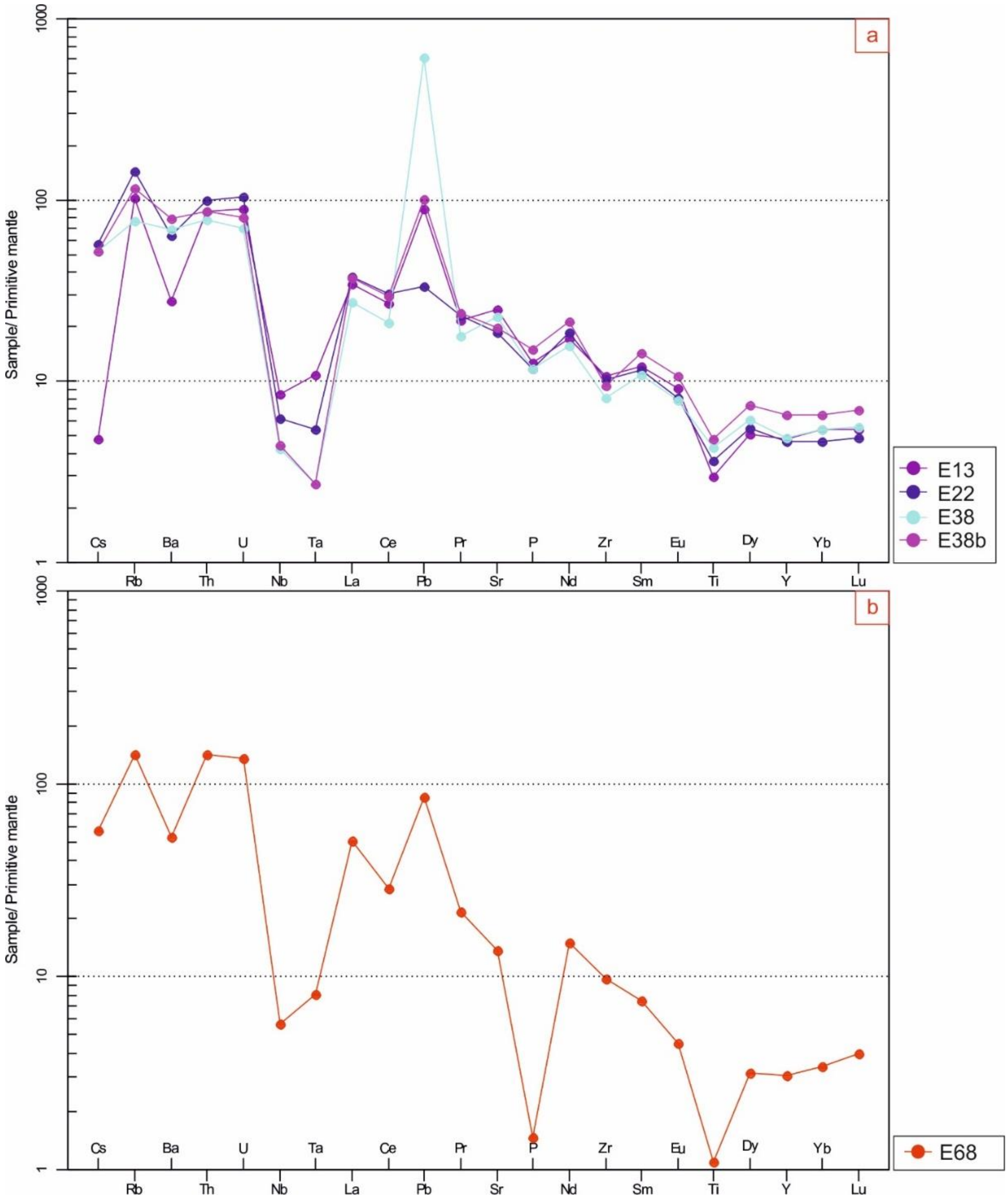

Figure 4.5 : Trace element spider diagrams normalized to primitive mantle after McDonough and Sun (1995) a) For andesite and basaltic andesite samples b) For dacitic sample.

4.3 Results and Discussion of Geochemical Analyses

Geochemical data (calc-alkaline characteristic, negative Nb-Ta anomaly, enriched LILE and light REE relative to HFSE) obtained from the volcanic rocks in İğneada clearly confirm the subduction signature and volcanic arc origin for all samples. These results are mostly compatible with the other geochemical studies about Upper Cretaceous magmatic arc rocks in Turkey and Europe. According to the geochemical and petrogenesis study of Karacık and Tüysüz (2010), Demirköy Igneous Complex, which is the plutonic member of Upper Cretaceous magmatic belt and 20 km away from İğneada, reveals its subduction-related origin with its calc-alkaline characteristic, relatively enriched LILE and depleted HFSE values. S. Georgiev et al. (2009) explained the geochemistry of magmatism in eastern Sredna-Gora segment of Apuseni – Banat – Timok – Sredna-Gora Upper Cretaceous magmatic belt. They suggested that the magmatism in Strandja region was initially high-K calc-alkaline. Then, the intra-arc rifting due to extension created by slab roll-back leads underplating of mantle-derived magmas at crust-mantle boundary and hence supplying the heat needed to melt lower crustal cumulates. Therefore, the fractional crystallization of Fe and Ti oxides (esspecially olivine and clinopyroxene) in a deep magma chamber caused the formation of shoshonitic basalts and basaltic andesites in eastern Sredna-Gora. The shoshonitic basalts and basaltic andesites differentiated and formed rocks with intermediate composition (S. Georgiev et al., 2009). The change from calc-alkaline to high-K calc-alkaline/shoshonitic magma is clearly seen for İğneada volcanics. Based on the comparison of geochemical data for each segment of Upper Cretaceous magmatic belt (Gallhofer et al., 2015), as distinct from the other three segments, east Sredna-Gora segment has high-K calc-alkaline and shoshonite magma series due to formation of volatile-rich magmas as a result of intra-arc extension. According to geochemical results, İğneada volcanics are also included these magma series.

Keskin and Tüysüz (2018) studied Upper Cretaceous volcanism on the SW margin of the Black Sea and divided it into two stages. Based on their geochemical results, the first stage of the arc volcanism is composed of calc-alkaline series and shows typical subduction signature whereas the second stage has OIB (ocean island basalt)-type alkaline within-plate characteristics instead of typical subduction component. They suggested that two contrasting mantle source, which are asthenospheric and metasomatized lithospheric mantle, coexist in the second stage (Keskin and Tüysüz, 2018). Boehm et al. (2019) also suggested that the volcanism is divided into two periods in western Pontides and based on their geochemical data, dominantly calc-alkaline/high-K calc-alkaline and seldom more tholeiitic volcanic arc basalts are present. However, the division between volcanic rocks and also OIB-type alkaline magma are not found in İğneada.

Although the geochemical characteristics of İğneada volcanics are mostly compatible with other volcanic and plutonic rocks within the Upper Cretaceous magmatic belt, some differences in terms of magma series and rock type exist. İğneada volcanics do not display OIB-type alkaline characteristics in contrast to western Pontides in Turkey. The alkaline characteristic may be absent since the upper levels of volcanism are not observed in İğneada. They also do not display any tholeiitic affinity in contrast to eastern Sredna-Gora region in which tholeiitic, calc-alkaline and high-K calc-alkaline rocks with basic, intermediate and acidic compositions are present. Additionally, the most mafic rocks which is found within İğneada volcanic-volcaniclastic sequence are basaltic andesites. Although basaltic blocks are found in the dacitic agglomerate within the second part of the D3 domain, basalts cannot be observed throughout the whole sequence. In order to see basaltic rocks and the geochemical variations in magma series, the continuation of the İğneada volcanics in Bulgaria, which can be seen from Beğendik Village, may need to be studied.

5. GEOLOGICAL EVOLUTION AND DISCUSSION

The basement rocks in the study are phyllite and schists of Strandja Massif which are metamorphosed in late Jurassic-early Cretaceous. The sedimentary rocks of İğneada Group unconformably overlie these metamorphic rocks. The sedimentation starts with shallow marine limestone including rudist and Orbitolina fossils. The age of this limestone is determined as Albian based on rudist and Orbitolina species (Arca, 2012), and Cenomanian based on other Orbitolina species (Pamir and Baykal, 1947). The sedimentary sequence continues with marl, carbonate-rich sandstone, laminated radiolarian siltstone and claystone indicating deepening upwards. The thin sections of these sedimentary rocks do not include any volcanic material. Therefore, it is understood that the volcanism had not yet begun during this sedimentation period.

The beginning of the volcanism is observed with andesitic tuff layers which conformably overlie the sedimentary sequence. This andesitic tuff layer, which is found in location 9 and considered as the base of volcanic-volcaniclastic sequence, represents the beginning of the volcanism in İğneada. The age of this layer is determined as Campanian (80.6 ±1.5 Ma) using U-Pb zircon dating. This age is obtained from only one zircon since the other zircons are xenocrystic. Another U-Pb zircon dating is done from a dacitic tuff level which is located in location 68. Since this layer is found in upper levels of volcanic-volcaniclastic sequence in İğneada, its age can be indicating close to the end of volcanism in İğneada. U-Pb zircon ages obtained from 22 zircons give the age as Santonian (84.85 ± 0.42 Ma). Campanian age obtained from the base of the volcanic-volcaniclastic sequence (location 9) and Santonian age obtained from the upper level of the sequence (location 68) geochronologically contradict each other. The reason for this contradiction may be the poor resolution of the age of this sample, based on a single zircon.

The volcanic-volcaniclastic sequence starts with andesitic tuff, lapilli-tuff and agglomerate. They are mostly found alternating with marl, carbonate-rich sand/siltstone and shale. The sedimentary rocks show poorly-developed turbiditic characteristics in some places indicating a submarine volcanism. This alternation is followed by andesite lava flow which has high-K calc-alkaline/shoshonitic characteristic. The alternation of andesitic volcaniclastic and volcanogenic sedimentary rocks continue to be observed above the andesite lava flow. The volcanism becomes clearly more basaltic after this long-continued alternation. The poorly-developed columnar basaltic andesites are observed indicating a decrease in the depth of the volcanism. Basaltic andesite lava flow found above this alternation has calc-alkaline to high-K calc-alkaline/shoshonite characteristic. The lava flow is followed again by the alternation of basaltic andesitic/andesitic volcaniclastic and volcanogenic sedimentary rocks. The biomicritic limestone level (location 75), which is found within this alternation, contains Turonian planktonic foraminifera, which are *Marginotruncana pseudolinneana, Marginotruncana marginata, Whitenella* sp.*, Whitenella praehelvetica, Muricohedbergella* sp.*,* and ?*Helvetoglobotruncana* cf. *Helvetica*. Another age determination by using planktonic foraminifera *Marginotruncana pseudolinneana, Marginotruncana coronate* and *Muricohedbergella flanderini* is done from biomicrite level (location 100) corresponding to the level found in location 75. Their ages are defined between uppermost Turonian and Santonian. It indicates that the volcanism was active during Turonian and Santonian in İğneada. The sequence continues with andesitic/basaltic andesitic volcanic/volcaniclastic rocks and volcanogenic sedimentary rocks which have well-developed turbiditic sedimentary structures again indicating deposition in submarine conditions. The composition of the volcanic and volcaniclastic rocks becomes more acidic in upper levels of the sequence. The dacitic volcanic and volcaniclastic rocks with high-K calc-alkaline/shoshonitic characteristic are started to be seen alternating with andesitic volcaniclastic rocks and volcanogenic sedimentary rocks. In uppermost levels of the sequence, the volcanism becomes basaltic andesitic and andesitic again. The basaltic andesite sample (sample 13) from the end of the volcanic-volcaniclastic sequence in İğneada has calc-alkaline to high-K calc-alkaline/shoshonitic characteristic. The interpretation of S-N seismic cross-section (Figure 5.1) taken from the study of Nikishin et al. (2015) shows a possible volcano which is located in the east of İğneada within Western Black Sea Basin. The non-eroded morphology of the volcano indicates that it was formed at least 2 km depth underwater (Nikishin et al., 2015). Similar volcanoes may have been the source of the volcaniclastic rocks in the İğneada region, which were probably deposited in an intraarc or the forearc.

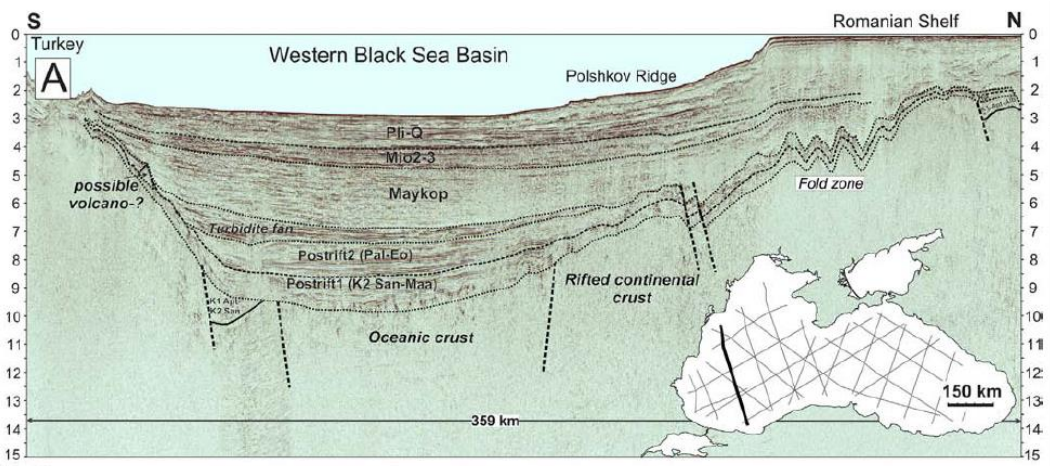

Figure 5.1 : Geologically interpreted seismic cross-section showing the possible volcano (modified from Nikishin et al., 2015).

The composition of volcanic and volcaniclastic rocks throughout the sequence in İğneada changes from andesite to basaltic andesite, then to dacite/andesite, and then again to andesite/basaltic andesite. The calc-alkaline and high-K calc-alkaline/shoshonite characteristic do not change throughout the sequence. According to geochemical data, calc-alkaline characteristics of all samples, negative Nb-Ta anomaly, enrichment in LILE and light REE relative to HFSE indicate a clear subduction signature and a volcanic arc setting. The sea floor alteration, which is found in all volcaniclastic and volcanic rock samples, the intercalated pelagic limestones, and turbiditic sedimentary structures show that the rocks were deposited in deep submarine conditions in an intra-arc to fore-arc environment.

Large and small-scale normal faults, which are observed in the whole sequence in various orientations, and tensile fractures indicate an extensional setting in the region whereas the presence of syncline indicates a compressional regime. It may be concluded that the region has undergone two different deformation phases. However, the ages of faulting and folding are not known, and their relative ages to each other cannot be understood from observations made from the sequence. The normal faulting may be resulted from extension which affected the region and formed Thrace Basin in the Middle to Late Eocene (Siyako and Huvaz, 2007; Okay et al., 2010). Therefore, if it is considered that the folds are associated with Alpine orogeny (Pamir and Baykal, 1947), the normal faulting in the region may be younger than folding.

It is stated that Upper Cretaceous volcanism in western Pontides is divided into two stages separated by a distinct pelagic limestone layer which was deposited during the pause in volcanism (Boehm et al., 2019; Keskin and Tüysüz, 2018; Tüysüz et al., 2012; Keskin et al.,2010). The initial stage (Coniacian-Turonian) of volcanism is explained as the arc volcanism formed as a result of northward subducting Tethys beneath southern Laurasian margin. After the first stage, the volcanic activity is paused and a red pelagic limestone layer is deposited during Upper Santonian. The second stage of volcanism (Campanian) is defined by rift magmatism comprising of two contrasting magma sources which are asthenospheric and metasomatized lithospheric mantle (Keskin and Tüysüz, 2018). There are different explanations for the pause in volcanism. Keskin et al. (2010) suggested a ridge-trench collision model. Keskin and Tüysüz (2018) and Boehm et al. (2019) suggested that arc rifting is started in the end of the first stage of volcanism. The rifting caused thinning and eventually rupturing of southern margin of Laurasia leading a slab roll-back process which gradually causes steepening and retreat of the slab. The stretching is increased as a result of this process and the red pelagic limestone started to deposit in the occurred subsidence (Keskin and Tüysüz, 2018). However, this red pelagic limestone layer, which should be laterally continuous, is not observed in İğneada. Additionally, U-Pb zircon ages obtained from location 68 indicate that the volcanism was active during Upper Santonian. Therefore, the arc volcanics and associated volcaniclastic rocks in İğneada cannot be divided into two stages. Based on the aforementioned ages obtained from U-Pb zircon and foraminifera datings, it is concluded that the volcanism in İğneada was continuous starting from Turonian to Campanian.

REFERENCES

Arca, İ. (2012). *Stratigraphy and facies characteristics of upper Cretaceous sequences around İğneada Kirklareli.* (MSc thesis). Dokuz Eylül University, İZMİR.

Aydın, Y. (1982) *Yıldız Dağları (Istranca) masifinin jeolojisi*. (Doctoral dissertation). İstanbul Technical University, İSTANBUL.

Aysal, N., Keskin, M., Peytcheva, I., and Duru, O. (2018). Geochronology, geochemistry and isotope systematics of a mafic–intermediate dyke complex in the İstanbul Zone. New constraints on the evolution of the Black Sea in NW Turkey. *Geological Society, London, Special Publications., 464*(1), 131-168.

Azer, M. K., Gahlan, H. A., Asimow, P. D., Alfaifi, H. J. (2018). Prehnite as an indicator mineral in the Wadi Nasb uralitized gabbro, South Sinai, Egypt. *Journal of Asian Earth Sciences., 160*, 107-117.

Boehm, K., Wagreich, M., Wolfgring, E., Tüysüz, O., Gier, S., and Yilmaz, İ. Ö. (2019). Upper Cretaceous volcaniclastic complexes and calcareous plankton biostratigraphy in the Western Pontides, NW Turkey. *Turkish Journal of Earth Sciences, 28*(2), 187-206.

Boynton, W. V. (1984). Cosmochemistry of the rare earth elements: meteorite studies. *Developments in geochemistry, Elsevier.*, Vol. 2, 63-114.

Çağlayan, M. A., and Yurtsever, A. (1998). Geological map of Turkey at 1:100000 scale, no. 20, 21, 22, 23, Burgaz-A3, Edirne-B2 and -B3, Burgaz A4, and Kırklareli-B4-B5-B6 and –C6 sheets, *Mineral Research and Exploration Institute (MTA) of Turkey publications*.

Cattò, S., Cavazza, W., Zattin, M., and Okay, A. I. (2018). No significant Alpine tectonic overprint on the Cimmerian Strandja Massif (SE Bulgaria and NW Turkey). *International Geology Review., 60*(4), 513-529.

Fisher, R. V. (1966). Rocks composed of volcanic fragments and their classification. *Earth-Science Reviews., 1*(4), 287-298.

Gallhofer, D., Quadt, A. V., Peytcheva, I., Schmid, S. M., and Heinrich, C. A. (2015). Tectonic, magmatic, and metallogenic evolution of the Late Cretaceous arc in the Carpathian-Balkan orogen. *Tectonics., 34*(9), 1813-1836.

Georgiev, N., Henry, B., Jordanova, N., Froitzheim, N., Jordanova, D., Ivanov, Z., and Dimov, D. (2009). The emplacement mode of Upper Cretaceous plutons from the southwestern part of the Sredna-Gora Zone (Bulgaria): structural and AMS study. *Geologica Carpathica., 60*(1), 15-33.

Georgiev, S., Marchev, P., Heinrich, C. A., Von Quadt, A., Peytcheva, and I., Manetti, P. (2009). Origin of nepheline-normative high-K ankaramites and the evolution of Eastern Srednogorie arc in SE Europe. *Journal of Petrology., 50*(10), 1899-1933.

Handler, R., Neubauer, F., Velichkova, S., and Ivanov, Z. (2004). 40Ar/39Ar age constraints on the timing of magmatism and postmagmatic cooling in the Panagyurishte region, Bulgaria. *Swiss Bulletin of Mineralogy and Petrology., 84*(1–2), 119–132.

Hastie, A.R., Kerr, A.C., Pearce, J.A., and Mitchell, S.F. (2007). Classification of altered volcanic island arc rocks using immobile trace elements: development of the Th–Co discrimination diagram. *Journal of Petroleum Science and Engineering., 48,* 2341-2357.

Karacık, Z., and Tüysüz, O. (2010). Petrogenesis of the Late Cretaceous Demirköy Igneous Complex in the NW Turkey: implications for magma genesis in the Strandja Zone. *Lithos., 114*(3-4), 369-384.

Keskin, M., and Tüysüz, O. (2018). Stratigraphy, petrogenesis and geodynamic setting of Late Cretaceous volcanism on the SW margin of the Black Sea, Turkey. *Geological Society, London, Special Publications., 464*(1), 95-130.

Keskin, M., Ustaömer, T., and Yeniyol, M. (2010). İstanbul kuzeyindeki Üst Kretase volkanojenik istiflerinin magmatik evrimi ve jeodinamik ortamı (Magmatic evolution and geodynamic setting of the Upper Cretaceous sequence in the north of İstanbul). *Symposium on the Geology of Istanbul III., 3,* 130–180.

Kouzmanov, K., Moritz, R., von Quadt, A., Chiaradia, M., Peytcheva, I., Fontignie, D., Ramboz, C., and Bogdanov, K. (2009). Late Cretaceous porphyry Cu and epithermal Cu– Au association in the Southern Panagyurishte District, Bulgaria: the paired VlaykovVruh and Elshitsa deposits. *Mineralium Deposita.,* doi:10.1007/s00126-009-0239-1.

Le Bas, M.J., Le Maitre, R., Streckeisen, A., and Zanettin, B. (1986). A chemical classification of volcanic rocks based on the total alkali-silica diagram. *Journal of Petroleum Science and Engineering., 27,* 745-750.

Marchev, P., Georgiev, S., and Singer, B. (2015). Onset of Late Cretaceous magmatism in the Eastern Balkan, Bulgaria: results from 40Ar/39Ar dating of amphibole from volcanic rocks. *National Conference "Geosciences 2015",* Sofia, Bulgaria, pp. 69–70.

McDonough, W. F., and Sun, S. S. (1995). The composition of the Earth. *Chemical geology, 120*(3-4), 223-253.

Moore, W.J., McKee, E.H., and Akıncı, Ö. (1980). Chemistry and chronology of plutonic rocks in the Pontide mountains, northern Turkey. *Symposium on the European Copper Deposits,* Belgrade, Yugoslavia, pp. 209–216.

Natalin, B. A., Sunal, G., Gün, E., Wang, B., and Zhiqing Y. (2016). Precambrian to Early Cretaceous rocks of the Strandja Massif (northwestern

Turkey): evolution of a long lasting magmatic arc, *Canadian Journal of Earth Sciences*, *53*(11), 1312-1335.

Nikishin, A. M., Okay, A. I., Tüysüz, O., Demirer, A., Amelin, N., and Petrov, E. (2015). The Black Sea basins structure and history: New model based on new deep penetration regional seismic data. Part 1: Basins structure and fill. *Marine and Petroleum Geology, 59*, 638-655.

Okay, A. I., Simmons, M., Özcan, E., Starkie, S., Bidgood, M., and Kylander-Clark, A. R. (2019). Eocene-Oligocene succession at Kıyıköy (Midye) on the Black Sea coast in Thrace. *Turkish Journal of Earth Sciences*, *29*, 139-153.

Okay, A. I., Yurtsever, A., and Siyako, M. (2006). Trakya bölgesi litostratigrafik birimleri, *Stratigrafi Komitesi Litostratigrafi Birimleri Serisi*, *2*, 53-66.

Okay, A.I., Satır, M., Tüysüz, O., Akyüz, S., and Chen, F. (2001). The tectonics of the Strandja Massif: late Variscan and mid- Mesozoic deformation and metamorphism in the northen Aegen, *International Journal of Earth Science*, *90*(2): 217-233.

Okay, A. I., Özcan, E., Cavazza, W., Okay, N., and Less, G. (2010). Basement types, Lower Eocene series, Upper Eocene olistostromes and the initiation of the southern Thrace Basin, NW Turkey. *Turkish Journal of Earth Sciences*, *19*: 1-25.

Pamir, H.N., and Baykal, F. (1947). Istranca masifinin jeolojik etüdü (Rapor No. 2257). Ankara : MTA Raporu.

Pearce, J.A. (1982). Trace element characteristics of lavas from destructive plate boundaries. In R. S. Thorpe (Ed.), *Orogenic Andesites and Related Rocks* (pp.525-548). Chichester, UK : John Wiley and Sons.

Pearce, J.A. (1996). A user's guide to basalt discrimination diagrams. In D. A. Wyman (Ed.), *Trace Element Geochemistry of Volcanic Rocks for Massive Sulphide Exploration* (Vol. 12: pp.79-113). Geological Association of Canada, Canada : Short Course Notes.

Peccerillo, A., and Taylor, S. R. (1976). Geochemistry of Eocene calc-alkaline volcanic rocks from the Kastamonu area, northern Turkey. *Contributions to mineralogy and petrology*, *58*(1), 63-81.

Peytcheva, I., von Quadt, A., Neubauer, F., Frank, M., Nedialkov, R., Heinrich, C., and Strashimirov, S. (2009). U–Pb dating, Hf-isotope characteristics and trace-REE-patterns of zircons from Medet porphyry copper deposit, Bulgaria: implications for timing, duration and sources of ore-bearing magmatism. *Mineralogy and Petrology, 96*, 19–41.

Shaw, D. M. (2006). Trace elements in magmas: a theoretical treatment. *Cambridge University Press* (pp.166).

Siyako, M., and Huvaz, O. (2007). Eocene stratigraphic evolution of the Thrace Basin, Turkey. *Sedimentary Geology, 198*: 75-91.

Tüysüz, O., Yılmaz, İ. Ö., Svabenicka and L., Kirici, S. (2012). The Unaz formation: a key unit in the Western Black Sea region, N Turkey. *Turkish Journal of Earth Sciences*, *21*(6), 1009-1028.

Url-1 < *nationalparksofturkey.com*>, date retrieved 20.11.2019.

Url-2 < *tr.climate-data.org*>, date retrieved 20.11.2019.

Üşümezsoy, Ş., and Öztunalı, Ö. (1981). Istranca ve Eybek masiflerinde kataklastik dokunun evrimi. *İstanbul Yerbilimleri*, 129-137.

von Quadt, A., Moritz, R., Peytcheva, and I., Heinrich, C.A. (2005). Geochronology and geodynamics of Late Cretaceous magmatism and Cu–Au mineralization in the Panagyurishte region of the Apuseni-Banat-Timok–Srednogorie belt, Bulgaria. *Ore Geology Reviews 27*, 95–126.

Winchester J., and Floyd P. (1977). Geochemical discrimination of different magma series and their differentiation products using immobile elements. *Chemical Geology 20*: 325-343.

APPENDICES

APPENDIX A: Geological map of the study area

APPENDIX B: NW-SE and SW-NE cross-sections

CURRICULUM VITAE

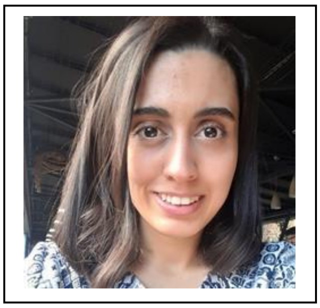

Name Surname : Ezgi Sağlam

Place and Date of Birth : Seyhan, 03.10.1994

E-Mail : saglamez@itu.edu.tr

EDUCATION

- **B.Sc.** : 2018, Istanbul Technical University, Geological Engineering

PROFESSIONAL EXPERIENCE AND REWARDS:

- **October 2018-May 2019:** Laboratory studies in ITU Sample Preparation and Mineral Separation Laboratory within the scope of TUBITAK scholarship of the project of Prof. Dr. Gültekin Topuz.

- **May 2019-continuing:** Research assistant at Eurasia Institute of Earth Sciences, İstanbul Technical University.

PUBLICATIONS, PRESENTATIONS AND PATENTS ON THE THESIS:

- **Sağlam, E., Duzman, T., Okay, A.I.** 2020. Upper Cretaceous Stratigraphy and Volcanism in the Igneada Region, Pontides, NW Turkey, EGU 2020 – General Assembly.